Gemp # 76-03499

UNITED TECHNOLOGIES RESEARCH CENTER

UNITED TECHNOLOGIES

East Hartford, Connecticut 06108

Report R76-912204

Investigation of Applications for High-Power, Self-Critical Fissioning Uranium Plasma Reactors

Contract NAS1-13291,
Modification No. 2

REPORTED BY Richard J. Rodgers

Thomas S. Latham

Nicholas L. Krascella

APPROVED BY Robert E. Olson
Manager, Fluid Dynamics Laboratory

DATE September 1976

NO. OF PAGES 89

COPY NO. _____

FOREWORD

An analytical and experimental research program on plasma core reactor technology was conducted by United Technologies Research Center (UTRC) under Contract NAS1-13291 with the National Aeronautics and Space Administration (NASA) Langley Research Center. The Technical Monitor of the Contract for NASA during the Contract period was Dr. F. Hohl. The Technical Program Manager for UTRC during the Contract period was Mr. T. S. Latham. The following three reports comprise the required Final Technical Report under the Contract:

1. Rodgers, R. J., T. S. Latham, and N. L. Krascella: Investigation of Applications for High-Power, Self-Critical Fissioning Uranium Plasma Reactors. United Technologies Research Center Report R76-912204, September 1976 (Present Report). Also issued as NASA CR-145048.

2. Roman, W. C.: Laboratory-Scale Uranium RF Plasma Confinement Experiments. United Technologies Research Center Report R76-912205, September 1976. Also issued as NASA CR-145049.

3. Krascella, N. L.: The Spectral Properties of Uranium Hexafluoride and Its Thermal Decomposition Products. United Technologies Research Center Report R76-912208, September 1976. Also issued as NASA CR-145047.

Report R76-912204

Investigation of Applications for High-Power Self-Critical Fissioning Uranium Plasma Reactors

TABLE OF CONTENTS

Report R76-912204

Investigation of Applications for High-Power Self-Critical Fissioning Uranium Plasma Reactors

SUMMARY

Analytical studies were conducted to investigate potentially attractive applications for gaseous nuclear cavity reactors fueled by uranium hexafluoride and its decomposition products at temperatures of 2000 to 6000 K and total pressures of a few hundred atmospheres. The objective of the investigations conducted was to determine approximate operating conditions and performance levels for a class of nuclear reactors in which fission energy removal is accomplished principally by radiant heat transfer from the high temperature gaseous nuclear fuel to surrounding absorbing media. The results show the radiant energy deposited in the absorbing media may be efficiently utilized in energy conversion system applications which include (1) a primary energy source for high-thrust, high-specific-impulse space propulsion, (2) an energy source for highly efficient generation of electricity, and (3) a source of high intensity photon flux for heating working fluid gases for hydrogen production or MHD power extraction.

These investigations were conducted as part of a planned program involving the National Aeronautics and Space Administration (NASA), Los Alamos Scientific Laboratory (LASL), United Technologies Research Center (UTRC), and other organizations to establish the feasibility of plasma core nuclear reactors and to identify unique and efficient applications which use the thermal radiant energy, and which can be demonstrated and advanced by laboratory experiments and analyses.

RESULTS AND CONCLUSIONS

1. Performance characteristics were calculated for a plasma core reactor with uranium hexafluoride (UF_6) fuel consisting of six unit cells imbedded in a beryllium oxide reflector-moderator and surrounded by a pressure vessel. The reactor with a nominal thermal power level of 2500 MW had the following characteristics: unit cell length = 4.35 m, unit cell diameter = 1.00 m, reactor length including pressure vessel = 8.2 m, reactor diameter = 4.05 m, critical mass = 86.4 kg of U-235, operating pressure = 650 atm.

2. Cylindrical aluminum lined transmission cells with a series of fused-silica transparent walls with intermediate regions of gaseous hydrogen and/or deuterium can provide a transparent light path for thermal radiation from the radiating plasma to a working fluid channel. The transmission cell can be used to locate working fluid channels at positions other than those adjacent to the fuel cavity, such as when it is necessary to minimize effects of neutron absorbing materials in the working fluid channels or when a significantly reduced pressure in the working fluid channel is required. For a radiant flux spectrum corresponding to a black-body radiating temperature of 4000 K, total transmissivity varies from approximately 0.50 to 0.85 for length-to-diameter ratios of 4.0 to 0.5 and fused silica thicknesses from 3.5 to 0.25 cm. The gaseous hydrogen and/or deuterium prevents neutron leakage through the cells.

3. Plasma core reactor rocket engines with specific impulses of 1150 to 1220 s and thrust-to-weight ratios of 0.15 to 0.47 require approximately 40 to 60 percent of the initial mass in earth orbit as chemical rockets for missions requiring boosts of 90,000 kg (approximately four space shuttle payloads) from low earth orbit to synchronous orbit.

4. Overall cycle efficiencies were calculated for closed-cycle helium gas turbine electric generator systems with an output power of 1000 MWe using plasma core reactors as thermal energy sources. The cycle efficiencies were calculated to be from 40 to 60 percent for turbine inlet temperatures from 1100 to 1900 K.

5. Significant fractions of plasma core reactor total radiant energy are available to induce photodissociation of bromine and iodine diatomic gases in a hydrogen production closed-cycle system for which water is the source species to be decomposed. Based on the radiant energy absorption spectra of bromine and iodine, radiant energy fractions of approximately 0.25, 0.35, and 0.44 can be utilized from plasma core nuclear reactors which are radiating at black-body temperatures of 4000 K, 5000 K, and 6000 K, respectively. The corresponding maximum hydrogen production rates are 0.443, 0.694, and 0.89 hydrogen moles per second per MW of incident radiant power, respectively, for the above radiating temperatures. For each of the spectra considered, thermal efficiencies between 0.41 and 0.55 were calculated for

instances in which the utilization of the wavelength dependent spectra was optimized, no recombination of dissociated species was allowed, and no recovery of either heat of reactions for the closed-cycle processes or of the energy devoted to preparation of initial constituents. The reaction processes were also prescribed such that the closed-cycle reactions can be carried out at low temperatures; that is, between 456 K and 700 K.

6. A Thorium--Uranium-233 breeding cycle was analyzed for a Uranium-233 fueled UF_6 plasma core nuclear reactor. Calculations were performed for a plasma core reactor in which a six cell cavity reactor configuration is embedded in a heavy-water reflector-moderator. One-dimensional neutron transport calculations indicate critical masses of approximately 75 to 106 kg of U-233 and maximum theoretical breeding ratios of approximately 1.055 to 1.12 for a Thorium--Uranium-233 thermal breeder. Doubling times of approximately 4 to 5 years are calculated for these configurations in which the total fuel inventory, including the fuel in the fuel recirculation system, is four times the critical mass value. Fuel partial pressures which include uranium, fluorine, electron, and uranium fluoride constituents are approximately 400 to 600 atm. Typically, 10 to 12 percent of the total pressure is due to the uranium species in the fuel region.

INTRODUCTION

Since 1955, various researchers have considered the prospects for utilizing nuclear energy with fissile fuel in the gaseous state. Most of this work was concentrated on the gaseous nuclear reactor technology required for high-performance space propulsion systems. This work was supported initially by the Air Force and later by NASA and the Atomic Energy Commission (AEC) as part of the larger nuclear rocket program. In 1973, virtually all work in nuclear space power and nuclear propulsion research was terminated. Subsequently, the Subcommittee on Aeronautics and Space Technology of the Committee on Science and Astronautics of the House of Representatives requested that funds be added to the fiscal year 1974 budget to maintain a viable long-range capability in advanced nuclear power and propulsion research (see Ref. 1). Research on plasma core nuclear reactors was one of the efforts chosen to be restarted. The current research program on gaseous nuclear reactors includes consideration of high-thrust, high-specific-impulse space propulsion applications and plasma core reactor applications for meeting terrestrial energy needs.

Extraction of energy from the fission process with the nuclear fuel in gaseous form allows operation at much higher temperatures than those of conventional nuclear reactors with solid fuel elements. Higher operating temperatures, in general, lead to more efficient thermodynamic cycles and, in the case of fissioning uranium plasma core reactors, result in many possible applications employing direct transfer of energy in the form of electromagnetic radiation. The applications for plasma core reactors require significant research and technology development, but the benefits in potential increases of domestic energy resources and utilization, reductions in environmental impact, and the development of new highly-efficient techniques for extracting energy from the fission process with nuclear fuel in the gaseous or plasma state justify an investment to establish the feasibility of fissioning uranium plasma core reactors as a prime energy source.

Possible applications for plasma core reactors are:

(1) High-thrust, high-specific-impulse space propulsion.

(2) Advanced closed-cycle gas turbine driven electrical generators.

(3) MHD power conversion systems for generating electricity.

(4) Photochemical or thermochemical processes such as dissociation of hydrogenous materials to produce hydrogen.

(5) Thorium--Uranium-233 thermal breeder nuclear reactor with gas turbine driven electrical generators.

(6) Direct nuclear pumping of lasers by fission fragment energy deposition in lasing gas mixtures.

(7) Optical pumping of lasers by thermal and nonequilibrium electromagnetic radiation from fissioning UF_6 gas and/or fissioning uranium plasmas.

Cavity reactor experiments have been conducted to measure critical masses in cavity reactors to obtain data for comparison with theoretical calculations at both LASL and the National Reactor Testing Station (NRTS) in Idaho Falls. Critical mass measurements have been made on both single cavity and multiple cavity configurations. In general, nucleonics calculations have corresponded to within a few percent of the experimental measurements. A review of these experiments is contained in Ref. 2. These studies provide the basis for selecting additional experiments to demonstrate the feasibility of the plasma core nuclear reactors.

A program plan for establishing the feasibility of fissioning UF_6 gas and uranium plasma reactors has been formulated by NASA and is described in Refs. 3 and 4. Briefly, the series of reactor tests consists of gaseous nuclear reactor experiments of increasing performance, culminating in an approximately 5 MW fissioning uranium plasma reactor experiment. Each reactor experiment in the series will yield basic physical data on gaseous fissioning uranium and basic engineering data required for design of the next experiment. Initial reactor experiments will consist of low-power, self-critical cavity reactor configurations employing undissociated, nonionized UF_6 fuel at near minimum temperatures required to maintain the fuel in gaseous form. Power level, operating temperatures, and pressures will be systematically increased in subsequent experiments to approximately 100 kW, 1800 K, and 20 atm, respectively. The final 5 MW reactor experiment will operate with a fissioning uranium plasma at conditions for which the injected UF_6 will be dissociated and ionized in the active reactor core.

The analytical investigations reported herein were performed to examine potentially attractive applications for gaseous nuclear reactors fueled by UF_6 and its decomposition products at operating temperatures of 2000 to 6000 K and pressures of approximately 100 to 650 atm. Emphasis was placed on predictions of performance and definition of technology required for use of this class of gaseous nuclear reactors (1) as the primary energy source for high-thrust, high-specific-impulse space propulsion applications, (2) as the energy source for highly efficient systems for generation of electricity, (3) as the source of high intensity photon flux for heating particle seeded working fluid gas for applications such as hydrogen production and MHD power extraction, and (4) in a Thorium--Uranium-233 nuclear fuel breeding cycle. Configurations to permit the coupling of the intense radiant energy

fluxes to working fluids are proposed and evaluated. Energy conversion systems using the gaseous nuclear reactor as the prime energy source were analyzed to determine system performance and thermodynamic efficiencies. Conceptual designs of the major system elements are presented which indicate the overall features of the application systems and the method of integration of the principal components with the gaseous nuclear reactor energy source.

A discussion of experimentally realized nuclear pumped lasers is given in Ref. 5.

PLASMA CORE REACTOR CONFIGURATION

Plasma core reactors with fissioning gaseous nuclear fuel could operate at significantly higher temperatures than those nominally associated with nuclear reactors having solid fuel elements. The fuel is a thermally-radiating gaseous mass which may be ionized or nonionized depending upon the application. Accordingly, the operating temperatures for the fuel are in the range of a few thousand degrees Kelvin to fifty thousand degrees Kelvin. This leads to the requirement that the radiating fuel mass be fluid-mechanically confined within a central volume of the core cavity by a buffer gas. The fuel is isolated thermally from the containment structure by a flowing stream of cooler buffer gas which is injected tangentially from the peripheral wall. For applications which employ thermal radiation emitted from the plasma, an internally-cooled transparent wall can be employed to isolate the nuclear fuel, fission fragments, and argon in a closed-circuit flow loop and permit transfer of the radiant energy from the plasma to an external working fluid. For applications which employ fission fragment induced short wavelength nonequilibrium radiation emitted from the plasma, the working fluid such as lasing gases can be either mixed with fissioning gas or injected into the peripheral buffer gas region such that there is no blockage of radiation due to the intrinsic absorption characteristics of transparent materials at short wavelengths.

Geometry of Reactor and Unit Cell

A sketch of a conceptual design of a plasma core reactor for use in generating electricity is shown in Fig. 1. The reactor consists of six unit cells which are imbedded in a beryllium oxide reflector-moderator and surrounded by a pressure vessel. Each of the six unit cells is a separate cylindrical unit consisting of a fuel region assembly and an outer working fluid assembly. A sketch of the unit cell is shown in Fig. 2. As shown in Fig. 1, the two assemblies can be withdrawn from opposite ends of the reactor configuration for periodic maintenance and inspection. The fuel assembly consists of a plasma fuel zone with nuclear fuel injected in the form of UF_6. The uranium used in the UF_6 can be either highly enriched U-235 or U-233. Gaseous nuclear fuel is confined in the central region of the fuel zone by argon buffer gas. The mixture of nuclear fuel and argon buffer gas is withdrawn from one or both endwalls at the axial centerline.

The working fluid assembly consists of a series of uncooled U-shaped fused-silica coolant tubes. The tubes have walls sufficiently thick to withstand compressive pressure loads should it be desirable to operate the working fluid at a pressure significantly lower than that in the fissioning uranium plasma region. Interstitial zones surrounding the tubes are filled with inert gas (argon or helium) at the same pressure as the plasma region. Helium working fluid passes through the fused-silica tubes and is heated by convection from high temperature graphite fins

inside the fused-silica tubes. These fins absorb thermal radiation emitted from the plasma. Helium working fluid is passed out to an energy conversion system such as a closed-cycle gas turbine electrical generator. The upper limit on helium working fluid outlet temperature imposed by an upper limit on the uncooled fused silica operating temperature would be approximately 1200 K.

An alternate unit cell configuration is shown in Fig. 3. In this configuration, the fuel and buffer gas zone is surrounded by a reflective aluminum liner with axial working fluid channels along portions of the periphery of the fuel cell surface. The reflective liner would be made of aluminum, for example, which has a reflectivity of approximately 0.9 for the spectral distribution of thermal radiation emitted from the nuclear fuel. The effect of cavity surface liner materials which are highly reflective to thermal radiation, is to reduce heating of the cavity surfaces and to concentrate the thermal radiation from the fuel onto the working fluid channels. In this alternate unit cell configuration, the working fluid is heated by being passed over graphite fins which are not surrounded by fused-silica tubes, in the axial channels. Thus, for the unit cell configuration shown in Fig. 3, the pressure in the working fluid channels must be equal to that in the fissioning uranium plasma regions. As an additional option, the graphite fins could be replaced by micron-sized particles added to the working fluid to absorb the thermal radiation from the fissioning plasma. Either concept would allow the working fluid to be heated to higher outlet temperatures than are possible when fused-silica U-tubes, which are subject to devitrification at a temperature of approximately 1200 K, are employed.

Critical Mass and Radiant Heat Transfer Calculations

Several experiments have been conducted to measure critical masses in cavity reactors to obtain data for comparison with theoretical calculations at both LASL (Refs. 6 and 7) and at the National Reactor Testing Station (NRTS) (Refs. 8 and 9) in Idaho Falls. Critical mass measurements have been made on both single cavity and multiple cavity configurations. In general, the results of nucleonic calculations have corresponded to within a few percent of the experimental measurements. By careful choice of moderator and structural materials, fuel densities can be achieved to allow plasma core reactors to be operated at pressures in the 100 to 1000 atm range. A calculation of the critical mass was performed using the one-dimensional neutron transport theory computer program, ANISN (Ref. 10), for the reactor configuration shown in Figs. 1 and 2. The volume of each region was transformed into equivalent-volume spherical zones. A twenty group neutron structure, as delineated in TABLE I, was used in the calculation for which neutron cross sections were obtained from the HRG (Ref. 11), TEMPEST-II (Ref. 12), and SOPHIST-I (Ref. 13) computer programs. A critical mass of 86.4 kg of U-235 was calculated for this configuration in which 14.4 kg of U-235 was the fuel loading in each of the six unit cells.

Nuclear fuel will be injected into the fuel region of plasma core reactors in the form of gaseous UF_6. Upon entering the plasma zone, the UF_6 will dissociate such that at high temperatures (>8000 K) the total pressure of the mixture will consist primarily of contributions from uranium atoms and ions, free fluorine atoms and ions, the corresponding electrons from ionized species, and some argon buffer gas which will mix into the plasma zone. The composition of UF_6 as a function of temperature and pressure were calculated using a UTRC computer code described in Ref. 14. The following species was included in the analyses: UF_6, UF_5, UF_4, UF_3, F, F^-, F_2, U^o, U^+, U^{+2}, U^{+3}, and electrons. Typical composition data are shown in Fig. 4 as a function of temperature for a total pressure of 1.0 atm. This total UF_6 pressure is typical of that near the edge-of-fuel region. At temperatures below approximately 4000 K, UF_6, UF_5, UF_4, UF_3, and neutral fluorine are the predominant species. At temperatures greater than 4000 K, the dominant species are U^o, U^+, U^{+2}, U^{+3}, e^-, and neutral fluorine. Further examination of the results of these calculations indicates that as the operating pressure increases, the temperature at which the UF_6 and UF_4 molecules dissociate increases. A composite plot of the variation of the ratio of fluorine to uranium and uranium fluoride species is shown as a function of temperature for several total pressures in Fig. 5(a). The abrupt increase in fluorine partial pressure with temperature occurs with the onset of the dissociation of UF_4. The variation of electron partial pressure ratio in UF_6 decomposition products is shown as a function of temperature in Fig. 5(b). Thus in a plasma core reactor fueled by UF_6 and operated at temperature levels greater than 8000 K,essentially complete dissociation of the UF_6 will occur. The total pressure will be equal to the sum of that due to the six fluorine species, the uranium species, and free electrons.

Estimates of the spectral characteristics of UF_6 and its dominant decomposition products over the range of pressure, temperature, and wavelength important to the plasma core reactor concept, were reported in Ref. 15. Results of current research on the experimental measurement of spectral emission and absorption characteristics by UF_6 and its decomposition products are reported in Ref. 16.

Radiant heat transfer calculations were performed for the unit cell configuration shown in Fig. 3. The results are presented in TABLES II and III for outward-directed radiant fluxes from the edge-of-fuel location which correspond to black-body radiating temperatures of 2000 K, 3000 K, 4000 K, and 5000 K. For each flux level, the fraction of aluminum reflective cavity surface area was varied to include ratios of working channel duct surface area to total cavity surface area of 0.0, 0.1, 0.2, 0.3, and 1.0, respectively. The reflective aluminum liner tends to trap photons in the fuel region. A portion of the reflected thermal radiation is reabsorbed by the nuclear fuel in the edge-of-fuel region which causes the local temperature to rise there.

The spectral heat flux incident on the aluminum liner was used to determine an aluminum spectrum-weighted average reflectivity which at the liner surface was 0.909. The net radiant heat flux at the edge-of-fuel location can be calculated from the outward-directed thermal heat flux at this location by

$$\mathcal{G}^{NET}_{EOF} = \mathcal{G}^{+}_{EOF}\left(1-\mathcal{R}_{EFF}\right) \tag{1}$$

from which the black-body radiating temperature corresponding to the net thermal radiant flux emitted from the fuel region can be determined. The value of $\mathcal{R}_{eff}$ is different from the spectrum-weighted average reflectivity of the aluminum liner because of geometrical factors. The diffusely reflected radiation from the liner had a cosine distribution about the inward normal. Some of the reflected radiation, therefore, does not intercept the fuel cloud but passes by the cloud and reflects off another portion of the liner. This subtended angle effect can be calculated for the case of an optically-thick cylindrical fissioning plasma surrounded by a reflecting surface by

$$\mathcal{R}_{EFF} = \mathcal{R}\left(\frac{A_L}{A_C}\right) - \sum_{n=1}^{N}\left(1-\mathcal{R}\left(\frac{A_L}{A_C}\right)\right)\left[\mathcal{R}\left(\frac{A_L}{A_C}\right)\left(1-\frac{R_F}{R_C}\right)\right]^n \tag{2}$$

where $\mathcal{R}$ is the reflectivity at the wall, A_L/A_C is the ratio of reflecting to total cavity surface area, R_F is the fuel region radius, R_C is the test cavity radius, and n+1 is the number of wall reflections. It is also assumed that the working channel duct is uniformly distributed about the cavity surface area. If $N\rightarrow\infty$, then

$$\mathcal{R}_{EFF} = \frac{\mathcal{R}\left(\frac{R_F}{R_C}\right)\left(\frac{A_L}{A_C}\right)}{1-\mathcal{R}\left(1-\frac{R_F}{R_C}\right)\left(\frac{A_L}{A_C}\right)} \tag{3}$$

The effect of fuel-to-cavity radius ratio and fraction of working channel duct area to total cavity surface area (where $A_{WCD}/A_C = 1-A_L/A_C$) on the effective reflectivity of the fuel is shown in Fig. 6 for an aluminum surface reflectivity of 0.909. The effective reflectivity is also calculated independently by the neutron transport theory program (see Ref. 10) in the flux iteration procedure when the program is modified to solve the thermal radiant heat transfer problem (see Refs. 15 and 17). The value of $\mathcal{R}_{eff}$ from Eq. (3) and that from the transport theory program calculations correspond exactly (see Refs. 15 and 18).

There is coupling between the temperature distribution calculated for the fissioning plasma region and the containment characteristics in the fuel and buffer-gas mixture. A reasonable constraint for containment is to require that from the edge-of-fuel location inward, the local density at any station be less than or equal to the density of the buffer gas at the edge-of-fuel location. With this constraint, and for constant total pressure, there exists an upper limit on the amount of uranium (which has a higher mass number) that can be confined with the fluorine and argon at a given local temperature. Calculations were performed to determine the ratios of uranium to fluorine and argon at local temperatures in the fuel region such that the total pressure is constant and the total density of uranium, fluorine, and argon is equal to or less than that of the argon at the edge-of-fuel location. The composition of fluorine, argon, and uranium as functions of temperature and pressure, including the effects of ionization at high temperatures, were taken from Refs. 19 and 20, and from the UF_6 decomposition calculations. By using UF_6 decomposition products and argon species in conjunction with the estimated spectral absorption cross sections, Rosseland mean opacities were calculated for the mixture of argon and UF_6 decomposition species in the fuel region. These opacities were used in a radiation diffusion analysis to determine the temperature distribution required to deliver a net heat flux at radial boundaries, which are located at 1.0 cm intervals from the centerline of the fuel zone, equal to the total energy release due to the fissioning of the nuclear fuel within each boundary (local argon, fluorine, and uranium densities and partial pressures were calculated using the program discussed above). The calculation procedure converges when the heat flux at the outer boundary corresponds to the net heat flux at the edge-of-fuel location and the contained uranium, based on the imposed density and total pressure constraints, equals the critical mass.

Temperature distributions were calculated for a parametric series of conditions listed in TABLE II, namely, edge-of-fuel temperatures of 2000 K, 3000 K, 4000 K, and 5000 K, and working channel duct to total cavity surface area ratios of 0.0, 0.1, 0.2, 0.3, and 1.0. The resulting temperature distributions are shown in Fig. 7 for an edge-of-fuel temperature of 4000 K. Similar temperature distributions were obtained for the other edge-of-fuel temperatures. The corresponding centerline temperatures and total cavity pressures which include the resulting UF_6 and argon decomposition product partial pressures are also given in TABLE II. The critical mass was held constant for the different operating conditions, so that the trend of the pressure increasing more rapidly than the temperature distribution increases is a measure of different degrees of UF_6 dissociation and can be seen from the results of TABLE II.

For the conditions at which the edge-of-fuel temperature is 4000 K and the working channel duct-to-cavity surface area ratio is 0.2, the calculated radial density distribution of the fuel, fluorine, and argon within the unit cell is shown in Fig. 8. A constant temperature of 500 K, equal to the aluminum liner temperature, was assumed over 90 percent of the buffer gas flow region. In the remaining 10 percent of the buffer gas flow region the temperature was assumed to decrease. This buffer gas region temperature variation and corresponding density variation was matched to the radial temperature and density distributions obtained from the radiation diffusion analysis of the fuel region.

The factors which determine the effective reflectivity for a given fuel region and reflective liner geometry were discussed previously such that a given steady-state outward-directed heat flux and the reflected component of the thermal radiation which is absorbed by the fuel cloud, are related uniquely when the fuel cloud is assumed to be a cylindrical, optically-thick radiating fuel cloud. The radiant energy which is not reabsorbed by the fuel cloud is either absorbed by the reflective liner or is incident on the working channel duct where it represents energy available for an energy extraction cycle. An expression for the fraction of outward-directed radiant energy which is absorbed by the reflective cavity liner is given by

$$\mathcal{R}_{ABS} = \frac{\left(1 - \mathcal{R}\right)\left(\frac{A_L}{A_C}\right)}{\left[1 - \mathcal{R}\left(\frac{A_L}{A_C}\right)\left(1 - \frac{R_F}{R_C}\right)\right]} \tag{4}$$

A corresponding expression for the fraction of outward-directed radiant energy incident on the working channel duct area is given by

$$\mathcal{R}_{WCD} = \frac{\left(1 - \frac{A_L}{A_C}\right)}{\left[1 - \mathcal{R}\left(\frac{A_L}{A_C}\right)\left(1 - \frac{R_F}{R_C}\right)\right]} \tag{5}$$

The expressions for $\mathcal{R}_{ABS}$ and $\mathcal{R}_{WCD}$ were obtained using the assumptions outlined in the previous discussion on the effective reflectivity, $\mathcal{R}_{EFF}$, of the fuel cloud. Results complementary to $\mathcal{R}_{EFF}$ (see Fig. 6) for the functional dependence of $\mathcal{R}_{ABS}$ and $\mathcal{R}_{WCD}$ on fuel-to-cavity radius ratio, R_F/R_C, and reflective liner to cavity surface area ratio, A_L/A_C, are given in Figs. 9 and 10, respectively, for a spectral-averaged aluminum wall reflectivity of 0.909. These results were then used to determine the corresponding radiant thermal powers associated with the liner and duct for the results of parametric calculations presented in TABLE III. Calculations

were also performed to estimate the convective removal of energy from the fuel cavity by the flowing gases as well as the energy deposited in the moderator by fission neutrons and gammas. The model used for the convective energy removal is similar to that described in Ref. 17. Using the temperature distributions calculated for each thermal heat flux condition and assuming a buffer gas cavity-residence time of 30 s and a fuel cavity-residence time of 60 s, the total convective energy removal, Q_{CONV}, was estimated and the results also shown in TABLE III. The assumed residence time values were based on results obtained in isothermal vortex containment tests. The power deposited in the moderator, Q_{MOD}, was calculated to be equal to 0.125 times the total reactor power and likewise is given in TABLE III for each configuration.

Transmission Cell Coupling of Plasma Region and Working Fluid Channel

Configurations for plasma core reactors which thus far have been discussed are such that the absorbing medium for the thermal radiant energy emitted from the fuel region is coupled neutronically to the reactor. This means that care must be taken to ensure the radiant energy absorbing media which are used in working fluid channels are not significant neutron absorbers. The neutronic coupling can occur when the working fluid channel is adjacent to the nuclear fuel cavity and is part of the fuel cavity peripheral wall. Applications for plasma core reactors are under consideration for which it is more advantageous to locate the working fluid channels at positions other than those adjacent to the fuel cavity, so that the neutron absorbing characteristics of material in the working fluid channels will be unimportant. To accomplish this, a means must be provided so that thermal radiant energy fluxes can be transmitted from the nuclear fuel cavity, through the moderator and perhaps through the pressure vessel, to the working fluid channels. A device which has been considered as the connecting structure, is the transmission cell.

A schematic of two possible plasma core reactor configurations which make use of the transmission cell is shown in Fig. 11. The configuration shown in Fig. 11(a) is an arrangement in which a transmission cell and working fluid channel are associated with each of six fuel cavities. This configuration possesses working fluid channels outside of the beryllium oxide neutron reflector-moderator and as such neutronic coupling between the fuel cavity and working fluid channel can be made insignificant. The working fluid channels are contained within the pressure vessel structure. Potential applications for this configuration are principally terrestrial. The configuration shown in Fig. 11(b) has a single centralized working fluid channel which receives thermal radiant energy from each of the surrounding six nuclear fuel cavities, and which is outside of the inner pressure vessel wall structure. This configuration has the potential for a significant amount of the total radiated energy being deposited into the working fluid such that a very high-temperature flowing gas stream can be achieved. This particular configuration can be employed

in providing a high temperature gaseous propellant stream for space propulsion applications. It appears also to have a further advantage of increased isolation capability between gaseous nuclear fuel and an effluent propellant. An additional feature is that radiant energy deposited in the reflective liner as well as neutron and gamma energy deposited in the moderator, could be extracted in a secondary cycle by flowing coolant through passages in the liner and moderator. The heated coolant could be used to provide on-board electrical power for the space vehicle.

An illustration of the manner in which the transmission cell will couple the fuel cavity to a working fluid channel is shown in Fig. 12. The transmission cell employs series of fused-silica transparent walls with intermediate regions of gaseous hydrogen and/or deuterium gas to balance pressure between the fuel cavity region and the transmission cell. The hydrogen and/or deuterium gas provide a transparent light path for the thermal radiation emitted from the plasma. Also, the gas scatters neutrons effectively and, therefore, reduces leakage of fast and thermal neutrons from the system. The transmission cell supporting structure is cylindrical in shape and the inner cylindrical wall is lined with a highly reflective material such as aluminum. The reflective liner minimizes the loss of radiant energy to the walls of the transmission cell as it is transmitted from the fuel cavity to the working fluid channel. The fused-silica walls which are components of the transmission cells are not completely transparent to thermal radiant energy. The spectral variation of the ratio of emitted radiation in the wavelength range from a given λ to $\lambda = \infty$, to the total emitted radiation from $\lambda = 0$ to $\lambda = \infty$ corresponding to a black-body radiating temperature of 4000 K is presented in Fig. 13. The spectral variation of the absorption coefficient for fused silica and the spectral variation of aluminum reflectivity is also shown in Fig. 13. It is apparent (see Fig. 13) that approximately 14 percent of the radiant energy is in the infrared portion of the spectrum (i.e., at wavelengths greater than 2 μm) and can potentially be absorbed by fused silica.

The absorption of radiant energy in the fused silica between wavelengths of 0.2 μm and 10 μm was calculated by

$$Q_{s_i o_2} = \sum^{i} \phi(\lambda)\Delta\lambda_i \left(1 - e^{-a_{\lambda_i}\Delta X}\right) A \qquad (6)$$

where $\phi(\lambda)$ is the spectral heat flux, $\Delta\lambda$ is the wavelength group width, a_λ is the absorption coefficient, ΔX is the effective thickness of the fused-silica wall, and "i" is the wavelength group index. The variation of both thermal radiation energy absorption, and neutron and gamma energy absorption with fused-silica wall thickness is shown in Fig. 14 in terms of energy flux removal. Thermal radiation absorption by fused silica for an incident thermal flux corresponding to a black-body radiating temperature of 4000 K is seen from Fig. 14 to approach a value of approximately 0.2 kW/cm^2. The energy absorption results in development of a temperature

gradient across the fused-silica wall. The upper limit on temperature gradient can be prescribed by limiting the thermal stresses developed within the fused-silica wall as a result of the temperature gradient across the wall. When one surface of an unrestrained plate of fused silica is at a higher temperature than the other, the expansion of the higher temperature surface results in a bending moment. If the plate is restrained to prevent bending, internal stresses develop which are compressive on the high temperature surface and tensile on the low temperature surface. The maximum resulting surface thermal stress is given by

$$\sigma_{TS} = \frac{E\alpha_T(\Delta T)}{2(1-\nu)} \tag{7}$$

where E is the modulus of elasticity, α_T is the thermal expansion coefficient, ΔT is the temperature differential, and ν is Poisson's ratio. Appropriate values for the thermal and mechanical properties of fused silica are given in the following table.

Modulus of Elasticity, E	7.17×10^{10} N/m^2
Poisson's Ratio, ν	0.16
Coefficient of Thermal Expansion, α_T	0.55×10^{-6} cm/cm·°K
Thermal Conductivity	3.3×10^{-3} g·cal/cm·s°K

The nominal tensile stress limit for fused silica is approximately 4.83×10^7 N/m^2. Using the thermal and mechanical properties of fused silica, and a strain point temperature of 1343 K, the maximum calculated thermal stress from Eq. (7) is 3.08×10^7 N/m^2, which is well below the tensile stress limit. For thermal stresses of 0.69×10^7 and 1.38×10^7 N/m^2, the corresponding temperature differentials are 300 and 600 K, respectively. For these temperature differentials and a fused-silica thermal conductivity as given above in the table, conductive heat fluxes were calculated for varying wall thickness. These results are shown on Fig. 14 where first-wall thicknesses of 0.1 and 0.2 cm are indicated for fused-silica wall temperature differentials of 300 and 600 K, respectively. The calculated first-wall thicknesses are based on the assumption that the entire heat load is deposited on the inner surface and subsequently conducted through the wall (i.e., no inner surface cooling). Therefore, these thicknesses should be considered as lower limits for a given heat load on the fused-silica surface. As the infrared portion of the incident energy spectrum is absorbed, successively thicker fused-silica walls may be employed.

A summary of transmission cell performance is given in TABLE IV. The results shown were calculated for an outward-directed thermal radiant energy flux corresponding to a black-body temperature of 4000 K, a cavity wall reflectivity of 0.909, and a transmission cell-to-cavity surface area fraction of 0.2. One component of transmissivity is related to the radiant energy absorbed by the fused silica and is a function of the wall thickness. This component varies from 0.941 to 0.84 for wall thicknesses of 0.25 and 3.5 cm, respectively. A second component of transmissivity is related to losses from the incident beam resulting from multiple wall reflections within the transmission cell along the path to the external working fluid channel. Based on the Monte Carlo technique developed in Ref. 21 in which the transmission of radiation from a diffuse source was calculated along a specular reflecting gray cylinder, the transmissivity of a right circular, cylindrical transmission cell with aluminum reflecting walls was calculated as a function of the cell length-to-diameter ratio. The transmissivity at the exit of the cell is shown in TABLE IV to vary from 0.56 to 0.92 as the length-to-diameter ratio is varied from 4.0 to 0.5. The total transmissivity of a transmission cell which incorporates both cylindrical reflecting walls and a series of fused-silica walls can be estimated, to a first approximation, by multiplying the two independent transmissivity components. Fresnel reflection losses must also be considered in determining the effective transmissivity of the transmission cell. These losses are responsible for the decreases in the incident radiant flux because of reflections at the interface of the fused-silica walls and the corresponding gases. For fused silica and gas interfaces with an index of refraction ratio of 1.5, the reflection loss at one surface is approximately 4 percent for a zero degree angle of incidence and approximately 9 percent for a 60 degree angle of incidence. A zero degree angle of incidence is normal to the surface of the fused silica. The transmission cell must have a minimum of two fused-silica walls and thus four potentially reflecting surfaces. However, not all of the reflected energy is lost. Some of the energy will be reflected back into the fuel region to be reabsorbed and, subsequently, re-radiated by the plasma; some will be re-reflected within the transmission cell and find its way to the working fluid channel. It is important to remember that the reflected energy is lost only when it is absorbed either by the fused silica or by the reflective liner of the transmission cell. As was previously discussed, the fused silica is a spectral absorber and, therefore, a maximum of 15 percent of the flux corresponding to a black-body radiating temperature of 4000 K can be absorbed out of the spectra by the fused silica, irregardless of the reflection history of the photons in the transmission cell.

Reflection losses occurring at the interfaces of the fused silica can also be reduced within a particular wavelength band by depositing antireflection layers of coatings on the surfaces. The coating materials must have a refractive index related to the refractive index of the two media and the thickness of the film coatings depends upon the wavelength for which maximum transmission is desired in the particular wavelength band most of the radiant energy is concentrated. The coating materials are usually metal oxide or fluoride compounds which are highly reflecting at some wavelengths and highly transparent at other wavelengths. Pure metals have the highest

absorptivity of the elements such that very little radiant energy, at the wavelengths of visible light or longer, is transmitted through metallic coatings more than a few wavelengths thick. Thin triple layer dielectric coatings consisting of MgF_2 + ZrO_2 + CeF_3 and MgF_2 + SiO_2 + CeF_3 on crown glass (see Ref. 22) have been demonstrated to reduce single surface reflectance to much less than 1 percent in the wavelength bands 400 to 850 nm matched at a wavelength of 550 nm, and 900 to 1600 nm matched at a wavelength of 1100 nm, respectively, for these coatings. The transmission is generally high for coatings which have a thickness of approximately one wavelength. This coating technique has been used in the preparation of optical elements. It may be possible to use antireflection coatings on fused silica matched to a particular incident thermal radiant energy spectra to significantly reduce the surface reflection losses. The coatings may also have high reflectivity outside the selected transmission wavelength band and as such cause the infrared portion of the incident spectra which would normally be absorbed by the uncoated fused silica, to be reflected back to the fuel region from the first fused silica surface of the transmission cell. Since the infrared contribution to the fused-silica wall heat load is greater than the neutron and gamma contribution, by one to two orders of magnitude depending on the fused-silica thickness, see Fig. 14, a significant reduction in the infrared heat load may allow thicker fused-silica walls to be used in the transmission cell. For example, reducing the infrared heat load by a factor of 10, will permit the first wall thickness to increase from 0.1 cm to approximately 0.5 cm for a maximum temperature differential of 300 K.

PLASMA CORE REACTOR APPLICATIONS

The salient feature of the plasma core reactor applications investigated is the coupling of power to working fluids by radiant heat transfer. The applications studied include high-thrust, high-specific-impulse, space propulsion systems, electric power generators using closed-cycle helium gas turbines, an MHD power conversion concept, and photochemical/thermochemical processes for the production of hydrogen. In addition, Thorium--U-233 breeder configurations of plasma core reactors were analyzed to determine possible ranges of breeding ratios and doubling times.

High-Thrust, High-Specific-Impulse Space Propulsion

Historically, research on gaseous nuclear reactors was focused on high-performance space propulsion systems. Research was conducted on two major concepts of gaseous nuclear rockets: the open-cycle, coaxial flow concept and the closed-cycle nuclear light bulb concept. Comprehensive surveys of the ranges of performance of the open-cycle and nuclear light bulb rocket engines are discussed in Refs. 23 and 24, respectively. In addition, a version of the nuclear light bulb engine with size and critical mass reduced by use of cold beryllium reflector-moderators (less than 300 K) backed by cold deuterium-compound moderator materials and by use of axial propellant channels is described in Ref. 25. TABLE V summarizes the performance characteristics of these propulsion systems.

The performance studies described below were done for closed-cycle gaseous nuclear rocket engines which employ gaseous UF_6 nuclear fuel and its decomposition products with radiating temperatures of 6000 K and lower and total pressures of a few hundred atmospheres. The resulting systems should be considered "first generation" plasma core reactor thrusters; the higher performance systems which should follow with technological improvements and growth having been thoroughly modeled and analyzed in earlier studies.

Engine performance characteristics were calculated for a derivative of the reference nuclear light bulb engine. Dimensional characteristics and component weights for this engine are given in Ref. 26. The assumptions employed to determine the performance of the engines over a range of fuel radiating temperatures from 4000 to 6000 K were as follows:

(1) Propellant exit temperature assumed to be 80 percent of fuel radiating temperature.

(2) Heat loads were assumed to be the same fraction of total power as those calculated for the reference nuclear light bulb engine in Ref. 26. Briefly, the ratio of these heat loads to total power are: neutron and

gamma heating, 0.075; nuclear and thermal radiation heating of transparent walls, 0.0004; and thermal radiation heating of cavity endwalls, 0.042. Thermal radiation and convection heat loads to propellant channel liners and convection heating of transparent walls were calculated using the analyses described in Ref. 26. Operating pressure and fuel and buffer gas heating were based on the calculations described in the preceding section.

(3) Specific impulse was reduced to 84 percent of the ideal value to allow for incomplete expansion, friction and recombination losses, nozzle transpiration coolant flow, and for the flow of tungsten seeds in the propellant to absorb thermal radiation.

(4) The total flow passing through the nozzle exit was increased by approximately 16 percent to include tungsten seed flow and transpiration coolant flow.

(5) Engine weight was determined by adding the reference nuclear light bulb moderator weight to the pressure vessel weight calculated using a weight factor given by $Z = W_{pv}/PV = 1.125$ kg/atm-m^3.

Performance characteristics for the cases considered are given in TABLE VI. For the derivative of the nuclear light bulb reference engine with radiating temperatures from 4000 to 6000 K, the performance characteristics are: engine mass 32,700 to 42,900 kg; operating pressure 540 to 900 atm; Isp 880 to 1220 s; thrust-to-weight, 0.14 to 0.47.

For comparison purposes, preliminary analyses based on the techniques described in Ref. 27 were conducted of the performance of the engines described in TABLES V and VI for missions requiring a total ΔV of approximately 12,000 m/s (i.e., low circular orbit to escape velocity, applicable to supply missions to synchronous orbit, for example). Comparisons were made in terms of Initial Mass required in Earth Orbit (IMEO) to a chemical rocket employing H_2/O_2 propellant with a specific impulse of 450 s, a weight of 1135 kg, and a thrust level of 890,000 N.

The missions comprised minimum energy Hohmann transfers from low circular earth orbit (100 nautical miles) to synchronous orbit and back using two rocket burns per transfer. Due to relatively low accelerations, gravity loss correction factors were included. The payload was assumed to be four space shuttle payloads, approximately 90,000 kg. Comparisons were made for two plasma core reactor rocket engines; a derivative of the nuclear light bulb reference engine with UF_6 fuel with an I_{sp} of 1220 s and a thrust-to-weight ratio of 0.47 (see column 3 of TABLE VI) and a small nuclear light bulb engine with an I_{sp} of 1150 s and a thrust-to-weight ratio of 0.15.

For the cases calculated, the IMEO's for the plasma core rocket engine were about 40 to 60 percent of those for the chemical system. The performance advantage increases with increased payload also. These results indicate that the plasma core reactor engine with UF_6 nuclear fuel with "first generation" performance characteristics could be a desirable system for ferrying space shuttle payloads to selected earth orbits and possibly for other operations in cis-lunar space. The benefits of performance extension by technology growth and improvements to the high-thrust, high-specific-impulse systems described by the performance ranges quoted in TABLE V from earlier work are clear.

Concepts which employ the reflective liners such as the small nuclear light bulb engines (see Ref. 25) and transmission cells described in the preceding section should be investigated to determine their adaptability and performance as hybrid systems which might serve as both intermittently operated thrusters and as space power systems. The plasma core reactor would operate as a thruster using transmission cells directed inward to heat propellant flowing through a central chamber as in the configuration shown in Fig. 11(b). In the space power mode of operation, the transmission cell could be shuttered off and the reactor operated at low temperature on pure UF_6 driving power conversion systems via a secondary fluid. Operating with pure circulating UF_6 would eliminate the need for a UF_6/argon buffer gas separation and recirculation system in the space power operating mode. In the thruster mode, the cryogenic hydrogen propellant provides an ideal fluid for a UF_6 cold trap and/or condenser for UF_6/argon buffer gas separation and recirculation (a separation-recirculation system will be described in more detail in the next section). Both the hybrid concept and other plasma core reactor rocket engine systems should be the subject of more extensive feasibility and performance investigations for earth orbit ferrying and cis-lunar missions.

Closed-Cycle Helium Gas Turbine Electrical Generators

Basic performance analyses of closed-cycle gas turbine systems which could effectively utilize the high temperature capability of plasma core reactors were performed. The closed-cycle system uses a helium-driven gas turbine coupled to an electrical generator with a nominal output of 1000 MWe. Heat from the reactor can be transferred directly to the closed-cycle helium working fluid or can be transmitted across a secondary heat exchanger. The cycle under consideration would employ a multistage turbine connected to compressor spools. The working fluid leaving the main turbine would enter a second multistage turbine directly connected to the electric generator. Several heat exchangers would be incorporated in the system (i.e., a regenerator, precooler, intercooler) to increase the system performance. A schematic diagram of the closed-cycle gas turbine system is shown in Fig. 15. Additional power generation is also possible by utilizing some of the heat from the

working fluid at the regenerator and intercooler exhaust temperatures to operate supplementary steam or organic working fluid power systems to increase the system overall efficiency. These additional systems were not investigated in this study.

The reactor configuration for electrical power generation was described in the preceding section entitled PLASMA CORE REACTOR CONFIGURATION. Sketches of the configuration and unit cells for power extraction are shown in Figs. 1, 2, and 3. The mechanisms for extracting heat from the reactor can be either the system employing fused-silica tubes with graphite fins within the tubes to absorb thermal radiation (Fig. 2) or the system with axial working fluid channels in which graphite fins absorb the thermal radiation without surrounding them with fused silica. The fused-silica tubes permit a pressure differential between the operating pressure of the reactor and the operating pressure of the helium gas turbine loop. For example, fused-silica tubes under a compressive loading of 500 atm would require a ratio of OD to ID of 1.19 for a design point compressive stress of 1.38×10^8 N/m^2 (20,000 psi). Due to the temperature limitation on fused silica, the helium outlet temperature for the fused-silica tube configuration is limited to approximately 1200 K. The alternate unit cell configuration with graphite fins, as shown in Fig. 3, would operate at working fluid pressures equal to those in the reactor fuel region. The working fluid would be ducted through a secondary heat exchanger across which a pressure drop could be sustained such that the helium gas turbine system could be operated at a desired cycle pressure. Helium outlet temperatures would be limited only by material limits in other system components. The latter unit cell would use less fused silica and structure in the reactor core and would be more adaptable to breeder reactor configurations where it is necessary to minimize parasitic neutron absorbers to maintain a desirable breeding ratio.

Performance was optimized by determining the overall system efficiency, equal to electrical power output divided by the total reactor thermal power, for a range of pressure ratios across the helium compressors and for turbine inlet temperatures of 1098, 1506, and 1922 K. Efficiencies of the compressors, turbines, and regenerators were assumed to be 0.9. The generator efficiency was assumed to be 0.98. Fractional pressure drops of $\Delta P/P = 0.02$ were assumed through all heat exchangers and through the reactor core. A compressor inlet temperature of 322 K was selected to permit use of a dry cooling tower for heat rejection (selection and evaluation of specific heat rejection systems was not included in the study, however). The variation of cycle efficiency with compressor pressure ratio is shown in Fig. 16. Based on these results, a compressor pressure ratio of 1.75 was selected for cases with turbine inlet temperatures of 1089 and 1505 K and a compressor pressure ratio of 2.0 was selected for the case with a turbine inlet temperature of 1922 K. Figure 17 shows the variation in cycle efficiency with turbine inlet temperature for three operating pressures considered, 20, 51, and 153 atm. It can be seen that the overall cycle efficiency is relatively insensitive to cycle pressure over the range from 20 to 150 atm. Thus, the principal impact of pressure selection would be on equipment size and cost. Figures 15, 18, and 19 show the block diagrams of the systems under

consideration with temperatures, pressures, and flow rates, and working fluid enthalpies shown at various locations in the cycle. In all cases, the output electrical power was normalized to 1000 MWe. The range of overall cycle efficiencies for the three turbine inlet temperatures chosen vary from approximately 40 percent to approximately 60 percent.

The variation of overall cycle efficiency with turbine inlet temperature is shown in Fig. 20 with inlet temperatures noted for various blade materials and turbine blade cooling schemes. The progression of gas turbine technology in the 1980's is discussed in Ref. 28. With the use of cooled molybdenum alloy (TZM) blades and vanes, operation with turbine inlet temperatures of about 1900 K might be feasible by the mid 1980's. The cross-hatched region on the plot to working fluid temperatures of the order of 2500 K is indicated with an MHD label. The description of possible concepts which could be used for MHD systems is given in the following subsection.

Argon buffer gas is used to separate the hot fissioning nuclear fuel from the cooler unit cell peripheral walls in the UF_6 fueled gaseous nuclear reactor concepts shown in Figs. 1 and 2. A system for separation and recirculation of the argon and UF_6 which exits the unit cell as a mixture is required for long-term steady-state operation. A schematic diagram of an argon/UF_6 separation and recirculation system is shown in Fig. 21. The diagram indicates temperatures and flow rates per unit cell throughout the separation-recirculation system.

The argon and UF_6 mixture which exits from the unit cell is cooled to 500 K by argon bypass flow (with some UF_6 carryover) to prevent corrosion of the exhaust port materials. The cooled mixture enters a condenser in which all but a mole fraction of ~ 0.004 (2 atm partial pressure out of 500 atm total pressure) of the UF_6 is condensed and removed in liquid form. About 90 percent of the flow is diverted as the bypass flow. The remaining flow enters an additional cold trap/condenser in which the UF_6 concentration is further reduced to a mole fraction of ~ 0.0002 (0.1 atm partial pressure). The mixture then passes through a chemical separation system to reduce the remaining UF_6 concentration to trace levels. The argon and UF_6 are then recirculated to the unit cell as shown. The argon injected as buffer gas into the unit cell requires thorough cleaning to prevent injection of fissile uranium near the reflective and transparent wall materials. Fission events occurring very near these materials could result in a fission fragment impingement and embedding which might cause gradual deterioration of the reflective and transmissive properties. The fission fragment range is only approximately 0.01 cm in argon at a pressure of 500 atm and temperature of 500 K. The presence of UF_6 in low concentrations in the bypass flow has negligible effect on materials or system performance.

Continuous chemical separation methods which have been proposed and/or operated are either solvent extraction methods using liquid absorption-distillation or adsorption-desorption methods utilizing fluidized beds of solid adsorbent such as NaF. The NaF adsorption beds also have been operated extensively as batch-type systems which can be regenerated by heating in a cyclic process. A comprehensive review of UF_6 separator processes is given in APPENDIX A of Ref. 29. Details of NaF adsorption bed performance are discussed in Refs. 30 and 31. The adsorption-desorption method utilizing NaF solid adsorbent is advantageous since it nearly completely strips the UF_6 from the inlet gas stream. Hence, NaF adsorption beds were selected for the chemical separation method shown in the block diagram in Fig. 21. The NaF desorption process can take several hours and requires relatively large amounts of adsorbent. Preliminary estimates indicate that 20 m^3 of NaF would be required to process the 22 kg/s of argon with 0.0002 mole fraction UF_6 for each unit cell. More detailed analyses of continuous separation processes and alternatives should be conducted to reduce the separator system size.

MHD Power Conversion Concepts

The high working fluid temperatures available from plasma core reactors make the use of MHD power extraction concepts attractive options for investigation . A comprehensive review of MHD power conversion systems based on gaseous nuclear reactor technology is given in Ref. 32. Plasma core reactors with fuel region radiating temperatures sufficiently high (4000 to 5000 K) to heat MHD working fluids to desired temperatures of 2000 to 2500 K have operating pressures on the order of 500 atm. Conductivity of MHD working fluid with alkali metal seeds decreases rapidly with increasing pressure ($\alpha P^{-\frac{1}{2}}$ for thermal ionization, αP^{-4} for nonequilibrium ionization). Therefore, MHD cycle performance for a given working fluid temperature tends to favor operation at a few atmospheres pressure. In the process of conceiving and evaluating configurations which might be used to couple MHD power extraction systems to plasma core reactors, two principal considerations are dominant: (1) the MHD duct operating pressure should be a few atmospheres while the reactor operating pressure is of the order of 500 atm; and, (2) space occupied by MHD duct magnets and electrodes and parasitic neutron absorptions by the MHD duct materials should be small to minimize their impact on reactor criticality. The transmission cell concepts described in the preceding section entitled PLASMA CORE REACTOR CONFIGURATION provide a means to satisfy both constraints.

The configurations shown in Fig. 11(a) and 11(b) are both adaptable for use as MHD systems. In both cases, the MHD ducts would be located outside the nuclear fuel and moderator zones and essentially neutronically isolated. As described earlier, the transmission cells with series of fused-silica tubes under compressive load would permit operation with the appropriate pressure differential between the reactor fuel region and the MHD duct. Two modes of operation would be possible. The MHD duct could be attached at the ends of the working fluid channels shown in

Figs. 11(a) and 11(b). Power would be extracted after the fluid was heated as in most MHD concepts. A second option could be to install the MHD ducts with magnets and electrodes in the working fluid channels. Power would be extracted as the working fluid was heated, resulting in a very efficient cycle since the working fluid temperature and conductivity would be approximately constant in the MHD duct. The latter constant temperature MHD power conversion system was first suggested in Ref. 33.

Preliminary investigations were made of possible MHD seeding materials. The most attractive working fluid and seeding materials identified for a plasma core reactor driven MHD system were suspensions of thermionically emitting particles of barium oxide or mixed oxides of barium, calcium, and strontium in argon gas. The main theoretical advantages of an emitter suspension over an alkali metal seeded gas are its higher conductivity at temperatures up to about 2000 K (especially at pressures of 10 atm and above) and its relatively small variation in conductivity with changes in pressure ($\alpha P^{-0.13}$). The latter property permits conceptual designs of MHD systems with operating pressures up to 50 atm with the resulting savings in component size. Discussions of theoretical and experimental investigations of the conductivities of gas borne suspensions of thermionic emitters are given in Refs. 34 and 35. Particle suspensions also tend to be broadband absorbers of radiant energy, making them ideally suited as plasma core reactor working fluids.

Related analyses of a closed-cycle nuclear MHD system using BaO solid particle suspensions described in Ref. 36 indicate that overall cycle efficiencies greater than 50 percent are theoretically possible with conventional nuclear reactors. Overall cycle analyses and identification of system components should be performed for a reference plasma core reactor driven MHD power plant to evaluate its potential as an efficient power generation system.

Photodissociation of Halogens to Produce Hydrogen

Plasma core reactors have been proposed (Ref. 3) as a high power source of radiant energy for which efficient use of high intensity photon fluxes emitted from the radiating ionized fuel cloud can be employed in thermochemical and photochemical processes in the production of hydrogen by dissociation of hydrogenous materials. A large-scale low-cost capability to produce hydrogen from water is an attractive solution in the quest for an essentially infinite energy supply. The concept of employing hydrogen as a fuel is attractive because it is nonpolluting. Hydrogen may be produced from energy sources such as nuclear reactors or solar radiation to the exclusion of production from fossil fuel sources. It also has the advantage of being an energy source which can be recycled on a much shorter time scale than the conventional energy sources of the present. However, for hydrogen to become a viable fuel, satisfying significant future energy requirements, a means of producing vast quantities in an economic process must be identified and demonstrated. It is only

under these tenets that the inherent large capital investment required for initial equipment and plant facilities will be made to accomplish the conversion to hydrogen as a primary energy source. Studies were conducted to evaluate methods for producing hydrogen using the intense photon fluxes emitted from plasma core reactors.

Past available technologies for the production of hydrogen depend on electrolysis of water or newer open-cylce processes based on fossil fuels for the starting reactant. In recent years emphasis has been placed on a number of closed-cycle, multistep, thermochemical processes for cracking water (Refs. 37 and 38). Multistep processes are required because the direct thermal decomposition of water requires temperatures in excess of 2500 K. Further, separation of the decomposition products, hydrogen and oxygen, at these temperatures is exceedingly difficult. Closed-cycle processes are attractive in that water and heat are used to produce hydrogen, oxygen, and degraded heat. Intermediate chemical species required in the process are regenerated without loss, thus only degraded heat need be rejected during the process. Similarly, processes have been devised for the photolytic decomposition of water in which sensitizers (cerric, cerrous ions, or ferric, ferrous ions) are incorporated to enable water photolysis with visible radiation. The direct photolysis of water requires radiation in the ultraviolet (UV) region at wavelengths less than 200 nm. However, few wall materials transparent to UV radiation are available for wavelengths less than about 180 nm, nor are efficient UV radiation sources readily available. In addition, the photolysis is conducted in aqueous solutions which tend to reduce product yield. In solution, the reaction products are confined to a small volume by the surrounding liquid (water) and tend to recombine before natural diffusion can cause separation of the products.

A relatively simple concept described herein for the photolytic decomposition of water in which the unique radiation emission characteristics of the plasma core reactor are utilized is shown in Fig. 22. Three successive working fluid channels are employed in the process. The first two channels provide a reaction site for the two-step closed-cycle photolytic decomposition of water and the third channel is provided to absorb the residual thermal radiation either by flowing particle laden gases or by graphite finned rods which transfer the absorbed energy to a flowing gas stream by convection. The concept utilizes radiation and the chemical properties of halogens and hydrogen halides and the unique radiation characteristics of the plasma core reactor to circumvent the problems associated with the direct thermal or photolytic decomposition of water. The key to the concept depends upon the ability of halogens to react with water to form the corresponding hydrogen halide and oxygen species.

In the concept a series of relatively low temperature thermal or photolytic reactions are used to effect decomposition of water and to permit easy separation of reaction products. Cycle-steps are depicted in the following reactions.

Reaction 1

$$Br_2(G) \overset{h\nu}{\rightleftarrows} 2Br(G)^* \tag{8}$$

$$H_2O(G) + 2Br(G) \rightleftarrows 2HBr(G) + \frac{1}{2} O_2(G)$$

Reaction 2

$$2I_2(G) \overset{h\nu}{\rightleftarrows} 4I(G) \tag{9}$$

$$2HBr(G) + 4I(G) \rightleftarrows 2HI(G) + 2IBr(G)$$

Reaction 3

$$2IBr(G) \rightleftarrows I_2(G) + Br_2(G) \tag{10}$$

Reaction 4

$$2HI(G) \rightleftarrows H_2(G) + I_2(G) \tag{11}$$

The combined overall reaction describing the process may be expressed as

$$Br_2(G) + 2I_2(G) + H_2O(G) \overset{h\nu}{\rightleftarrows} H_2(G) + Br_2(G) + 2I_2(G) + \frac{1}{2} O_2(G) \tag{12}$$

Results of composition calculations indicate that molecular bromine (Br_2) does not appreciably react with water. However, similar composition calculations indicate that atomic bromine (Br) and water react to yield hydrogen bromide (HBr) and oxygen (O_2) as the principal products. The results of these calculations, shown

*(G) signifies a gaseous material.

in Fig. 23, indicate that a means of dissociating the molecular bromine into the atomic species must be provided. Thermal dissociation of the halogens occurs to an appreciable degree (> 50 percent) only at temperatures greater than 1500 K as shown in Fig. 24. The spectral ranges over which halogens and halide gases used in the process steps exhibit strong absorption are shown in Fig. 25. Also shown is the fractional flux spectral distribution for a 4000 K black-body. In the concept, the radiant flux is used to induce photodissociation of the bromine and iodine molecular species and thermal dissociation is used for the hydrogen iodide and iodine monobromide species. The feasibility of the approach is indicated in Fig. 26 by the high dissociation fractions for these species which occur at relatively low temperature. Gaseous molecular bromine (Br_2) and water (H_2O) are allowed to react at approximately 450 K in the presence of radiation ($365 \leq \lambda \leq 535$ nm) to yield gaseous hydrogen bromide and oxygen (Reaction 1).

Gas properties listed in TABLE VII suggest possible separation methods for various reactants and products. For example, unreacted Br_2, H_2O, as well as O_2 and HBr, result from the chemical reaction of Br and H_2O. The solubility of HBr (TABLE XII) is such that large quantities are dissolved by liquid water compared to Br_2 or O_2, thus affording a simple procedure for removing Br_2 and O_2. Similarly, the boiling points for Br_2 and O_2 are greatly different; Br_2 may be condensed from the Br_2/O_2 mixture at 332 K. Similar approaches appear feasible for other reactant/product species.

Hydrogen bromide is separated by solution in a HBr-H_2O mixture up to a concentration of about 87 percent HBr to 13 percent H_2O (by weight). Since oxygen is relatively insoluble in water, separation is effected. Subsequent distillation of the concentrated HBr-H_2O mixture drives off HBr until the concentration of HBr in H_2O reaches 47 percent HBr. (HBr forms a constant boiling mixture, T = 339 K, containing 47 percent HBr.) Since HBr is not appreciably dissociated at temperatures below approximately 1500 K, HBr is allowed to react with iodine (I_2) at 456 K in the presence of radiation ($430 \leq \lambda \leq 740$ nm) to yield gaseous hydrogen iodine (HI) and iodine monobromide (IBr) (Reaction 2, some unreacted HBr is also present). Cooling the reaction mixture below the boiling point of IBr permits separation of liquid IBr from gaseous HI and HBr. Iodine (I_2) and bromine (Br_2) are regenerated from IBr at a temperature of about 700 K. The HI-HBr mixture is heated to about 700 K to thermally decompose HI to hydrogen (H_2) and I_2 (Reaction 4, hydrogen bromide is not dissociated at this temperature). Upon quenching to a temperature below 456 K, I_2 is liquefied and separated from the H_2 and HBr. Finally, the solubility of HBr in H_2O is utilized to separate H_2 from HBr.

Calculations were performed to estimate the amount of hydrogen which could be produced using plasma core reactors with thermal radiant energy fluxes corresponding to black-body radiating temperatures of 4000 K, 5000 K, and 6000 K. The reactants were assumed to flow through working fluid channels extending the entire length of the cylindrical plasma cavity. For the radiation spectra from plasma core reactors with radiating temperatures between 4000 K and 6000 K, iodine would absorb over a larger fraction of the available energy spectra than bromine, and overlaps portions of the energy spectra in which bromine also absorbs. To maximize bromine photodissociation to atomic bromine, the bromine region was positioned to intercept the incident thermal radiation first and was made of sufficient thickness to reduce the spectral flux to less than one percent of its incident value. The iodine region was located behind the bromine region in the thermal radiation path and was also of sufficient thickness to absorb all but one percent of the spectral flux in its photodissociation wavelength range. Calculated halogen temperatures, halogen partial pressures, and working channel thicknesses are given in TABLE VIII.

For plasmas with black-body radiating temperatures of 4000 K, 5000 K, and 6000 K the number of bromine moles converted to atomic bromine per MW-s of total radiated energy incident on the working fluid channels are 0.443, 0.694, and 1.148, respectively. It was assumed that no recombination of the atomic species to molecular species took place in these calculations. As can be seen from the total reaction given in Eq. (12), photodissociation of at least two moles of iodine and one mole of bromine is required to produce one mole of hydrogen. The iodine-to-bromine photodissociation ratios were 2.48, 2.11, and 1.36 for the thermal radiation spectra corresponding to black-body radiating temperatures of 4000 K, 5000 K, and 6000 K, respectively, as indicated in TABLE VIII.

The iodine-to-bromine photodissociation ratios are greater than 2.0 for black-body radiating temperatures of 4000 and 5000 K due to the combined spectral characteristics of the gases and the thermal radiation fluxes. However, at a radiating temperature of 6000 K, the spectral flux distribution shifts more into the UV with the net effect that more bromine is photodissociated and less iodine is photodissociated, as indicated by an iodine-to-bromine photodissociation ratio of 1.36. To make efficient use of the spectral flux available at a radiating temperature of 6000 K, the bromine partial pressure should be reduced from 0.5 atm to 0.15 atm so that approximately 22 percent of the thermal radiation flux in the bromine photodissociation absorption band will survive the bromine region and thus be available to increase the amount of iodine photodissociated. Average iodine and bromine absorption cross sections of 5.0×10^{-19} and 2.0×10^{-19} cm^2/molecule were assumed. This effect is indicated in TABLE VIII for a radiating temperature of 6000 K (optimized), for which the iodine-to-bromine photodissociation ratio is exactly 2.0. The number of hydrogen moles which can be produced per MW·s of total radiated energy incident on the working channels via the reactions given in Eq. (12) are then 0.443, 0.694, 0.782, and 0.89 for radiating temperatures of 4000 K, 5000 K, 6000 K, and 6000 K (optimized). The fractions of radiant energy available to induce

photodissociation of bromine and iodine are 0.25, 0.353, 0.455, and 0.438 for black-body radiating temperatures of 4000 K, 5000 K, 6000 K, and 6000 K (optimized), respectively. The fraction of radiant energy used is less for the 6000 K (optimized) case than for the 6000 K case because a portion of the bromine absorption spectrum which does not overlap the iodine absorption spectrum has a 22 percent survival flux which emerges from the bromine region because the bromine partial pressure was reduced from 0.5 atm to 0.15 atm.

Results are presented in TABLE IX showing the energy requirements associated with the reactions indicated in Eqs. (8) through (11). The corresponding hydrogen production rates are specified in TABLE VIII for thermal spectral radiation corresponding to black-body radiating temperatures of 4000 K, 5000 K, and 6000 K. It is evident from the results in TABLE IX that a substantial fraction of the total energy required is devoted to the photodissociation of bromine and iodine diatomic gases into their corresponding monatomic species. For example, the 6000 K (optimized) spectrum uses (40.705 + 63.902)/148.691 or 0.705 of the required energy for the bromine and iodine photodissociation reaction. Spectroscopic measurements indicate photodissociation energies of 1.971 and 1.542 ev for bromine and iodine gases, respectively, and these are comparable with the standard chemical values for the heat of formation of -45.8 and -35.9 K-cal/mole for these gases.

The concept process also requires two other dissociation reactions; namely, HI and IBr into H_2, I_2, and Br_2 with corresponding values of heat of formation of -1.6 and -1.4 K-Cal/Mole, respectively. The dissociation of HI and IBr can be carried out thermally in a consecutive sequence of separation chambers which exhibit a high degree of dissociation at relatively low temperature as shown in Fig. 26. By considering these photodissociation and thermal dissociation reactions only, and assuming the higher heating value of water equal to 68.4 K-Cal/Mole of hydrogen consumed, a maximum thermal efficiency of 0.553 was calculated for the case where recombination and other thermal losses are neglected. The other three thermal energy requirements considered were those related to heating the initial species of H_2O (liquid), bromine (liquid), and iodine (solid) from room temperature, to the gaseous state at a temperature of 456 K and at which the gaseous constituents enter the working fluid channels where they are exposed to the incident thermal radiant flux. Thermal efficiencies were calculated for the reaction rates specified in TABLE VIII for each spectrum considered and were in the range of 0.31 to 0.41, see TABLE IX. The only spectrum optimized was that at 6000 K; however, by optimizing the 4000 K and 5000 K spectra utilization, thermal efficiencies of 0.41 might also be realized. The calculated efficiencies are based on the assumption that there is no recombination of dissociated species and that there is no recovery either of the heats of reaction for the closed-cycle process or of the energy devoted to initial heating of the constituents. Thus in an actual process, the range of thermal efficiency would be expected to be between 0.41 and 0.55 provided the spectrum utilization is optimized; i.e., an iodine-to-bromine photodissociation ratio of 2.0 is obtained.

Because of the selective manner by which the thermal radiant energy spectra are absorbed in the production of hydrogen for the photodissociation reactions of bromine and iodine, the residual energy in the spectra may be a considerable fraction of the total radiant energy available. This energy could be utilized for some other energy conversion system. The actual fraction of residual energy available depends upon the radiating temperature of the plasma and the spectral flux distribution emanating from the fuel region. For radiating temperatures between 4000 K and 6000 K, a maximum of approximately 25 and 45 percent, respectively, of the spectral flux is available for use in bromine and iodine photodissociation reactions. For a plasma core reactor operating over this range of radiating temperature, this hydrogen production concept could be used as an auxiliary cycle to a primary energy conversion system such as the closed-cycle helium gas turbine system described in a previous subsection. The advantage of this dual energy extraction possibility is that the reactor can be operated at normal power during times when demand for electric power is not high and hydrogen may be produced. The hydrogen could be stored for subsequent usage. It is also possible to operate in a mode such that hydrogen production and the helium gas turbine system operate simultaneously. Here the hydrogen produced could either be consumed in fuel cells to aid in meeting the immediate power demand or stored for subsequent use.

This hydrogen production concept which uses a plasma core reactor as the prime energy source has by no means been optimized. Continued investigations are needed to determine the operating conditions to optimize the output power in dual energy extraction systems employing plasma core reactors.

Thorium--Uranium-233 Breeder Reactor

Plasma core reactors have several features which are of benefit in terrestrial applications in addition to increased thermodynamic cycle efficiency resulting from high temperature operation. One of these features involves use of the Thorium--U-233 breeding cycle. Exploratory investigations have been performed to examine gaseous core reactors as both fast and thermal breeders, see Refs. 39 and 40. These studies were directed toward analyses of open-cycle type gaseous core reactors. The present studies were performed to estimate the operating characteristics of the plasma core reactor configuration shown in Fig. 27 operating as a thermal breeder on the thorium--U-233 cycle.

Fuel bred in a fertile blanket can be separated on-site and incorporated directly into the reactor fuel cycle flowing inventory or stored for use in other reactors. Such on-site reprocessing of the nuclear fuel would eliminate fuel element fabrication costs and avoid the necessity to transport expended fuel elements to remote locations. A thorough study of the safety of plasma core reactors has not been conducted; however, it is expected that the consequence of an accident in a

plasma core reactor would be minimal because fission products are separated and removed continuously in the on-site reprocessing facility. The high pressure, power producing core region contains relatively small amounts of radioactive materials which could potentially be released from the reactor in the event of an accident.

A sketch of the conceptual design for a breeder reactor which also could provide high temperature working fluids for closed-cycle gas turbine systems is shown in Fig. 27. In the design of a plasma core reactor as a breeder reactor, it is important to minimize parasitic neutron absorption by structural components of the reactor. In the configuration shown in Fig. 27 structural neutron poisons are minimized by employing heavy-water as the reflector-moderator material and by encasing the working fluid and fuel region zones in Zircalloy tanks. A graphite-lined, fertile thorium breeding blanket surrounds the heavy-water moderator. The complete assembly is contained within a pressure vessel. The reactor configuration consists of six 1-m-dia by 4.35-m-long cylindrical fuel cavities embedded in the heavy-water reflector-moderator. The 0.254 cm wall thickness Zircalloy tanks are sufficient to withstand the heavy-water hydrostatic pressure. The fertile thorium blanket is composed of a molten salt solution (ThF_4-BeF_2-LiF with mole fractions of 0.27, 0.02, and 0.71, respectively) similar to that employed in the molten salt breeder reactor concepts described in Ref. 41. The fissile nuclear fuel is U-233 which allows exploitation of the Th-232 and U-233 breeding cycle. The technology required for removing the U-233 produced in the molten salt fertile thorium solution is well-developed and could be employed for a plasma core breeder reactor configuration. The unit cells of the breeder configuration are similar to those in the non-breeder plasma core reactor configuration shown in Fig. 2. However, in the breeder the graphite fins might not be enclosed in fused-silica tubes due to neutron absorption in the fused silica.

Calculations of critical mass and breeding ratio were performed using the neutron transport theory computer program, ANISN (Ref. 10), for the one-dimensional model which is shown in Fig. 28 of the reactor configuration shown in Fig. 27. The volume of each region was transformed into an equivalent-volume spherical zone. Fast group neutron cross sections were calculated using the HRG code, Ref. 11. Thermal group neutron cross section were calculated using the TEMPEST-II code for average cross sections and the SOPHIST-I code for group-to-group scattering transfer probabilities (Refs. 12 and 13). The twenty neutron-group structure used in the calculations are given in TABLE I. Neutron spectrum cell-weighted cross sections were determined for each critical mass calculation and those cross sections were employed in the fuel region of the spherical model critical mass calculation. The results of critical mass calculations are given in TABLE X for several breeder reactor geometries. In the set of calculations for which the thickness of the outer heavy-water reflector-moderator zone was reduced from 107 to 12 cm while the inner heavy-water thickness was maintained at 149 cm, the critical mass increased from 22.3 to 94 kg of U-233.

The fuel pressure was calculated based on a reactor operating at approximately 2500 MW thermal with an edge-of-fuel temperature of 5000 K and a centerline fuel region temperature of approximately 30,000 K. The operating pressure in the fissioning uranium plasma region is defined by the combined partial pressures of nuclear fuel required for criticality, dissociation products (i.e., fluorine), electrons from ionized species, and some argon buffer gas present in the fuel region. In general, for plasma conditions with the temperature at the edge of the fuel region equal to or greater than 5000 K, operating pressures in the fissioning uranium plasma are on the order of 500 atm. The total nuclear fuel inventory for these configurations might be on the order of four critical masses when the fuel in the recirculation system is included in the inventory.

The breeding ratio was determined from the critical mass calculations as the ratio of the absorption rate of neutrons by Th-232 in the fertile blanket to the absorption rate of neutrons by the U-233 in the plasma fuel zone. The corresponding breeding ratio varied from 0.547 to 1.08. The effect of reducing the heavy-water reflector-moderator thickness is to increase the fraction of thermal neutrons which traverse the reflector-moderator and are then absorbed in the fertile breeding blanket. The corresponding fuel partial pressures for these reactors in which the fuel is injected in the form of UF_6 varied from 132 to 555 atm. A second set of calculations was performed for which the heavy-water moderator region interior to the six fuel cavities was reduced in thickness from 149 cm to 19 cm and the thickness of the outer heavy-water reflector-moderator was maintained at 17 cm. The removed heavy-water was replaced with additional thorium blanket solution. The purpose of adding an internal fertile blanket is to determine whether a further increase in the breeding ratio is possible and to flatten the thermal neutron flux distribution across the region containing the unit cell fuel cavities. The results of these calculations are also indicated in TABLE X.[34] For a fixed outer heavy-water thickness thorium blanket thickness is varied. This occurs because the critical mass is increasing faster than the corresponding increase in the breeding ratio as the fertile blanket thickness is increased beyond the minimum. These calculations resulted in the critical mass increasing from 73.9 to 146.7 kg of U-233 while the breeding ratio was likewise increasing from 1.055 to 1.140 and fuel pressure was increasing from 436 to 866 atm.

The doubling time for plasma core breeder reactors can be quite short since the total fuel inventories are 300 to 500 kg of U-233. The equation describing doubling time for a breeder reactor is

$$D = \frac{M}{G\, Q_{TOT}(1+\bar{\alpha})} \qquad (13)$$

where D is the doubling time in days, M is the total fuel inventory for the reactor in grams, G is the breeding gain and is equal to the breeding ratio minus one, Q_{TOT} is the operating power level in MW, and alpha is the capture to fission ratio of U-233 (≈ 0.1). Using Eq. (13), for a nominal-thermal power level of 2500 MW and capture to fission rate ratios of U-233 obtained from the neutron transport theory calculations, doubling times of approximately five years were calculated for the calculated critical masses and breeding ratios. The calculations assumed that each thorium atom converted to a U-233 could be recovered for use as nuclear fuel and as such represent maximum values of the breeding ratio. The indications are that a plasma core breeder reactor offers the opportunity to exploit the Th-232--U-233 breeding cycle with potential doubling times (≈ 5 years) much shorter than doubling times of other breeder reactor concepts (Ref. 41) which are in the range of ten to twenty years.

For the breeder reactor configurations described above, the breeding ratios given in TABLE X represent the maximum value obtained from absorption rates obtained in one-dimensional transport theory critical mass search calculations using twenty neutron groups. Detailed analysis of the breeding ratio actually achievable was performed for one case. This case was selected because it possessed a doubling time of less than five years. The reactor has a calculated critical mass of 84.4 kg of of U-233, an operating fuel partial pressure of 498 atm, and a maximum calculated breeding ratio of 1.080, assuming that all Th-232 absorptions in the fertile breeding blanket are converted to U-233 atoms. However, in an operating breeder reactor, the complete conversion and reclaimation of U-233 atoms from the Th-232 atoms which absorb neutrons is not possible and, hence, the actual achievable breeding ratio is somewhat reduced. The Th--U-233 breeding chain is shown in Fig. 29. Included in the description of the breeding chain, are the processes by which (1) uranium is reclaimed by fluoridation ($UF_4+F_2 \rightarrow UF_6$ gas) and removed from the molten fertile breeding blanket, and (2) protactinium (Pa) is removed via a chemical process.

The particular leg of the U-233 production chain which would maximize the breeding ratio is

$$Th^{232} \xrightarrow{n\gamma} Th^{233} \xrightarrow[23.5\,m]{\beta^-} Pa^{233} \xrightarrow{\lambda_{CP}} Pa^{233} \xrightarrow[27.4\,d]{\beta^-} U^{233} \xrightarrow[1.62 \times 10^5\,y]{\alpha} \qquad (14)$$

where λ_{CP} is equivalent to a decay constant describing the removal rate of Pa from the fertile breeding blanket by chemical processing. In the presence of a neutron flux field, the isotopes of Th, Pa, and U undergo transmutation to other isotopes in the chain via (n,γ) absorption reactions or by fission reactions. The only desired neutron absorption reaction is the transmutation of Th^{232} to Th^{233} via the (n,γ) reaction. All other neutron absorption reactions and fission reactions are

loss channels which diminish the breeding ratio. The isotope designations shown in Fig. 29 are as follows: (1) unprimed isotopes are those remaining in the breeding blanket; (2) primed isotopes are the Pa isotopes which have been removed from the breeding blanket by continuous chemical processing and are no longer in the high neutron flux field, as well as the U isotopes which result from the β decay of the Pa isotopes removed from the neutron flux field; and (3) the double primed isotopes are the U isotopes which have been removed from the fertile breeding blanket by a continuous fluoridation process and are no longer in the high neutron flux field. A computer program, ISOCRUNCH (Ref. 42), which solves the general differential equation describing the production and removal of an isotope in a reaction and decay scheme, has been modified and a procedure has been implemented to solve the differential equations which describe the production and removal of the isotopes as depicted in the Th--U-233 breeding cycle chain shown in Fig. 29. The procedure makes use of the twenty neutron group flux distributions from one-dimensional spherical critical mass calculations to determine corresponding fission and absorption rates for each of the unprimed isotopes, as shown in Fig. 29. The fission and absorption rates are used as input to the ISOCRUNCH computer program.

The general differential equation which describes the production and removal of an isotope in a single reaction and decay chain is

$$\frac{dN_i}{dt} = p_i N_{i-1} - r_i N_i \qquad (15)$$

In this equation, p_i is a coefficient describing the production of N_i from its parent isotope having a density N_{i-1}, and r_i is a coefficient describing the removal rate of N_i: $p_i = \bar{\lambda}_{i-1}$ (decay constant of N_{i-1}), or

$\phi\sigma_{c_{i-1}}$ (flux times the cross section of N_{i-1}),

$r_i = \bar{\lambda}_i + \phi\sigma_{c_i} + \phi\sigma_{f_i}$,

where σ_{c_i} = neutron capture cross section of N_i,

σ_{f_i} = fission cross section of N_i.

Breeding ratio results for the previously mentioned breeder reactor configuration are shown in Fig. 30 for two different continuous chemical processing and fluoridation rates. The independent chemical processing and fluoridation rates were assumed to be equal for each of the cases shown in Fig. 30. The chemical processing and fluoridation half-life for the two cases shown are 12 hours and 7 days (the half-life is defined as the time required to remove half of the desired isotope from the breeding blanket by the chemical or fluoridation processes). The calculated breeding ratios asymptotically approach 1.077 and 1.067 for the chemical processing

and fluoridation half-lives of 12 hours and 7 days, respectively. The concentration of Th-232 atoms in the breeding blanket was assumed to be constant with time for these calculations. For continuous chemical processing and fluoridation half-lives of 12 hours, the breeding ratio is greater than 1.0 after approximately twenty-six days and is greater than 1.06 after approximately seventy days. Similarly, for continuous chemical processing and fluoridation half-lives of 7 days, the breeding ratio is greater than 1.0 after 150 days and not greater than 1.06 until approximately two years. The variation in the quantity of reclaimed P_a-233 and U-233 with reactor time at full power (2500 MW thermal) is given in Figs. 31 and 32 for chemical processing and fluoridation half-life removal rates of 12 hours and 7 days, respectively. For this breeder configuration operating for a time of five years, approximately 98 percent, and 80 percent of the reclaimed U-233 is achieved by processing the P_a-233 on a 12 hour and 7 day half-life, respectively, out of the blanket and allowing it to beta decay to U-233. At a power level of 2500 MW, approximately 1040 kg of U-233 will be consumed per year. From the results of Figs. 31 and 32, an excess of P_a-233 and U-233 reclaimed over the amount of U-233 consumed is approximately 320 and 405 kg for operating times of four years and five years, respectively, with chemical processing and fluoridation half-lives of 12 hours, and 240 and 350 kg for operating times of four years and five years, respectively, at half-lives of 7 days. These calculations indicate time-averaged breeding ratios which imply doubling times of slightly greater than four years and slightly less than five years for the processing half-lives of 12 hours and 7 days, respectively, when the doubling time is the time to reclaim four critical masses or 337.6 kg of U-233.

It has been calculated that a plasma core breeder reactor operating at a thermal power level of 2500 MW with a constant breeding ratio of 1.06, will have a doubling time of approximately five years for a total fuel inventory which indicates fuel in the recirculation system equal to four times the critical mass. To achieve doubling times of approximately five years, it is necessary to have a time-averaged breeding ratio of 1.06, indicating that short chemical processing and fluoridation half-lives on the order of 12 hours to 7 days are necessary to bring the system to secular equilibrium as quickly as possible and to minimize U-233 losses from the breeding blanket due to unwanted neutron reactions.

REFERENCES

1. Anon.: Advanced Nuclear Research - Hearing Before the Subcommittee on Aeronautics and Space Technology of the Committee on Science and Astronautics U. S. House of Representatives, Ninety-third Congress, Second Session, February 7, 1974.

2. Latham, T. S., F. R. Biancardi, and R. J. Rodgers: Applications of Plasma Core Reactors to Terrestrial Energy Systems. AIAA Paper 74-1074, AIAA/SAE 10th Propulsion Conference, San Diego, CA., October 21-23, 1974.

3. Helmick, H. H., G. A. Jarvis, J. S. Kendall, and T. S. Latham: Preliminary Study of Plasma Nuclear Reactor Feasibility. Los Alamos Scientific Laboratory Report LA-5679, Prepared under NASA Contract W-13721, August 1974.

4. Thom, K., R. T. Schneider, and F. C. Schwenk: Physics and Potentials of Fissioning Plasmas for Space Power and Propulsion. International Astronautics Federation, XXVth Congress, Amsterdam, 30 September - 5 October 1974.

5. Schneider, R. T., K. Thom, and H. H. Helmick: Lasers From Fission (Gaseous Core Reactors and Nuclear Pumped Lasers for Space Power Generation and Transmission). International Astronautics Federation, XXVIth Congress, Lisbon, Portugal, September 21-27, 1975.

6. Jarvis, G. A. and C. C. Byers: Critical Mass Measurements for Various Fuel Configurations in the LASL D_2O Reflected Cavity Reactor. AIAA Paper 65-555, AIAA Propulsion Joint Specialist Conference, June 1965.

7. Bernard, W., H. H. Helmick, G. A. Jarvis, E. A. Plassmann, R. H. White: Research Program on Plasma Core Assembly. Los Alamos Scientific Laboratory Report LA-5971-MS, Prepared under NASA Contract W-13755, May 1975.

8. Kunze, J. F., J. H. Lofthouse, C. G. Cooper, and R. E. Hyland: Benchmark Gas Core Critical Experiment. Nuclear Science and Engineering, Vol. 47, January 1972, p. 59.

9. Kunze, J. F. and P. L. Chase: Critical Experiments on a Modular Cavity Reactor. Idaho Nuclear Corporation Report IN-1372, May 1970. Also issued as NASA CR-72681.

10. Engle, W. W., Jr.: A User's Manual for ANISN, A One-Dimensional Discrete Ordinates Transport Code With Anisotropic Scattering. Union Carbide Corporation Report K-1693, 1967.

REFERENCES (Continued)

11. Carter, J. L.: HRG3 - A Code for Calculating the Slowing-Down Spectrum in the P1 or B1 Approximations. Battelle-Northwest Laboratory Report BNWL-1432, June 1970.

12. Shudde, R. H. and J. Dyer: TEMPEST-II, A Neutron Thermalization Code. North American Aviation Report AMTD-111, September 1960.

13. Canfield, E. H., R. N. Stewart, R. P. Freis, and W. H. Collins: SOPHIST-I, An IBM 709/7090 Code Which Calculates Multigroup Transfer Coefficients for Gaseous Moderators. University of California, Lawrence Livermore Radiation Laboratory Report UCRL-5756, October 1961.

14. Roback, R.: Thermodynamic Properties of Coolant Fluids and Particle Seeds for Gaseous Nuclear Rockets. United Aircraft Research Laboratories Report C-910092-3, September 1964, Prepared under NASA Contract NASw-847.

15. Rodgers, R. J., T. S. Latham, and N. L. Krascella: Analyses of Low-Power and Plasma Core Cavity Reactor Experiments. United Technologies Research Center Report R75-911908-1, Prepared under Contract XP4-54459-1, May 1975.

16. Krascella, N. L.: The Spectral Properties of UF_6 and Its Thermal Decomposition Products. United Technologies Research Center Report R76-912208, Prepared under Contract NAS1-13291, Mod. 2, September 1976.

17. Rodgers, R. J., T. S. Latham, and H. E. Bauer: Analytical Studies of Nuclear Light Bulb Engine Radiant Heat Transfer and Performance Characteristics. United Aircraft Research Laboratories Report K-910900-10, Prepared under Contract SNPC-70, September 1971.

18. Latham, T. S. and R. J. Rodgers: Analytical Design and Performance Studies of Nuclear Furnace Tests of Small Nuclear Light Bulb Models. United Aircraft Research Laboratories Report L-910900-17, Prepared under Contract SNPC-70, September 1972.

19. Krascella, N. L.: Theoretical Investigation of the Spectral Opacities of Hydrogen and Nuclear Fuel. Air Force Systems Command Report RTD-TDR-63-1101, Prepared by United Aircraft Research Laboratories, November 1963.

REFERENCES (Continued)

20. Krascella, N. L.: Spectral Absorption Coefficients of Argon and Silicon and Spectral Reflectivity of Aluminum. United Aircraft Research Laboratories Report L-910904-3, Prepared under Contract SNPC-70, September 1972.

21. Corlett, R. C.: Direct Monte Carlo Calculation of Radiative Heat Transfer in Vacuum. J. of Heat Transfer, Trans. ASME, Series C, Vol. 88, 1966, p. 376.

22. Cox, J. T., G. Hass, and A. Thelen: Triple-Layer Antireflection Coatings on Glass for the Visible and Near Infrared. J. of Optical Soc. of Amer., Vol. 52, No. 9, September 1962, p. 965.

23. Ragsdale, R. G. and E. A. Willis: Gas-Core Rocket Reactors - A New Look. NASA TM X-67823, 1971.

24. Latham, T. S.: Summary of the Performance Characteristics of the Nuclear Light Bulb Engine. AIAA Paper 71-642, AIAA/SAE 7th Propulsion Joint Specialist Conference, June 1971.

25. Latham, T. S. and R. J. Rodgers: Small Nuclear Light Bulb Engines With Cold Beryllium Reflectors. AIAA Paper 72-1093, AIAA/SAE 8th Joint Propulsion Specialist Conference, November 1972.

26. Rodgers, R. J. and T. S. Latham: Analytical Design and Performance Studies of the Nuclear Light Bulb Engine. United Aircraft Research Laboratories Report L-910900-16, Prepared under Contract SNPC-70, September 1972.

27. Titus, R. R.: Evaluation of NLB for Space Missions. United Aircraft Research Laboratories Report J-170817-1, February 1971.

28. Biancardi, F. R., G. T. Peters, and A. M. Landerman: Advanced Nonthermally Polluting Gas Turbines in Utility Applications. United Aircraft Research Laboratories Report J-970978-8, March 1971. Also issued as EPA Report 6130 DNE 0371.

29. Masson, L. S.: A Study of the Feasibility of a Flowing Gas Critical Experiment in the Cavity Reactor Configuration. Idaho Nuclear Corporation Report IN-1395, April 1970. Also issued as NASA CR-72611.

REFERENCES (Continued)

30. Smiley, S. H., et al.: Quantitative Recovery of Uranium Hexafluoride From a Process Gas Stream. Industrial and Engineering Chemistry, Vol. 51, February 1959, pp. 191-196.

31. Stephenson, M. J.: A Design Model for the Dynamic Absorption of Uranium Hexafluoride on Fixed Beds of Sodium Fluoride. Union Carbide Corp., Nuclear Division, Oak Ridge Gaseous Diffusion Plant, Report K-L-6195-2, December 1968.

32. Williams J. R.: Nuclear Power From Space. Final Report Prepared Under NASA Grant NGR-11-002-181. Georgia Institute of Technology, November 1974.

33. McLafferty, G. H.: Nuclear Magnetohydroelectric Generator. U. S. Patent No. 3,140,410, July 7, 1964.

34. Sodha, M. S., C. J. Palumbo, and J. T. Daley: Enhancement of Gas Conductivity by Dust Suspensions and Its Application to Closed Cycle MHD Power Generation. Proceedings, International Symposium, MHD Electrical Power Generation, Paris, France, Vol. 2, 1964.

35. Waldie, B. and I. Fells: An Experimental Study of Gas Borne Suspensions of Thermionic Emitters as MHD Working Fluids. Phil. Trans. Royal Soc., London, England, Series A, 261, July 1967, pp 490-495.

36. Hooper, A. T., D. Newby, and A. H. Russel: Closed Cycle Nuclear MHD Studies Using Dust Suspensions. Proceedings of Symposium on Electricity from MHD. Salzburg, Austria, July 1966.

37. Chao, R. E.: Thermochemical Water Decomposition Process. Ind. Eng. Chem. Prod. Res. Develop., Vol. 13, No. 2, 1974.

38. DeBeni, G. and C. Marchetti: Mark 1, A Chemical Process to Decompose Water Using Nuclear Heat. Symposium on Nonfossil Chemical Fuels, ACS 163rd National Meeting, Boston, Mass., April 10-14, 1972.

39. Kallfelz, J. M. and J. R. Williams: Exploratory Calculations for a Gaseous Core Fast Breeder Reactor. Trans. Amer. Nuclear Soc., Vol. 13, No. 2, 1970, p. 832.

REFERENCES (Concluded)

40. Kallfelz, J. M. and J. R. Williams: Exploratory Calculations for a Gaseous Core Breeder Reactor. Second Symposium on Uranium Plasmas: Research and Applications, Atlanta, GA., November 1971.

41. Kasten, P. R., et al.: Summary of Molten-Salt Breeder Reactor Design Studies: Thorium Fuel Cycle. Proceedings of 2nd International Thorium Fuel Cycle Symposium, Gatlinburg, Tenn., May 3-6, 1966, p. 41.

42. Friend, C. W. and J. R. Knight: ISOCRUNCH - Modifications to the CRUNCH Program for the IBM 7090. Oak Ridge National Laboratory Report ORNL-3689, January 1965.

43. Herzberg, G.: Molecular Spectra and Molecular Structure. Van Nostrand Co., Inc., Princeton, New Jersey, 1957.

LIST OF SYMBOLS

A_L/A_C	Ratio of reflecting-to-total cavity surface area, dimensionless
A_{WCD}/A_C	Ratio of working channel duct-to-total cavity surface area, dimensionless
a_λ	Spectral absorption coefficient, cm^{-1}
BR	Breeding ratio, dimensionless
D	Doubling time, d
E	Modulus of elasticity, N/m^2
F_Q	Fractional radiant energy flux, dimensionless
G	Breeding gain, dimensionless
L/D	Transmission cell length-to-diameter ratio, dimensionless
M	Mass, kg
M_{CRIT}	Critical mass, kg
M_i	Mole fraction, dimensionless
N_i	Number density, $atoms/cm^3$
P	Pressure, atm
P_{e^-}/P_T	Electron partial pressure ratio, dimensionless
$P_F/(P_U+P_{UF_X})$	Fluorine to uranium bearing species pressure ratio, dimensionless
PR	Compressor pressure ratio, dimensionless
P_{TOT}	Total pressure, atm
Q/A	Surface heat flux, kW/cm^2
Q_{CONV}	Convective power removal by fuel and buffer flows, MW/Cell
$Q_{Br2}^{h\nu}$	Bromine photodissociation energy requirement, K-Cal/MW-s of incident power

LIST OF SYMBOLS (Continued)

$Q_{I2}^{h\nu}$	Iodine photodissociation energy requirement, K-Cal/MW-s of incident power
Q_{HI}	Hydrogen iodine thermodissociation energy requirement, K-Cal/MW-s of incident power
Q_{IBR}	Iodine monobromide thermodissociation energy requirement, K-Cal/MW-s of incident power
Q_{INPUT}	Total energy input requirement, K-Cal/MW-s of incident power
Q_{Br2}^{TH}	Thermal energy requirement for Bromine liquid to gas, K-Cal/MW-s of incident power
$Q_{H_2O}^{TH}$	Thermal energy requirement for H_2O liquid to gas, K-Cal/MW-s of incident power
Q_{I2}^{TH}	Thermal energy requirement for Iodine solid to gas, K-Cal/MW-s of incident power
Q_{MOD}	Power deposited in moderator, MW/Cell
Q_{RADD}	Radiated thermal power to duct, MW/Cell
Q_{RADL}	Radiated thermal power to liner, MW/Cell
Q_{SiO_2}	Total power deposited in fused-silica wall of transmission cell, MW/Cell
Q_{TOT}	Total power, MW/Cell
g_{EOF}^{NET}	Net thermal heat flux at edge-of-fuel location, MW/cm^2
g_{EOF}^{+}	Thermal heat flux directed radially outward at edge-of-fuel location, MW/cm^2
R	Radius, cm
R_{EOF}	Edge-of-fuel radius, cm
R_F/R_C	Fuel-to-cavity radius ratio, dimensionless

LIST OF SYMBOLS (Continued)

$\mathcal{R}$	Aluminum reflectivity, dimensionless
$\mathcal{R}_{ABS}$	Fraction of radiant energy absorbed by reflecting surface of cavity, dimensionless
$\mathcal{R}_{EFF}$	Fraction of radiant energy reflected to fuel, dimensionless
$\mathcal{R}_{WCD}$	Fraction of radiant energy incident on working channel duct, dimensionless
$\mathcal{R}_{\lambda}$	Spectral reflectivity, dimensionless
T	Temperature, deg K
t	Time at power, d
$(t\frac{1}{2})_{CP}$	Time required to remove half of the protactinium atoms from the breeding blanket by chemical processing, hr or d
$(t\frac{1}{2})_{F}$	Time required to remove half of the uranium atoms from the breeding blanket by fluoridation, hr or d
$(T^{*}_{BB})_{NET}$	Black-body temperature corresponding to net radiant flux at edge-of-fuel location, deg K
$(T^{*}_{BB})_{OUT}$	Black-body temperature corresponding to outward-directed radiant flux at edge-of-fuel location deg K
T_{CL}	Centerline temperature, deg K
W	Flow rate, kg/s
α	Absorption coefficient, cm^{-1}
$\overline{\alpha}$	Capture to fission ratio, dimensionless
α_{T}	Thermal expansion coefficient, cm/cm-deg K
δ	Thermal dissociation fraction, dimensionless
ΔT	Temperature differential, deg K

LIST OF SYMBOLS (Concluded)

ΔX	Fused-silica thickness, cm
η	Thermal efficiency, dimensionless
λ	Wavelength, μm or nm
λ_{cp}	Reciprocal of average residence time of protactinium atoms in breeding blanket before chemical processing removal, hr^{-1} or d^{-1}
λ_F	Reciprocal of average residence time of uranium atoms in breeding blanket before fluoridation removal, hr^{-1} or d^{-1}
$\overline{\lambda}_i$	Radioactive decay constant, s^{-1}
ν	Poisson's ratio, dimensionless
ρ	Density, g/cm^3
σ	Absorption cross section, cm^2/molecule
σ_c	Neutron capture cross section, cm^2/atom
σ_F	Neutron fission cross section, cm^2/atom
σ_{TS}	Thermal stress, n/m^2
ϕ	Neutron flux, neutrons/cm^2-s
$\phi(\lambda)$	Spectral radiant flux, MW/cm^2 -nm

TABLE I

MULTIGROUP NEUTRON ENERGY STRUCTURE USED IN CRITICAL MASS CALCULATIONS

Neutron Energy Group	Upper Energy of Group, eV
1	1.0×10^7
2	3.0×10^6
3	1.4×10^6
4	9.0×10^5
5	4.0×10^5
6	1.0×10^5
7	1.7×10^4
8	3.0×10^3
9	4.54×10^2
10	61.4
11	22.6
12	8.32
13	3.06
14	1.125
15	0.414
16	0.250
17	0.055
18	0.025
19	0.006
20	0.00175*

*Group 20 lower energy limit = 0.0 eV

TABLE II

PERFORMANCE CHARACTERISTICS FOR UF_6-FUELED GASEOUS NUCLEAR REACTORS
Cylindrical Reactor With Six Unit Cells -- See Fig. 1
Critical Mass = 86.4 kg of U-235

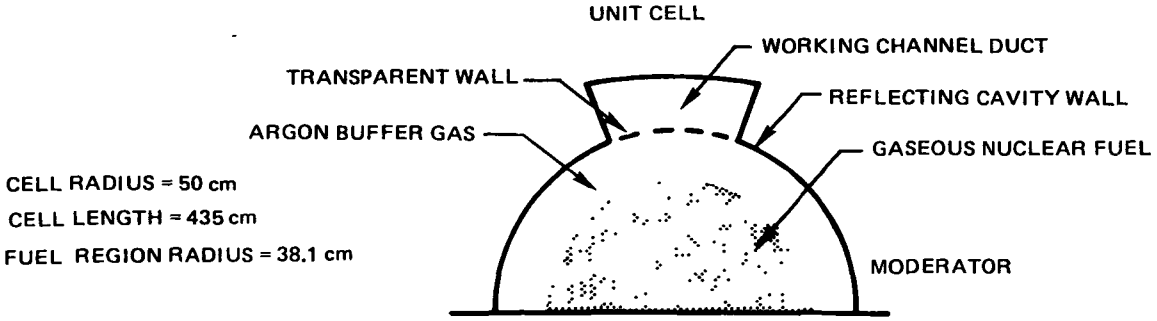

See Table III for Energy Balance

Black-Body Temperature For Outward Directed Radiant Flux, $(T^*_{BB})_{OUT}$, Deg K	Duct-To-Cavity Area Ratio, A_{WCD}/A_C, Dimensionless	Black-Body Temperature For Net Radiant Flux, $(T^*_{BB})_{NET}$, Deg K	Centerline Temperature, T_{CL}, Deg K	Cavity Pressure, P_{TOT}, Atm
2000	0.0	1170	5500	110
2000	0.1	1385	6300	95
2000	0.2	1520	6900	80
2000	0.3	1620	7300	85
2000	1.0	2000	8900	90
3000	0.0	1760	10,500	190
3000	0.1	2075	12,500	230
3000	0.2	2280	13,700	255
3000	0.3	2430	14,600	270
3000	1.0	3000	18,000	330
4000	0.0	2345	14,400	320
4000	0.1	2765	17,200	365
4000	0.2	3040	18,800	395
4000	0.3	3245	19,900	420
4000	1.0	4000	24,000	505
5000	0.0	2930	18,200	400
5000	0.1	3460	21,200	465
5000	0.2	3800	22,800	505
5000	0.3	4055	24,300	530
5000	1.0	5000	29,800	650

*Equivalent Black-Body Radiating Temperature

TABLE III

ENERGY BALANCE FOR UF_6-FUELED GASEOUS NUCLEAR REACTORS

See TABLE II For Associated Parameters

Black-Body Temperature For Outward Directed Radiant Flux, $(T^*_{BB})_{OUT}$, Deg K	Duct-To-Cavity Area Ratio, A_{WCD}/A_C, Dimensionless	Total Power, Q_{TOT}, MW/Cell	Radiated Thermal Power To Duct, Q_{RADD}, MW/Cell	Radiated Thermal Power To Liner, Q_{RADL}, MW/Cell	Power Convected by Fuel and Buffer Flows, Q_{CONV}, MW/Cell	Power Deposited in Moderator, Q_{MOD}, MW/Cell
2000	0.0	3.31	0.00	1.21	1.69	0.41
2000	0.1	4.71	1.29	1.06	1.77	0.59
2000	0.2	6.51	2.51	0.91	2.28	0.81
2000	0.3	8.21	3.66	0.78	2.74	1.03
2000	1.0	16.54	10.27	0.00	4.20	2.07
3000	0.0	13.24	0.00	6.13	5.46	1.65
3000	0.1	20.60	6.54	5.36	6.13	2.57
3000	0.2	27.29	12.72	4.63	6.53	3.41
3000	0.3	33.50	18.56	3.94	6.81	4.19
3000	1.0	68.70	52.02	0.00	8.09	8.59
4000	0.0	30.30	0.00	19.36	7.15	3.79
4000	0.1	52.28	20.67	16.93	8.15	6.53
4000	0.2	72.80	40.18	14.63	8.89	9.10
4000	0.3	92.03	58.65	12.45	9.43	11.50
4000	1.0	201.35	164.39	0.00	11.79	25.17
5000	0.0	64.30	0.00	47.26	9.00	8.04
5000	0.1	116.94	50.45	41.32	10.55	14.62
5000	0.2	166.21	98.11	35.71	11.62	20.77
5000	0.3	212.67	143.18	30.40	12.51	26.58
5000	1.0	479.28	401.35	0.00	18.02	59.91

*Equivalent Black-Body Radiating Temperature.

TABLE IV

TRANSMISSION CELL PERFORMANCE

See Fig. 12 for Configuration Details

$A_{WCD}/A_C = 0.2$
Spectral-Weighted Al Reflectivity = 0.909
$(T^*_{BB})_{OUT} = 4000$ K

Cell L/D	Cell Transmissivity Without SiO_2	Total SiO_2 Thickness, cm	Transmissivity of SiO_2
0.5	0.92	0.25	0.941
1.0	0.83	0.50	0.923
2.0	0.72	1.0	0.900
4.0	0.56	2.0	0.874
		3.5	0.850

TABLE V

PERFORMANCE CHARACTERISTICS OF GASEOUS NUCLEAR ROCKET ENGINES

Coaxial Flow, Open-Cycle Performance From Ref. 23
Nuclear Light Bulb Performance From Ref. 24
Small Nuclear Light Bulb Performance From Ref. 25

	Coaxial Flow Open Cycle	Nuclear Light Bulb	Nuclear Light Bulb Reference Engine	Small Nuclear Light Bulb
Engine Mass, kg	40,000-210,000	29,500-45,500	31,750	15,000-26,000
Operating Pressure, atm	490-2000	400-900	500	500-650
Specific Impulse, s	2500-6000	1100-2500	1870	925-1550
Thrust-to-Weight	0.05-0.20	0.3-1.6	1.3	0.14-0.29

TABLE VI

PERFORMANCE OF NUCLEAR LIGHT BULB ROCKET ENGINE
WITH URANIUM HEXAFLUORIDE FUEL

Engine Parameter	Fuel Radiating Temperature		
	4000 K	5000 K	6000 K
Operating Pressure, Atm	540	720	900
Uranium Partial Pressure, Atm	60	80	100
Power, MW	244	596	1236
Propellant Exit Temperature, Deg K	3200	4000	4800
Primary Propellant Weight Flow, kg/s	5.21	9.55	16.61
Corrected Specific Impulse, s	880	1030	1220
Thrust, N	45,000	96,500	198,800
Engine Mass, kg	32,700	37,900	42,900
Thrust-to-Weight Ratio	0.14	0.26	0.47

TABLE VII

PROPERTIES OF SPECIES EMPLOYED IN HALOGEN PHOTO-DISSOCIATION PROCESS FOR PRODUCING HYDROGEN FROM WATER

See Ref. 43 for Dissociation Data

Species	Dissociation Energy ev	nm	Melting Point Deg K (Deg C)	Boiling Point Deg K (Deg C)	Temperature Solubility at 20 C g/100 g H_2O
I_2	1.542	804	387(114)	456(183)	0.034
Br_2	1.971	629	265.7(-7.3)	331.8(58.8)	15.5
Cl_2	2.475	501	171(-102)	239.3(-33.7)	0.64
HI	3.056	406	222.2(-50.8)	237.6(-35.4)	~ 2.5
HBr	3.754	330	184.5(-88.5)	206(-67)	194
HCl	4.430	280	161(-112)	189.3(-83.7)	69.8
H_2	4.553	272	18.8(-254.2)	20.2(-252.8)	negl.
O_2	5.080	244	54.6(-218.4)	90 (-183.0)	negl.
H_2O	5.12	242	273(0)	373(100)	--

TABLE VIII

PERFORMANCE CHARACTERISTICS FOR HYDROGEN PRODUCTION VIA PHOTO-DISSOCIATED BROMINE, IODINE AND GASEOUS H_2O REACTANTS

Iodine Partial Pressure = 1.0 Atm

Thickness of Bromine Working Channel Region = 3.1 cm

Temperature of Bromine and Iodine regions = 456 K

Thickness of Iodine Working Channel Region = 0.62 cm

Incident Spectrum - Black-Body Temperature, Deg K	Bromine Photo-Dissociated, Moles / MW-s	Iodine Photo-Dissociated, Moles / MW-s	Iodine-to-Bromine Photo-Dissociation Ratio	Maximum Hydrogen Produced, Moles / MW-s	Fraction of Radiant Energy For Bromine Photo-Dissociation	Fraction of Radiant Energy For Iodine Photo-Dissociation	Bromine Partial Pressure, Atm
4000	0.443	1.098	2.48	0.443	0.085	0.165	0.5
5000	0.694	1.464	2.11	0.694	0.133	0.220	0.5
6000	1.148	1.564	1.36	0.782	0.220	0.235	0.5
6000 (optimized)	0.890	1.780	2.00	0.890	0.172	0.266	0.15

TABLE IX

ENERGY REQUIREMENTS FOR HYDROGEN PRODUCTION
VIA PHOTODISSOCIATION OF BROMINE AND IODINE PROCESSES

See Fig. 22 For Conceptual Configuration
See Table VIII For Gaseous Production Rates
1 MW·s = 238.89 K-Cal
Higher Heating Value of H_2O = 68.4 K-Cal/Mole H_2 Consumed

Energy Requirement, K-Cal/MW-s of Incident Power	Black-Body Radiating Temperature Spectrum			
	4000 K	5000 K	6000 K	6000 K (OPT)
Bromine Photodissociation Energy, $Q_{Br_2}^{h\nu}$	20.261	31.741	52.505	40.705
Iodine Photodissociation Energy, $Q_{I_2}^{h\nu}$	39.418	52.558	56.148	63.902
Hydrogen Iodide Thermo-dissociation Energy, Q_{HI}	1.435	2.249	2.534	2.884
Iodine Monobromide Thermo-dissociation Energy, Q_{IBr}	1.249	1.957	2.205	2.510
Thermal Energy Requirement (H_2O Liquid (298 K) to H_2O Gas (456 K)), $Q_{H_2O}^{TH}$	5.226	8.189	13.546	10.502
Thermal Energy Requirement (Bromine Liquid (298 K) to Bromine Gas (456 K)), $Q_{Br_2}^{TH}$	4.128	6.467	10.697	8.293
Thermal Energy Requirement (Iodine Solid (298 K) to Iodine Gas (456 K)), $Q_{I_2}^{TH}$	13.275	16.363	17.481	19.895
Total Energy Input Requirement, Q_{INPUT}	83.992	119.524	155.116	148.691
Thermal Efficiency* Based on Higher Heating Value (HHV) of H_2O, η	0.36	0.40	0.31	0.41

*NOTE: Thermal efficiency calculated as product of (HHV/Q_{INPUT}) and number of H_2 moles produced per MW·s from TABLE VIII.

TABLE X

PLASMA CORE BREEDER REACTOR CHARACTERISTICS
See Fig. 28 for Detail of Calculational Model

Outer D_2O Thickness cm	Inner D_2O Thickness cm	Critical Mass kg	Fuel Partial Pressure* Atm	Breeding Ratio	Doubling Time** yr
107	149	22.3	132	0.547	-
57	149	28.8	170	0.727	-
32	149	43.2	255	0.925	-
22	149	59.4	350	1.014	16.45
17	149	73.9	436	1.055	5.27
15	149	83.5	493	1.068	4.87
12	149	94.0	555	1.080	4.69
17	112	76.6	452	1.059	5.19
17	75	84.4	498	1.080	4.19
17	37	106.3	627	1.118	3.59
17	19	146.7	866	1.140	4.14

*Pressure includes the uranium, electron, fluorine, and fluoride constituents.
**The doubling time is for a total fuel inventory which includes an amount of fuel in the recirculation system equal to four critical masses.

PLASMA CORE REACTOR FOR ELECTRIC POWER GENERATION

NOMINAL THERMAL POWER–2500 MW

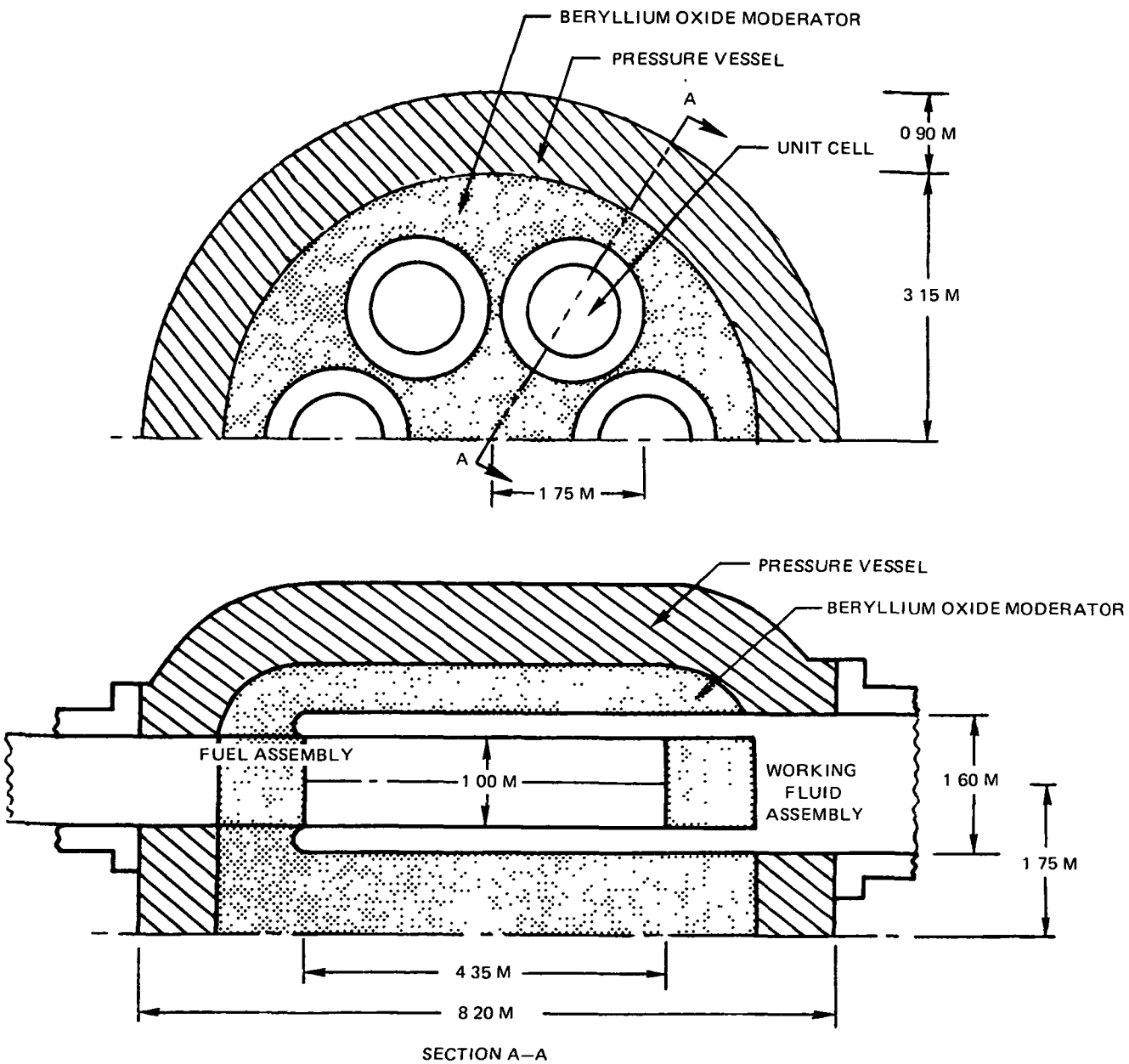

SECTION A–A

76–04–69–4

PLASMA CORE UNIT CELL CONFIGURATION FOR CLOSED CYCLE HELIUM GAS TURBINE

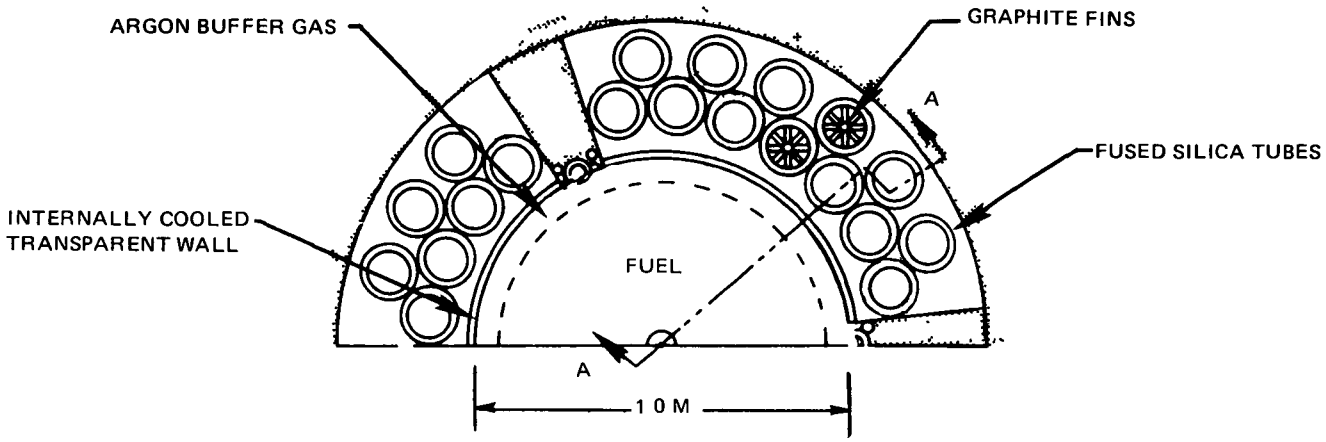

SECTION A–A

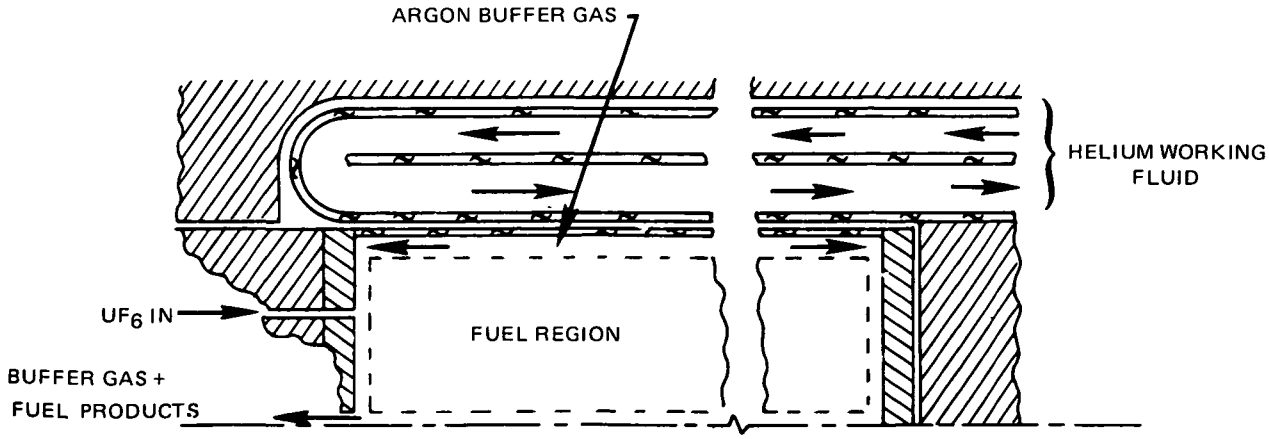

76–04–179–1

PLASMA CORE UNIT CELL CONFIGURATION FOR MHD ENERGY EXTRACTION OR HYDROGEN PRODUCTION CONCEPTS

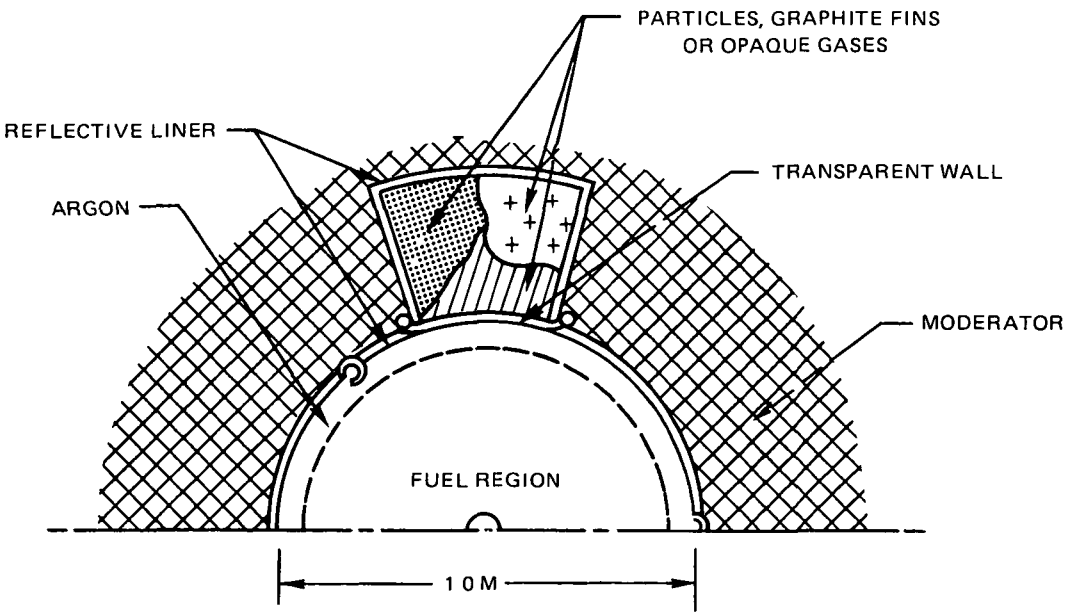

COMPOSITION OF URANIUM HEXAFLUORIDE AS A FUNCTION OF TEMPERATURE

P_{TOT} = 1 ATM

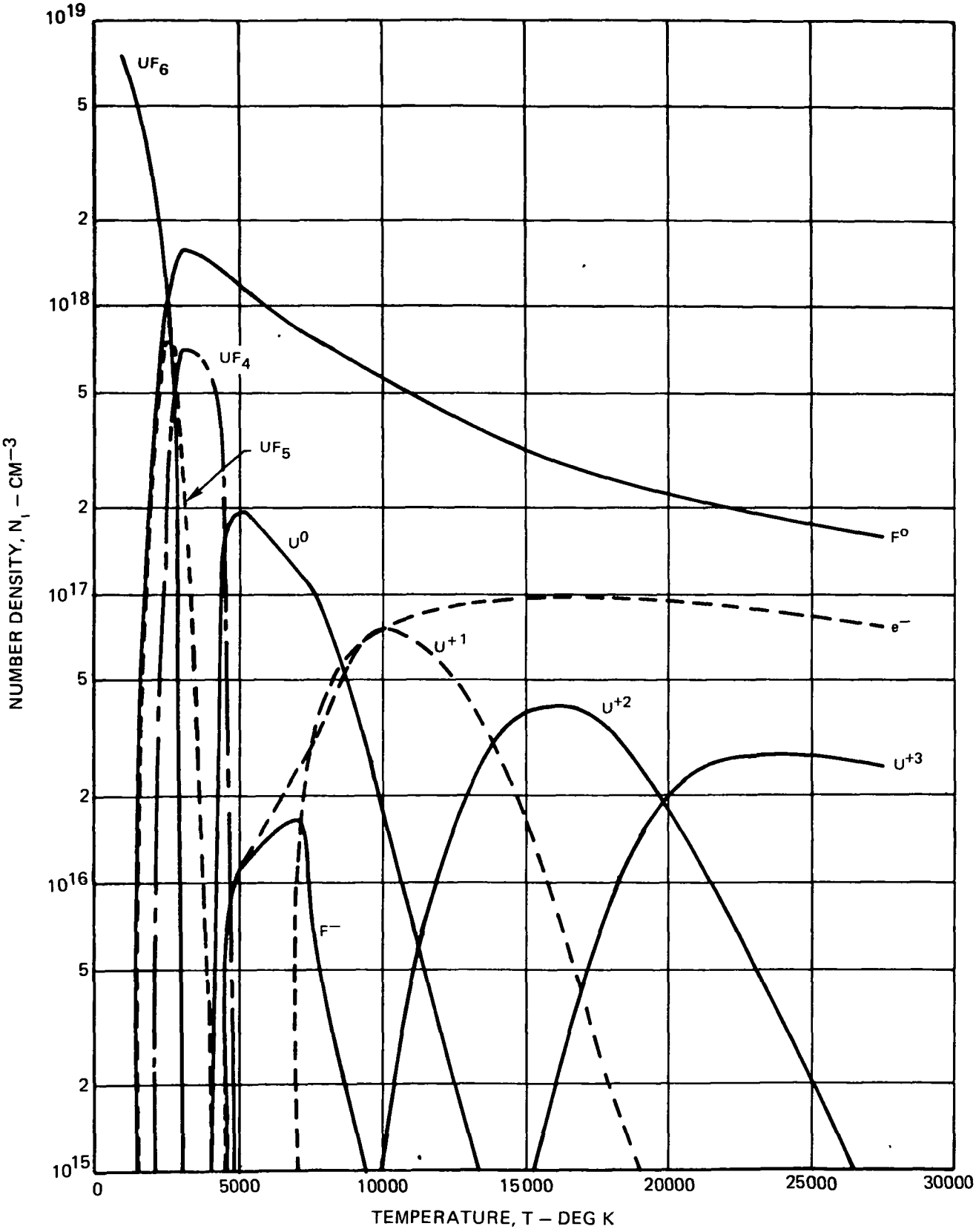

VARIATION OF RATIO OF FLUORINE TO URANIUM AND URANIUM FLUORIDE SPECIES AND VARIATION OF ELECTRON PARTIAL PRESSURE IN UF_6 DECOMPOSITION PRODUCTS

(a) RATIO OF FLUORINE TO URANIUM AND URANIUM FLUORIDE SPECIES

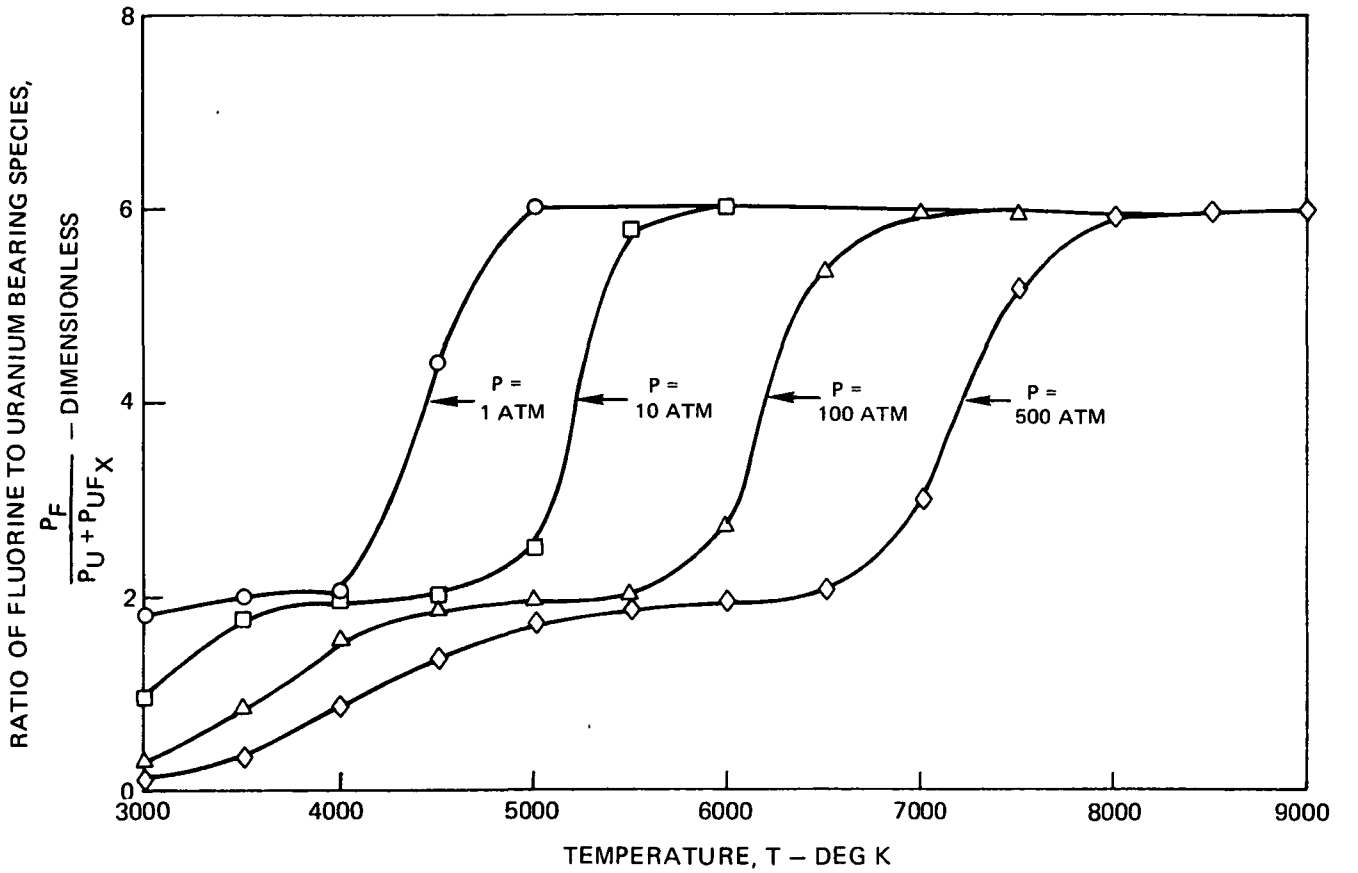

(b) ELECTRON PARTIAL PRESSURE RATIO

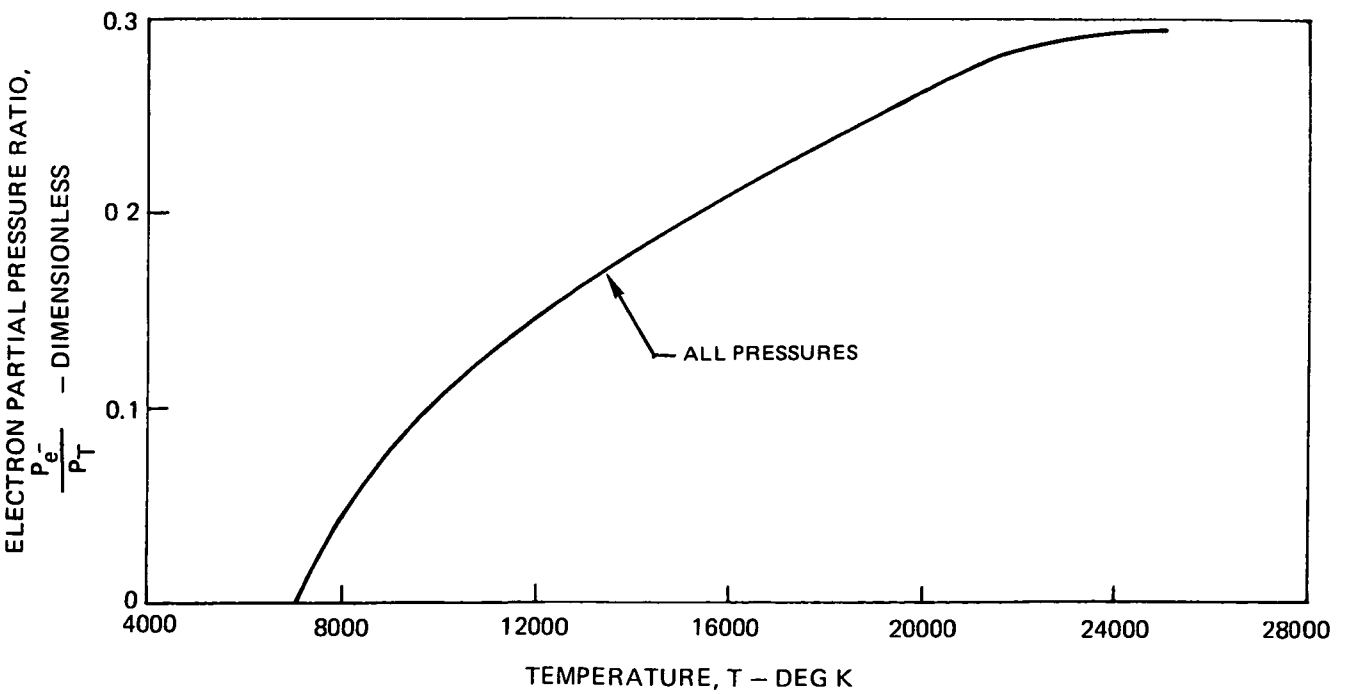

R05–128–1

FIG. 6

VARIATION OF FRACTION OF ENERGY REFLECTED TO FUEL REGION WITH REFLECTING SURFACE AREA FOR SEVERAL FUEL TO CAVITY RADIUS RATIOS

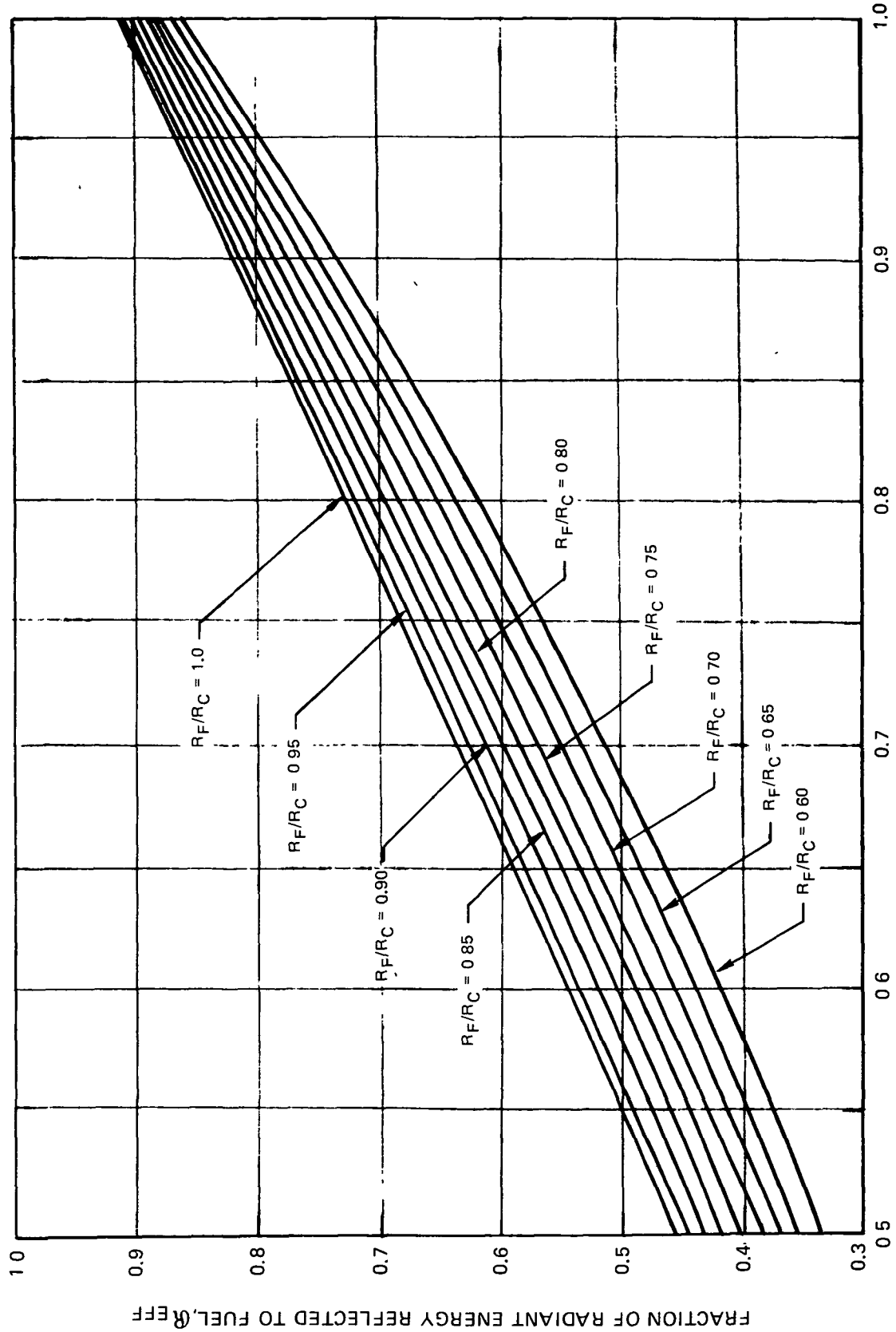

76–04–176–2

FIG. 7

CALCULATED RADIAL TEMPERATURE DISTRIBUTIONS FOR A 4000K EDGE–OF–FUEL TEMPERATURE WITH VARYING FRACTIONS OF REFLECTING CAVITY SURFACE AREA

R_{EOF} = 38.1 CM

M_{CRIT} = 86.4 Kg OF U–235 (FOR 6 UNIT CELL CONFIGURATION)

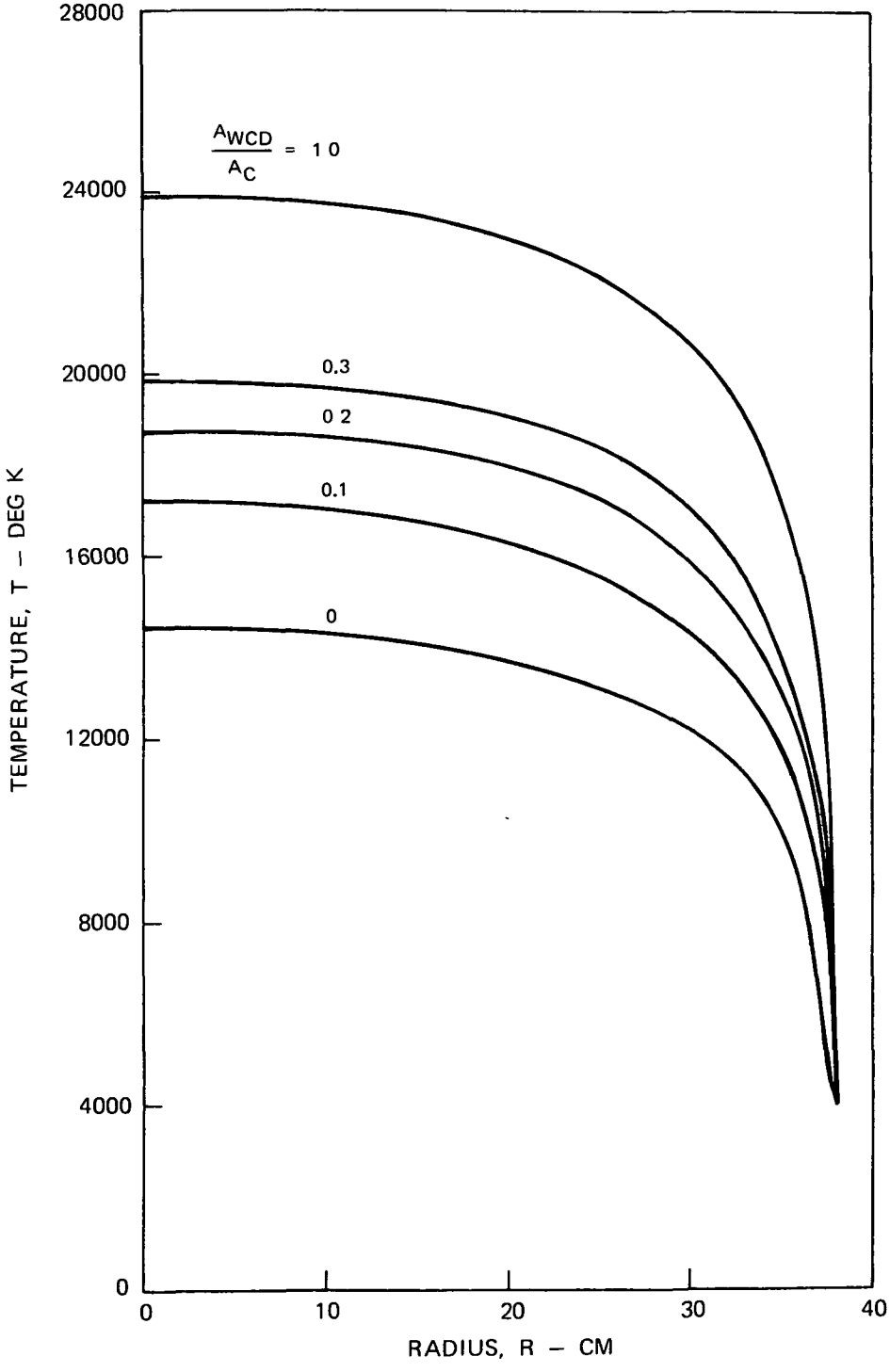

DENSITY AND TEMPERATURE DISTRIBUTIONS FOR PLASMA CORE REACTOR WITH AN EDGE–OF–FUEL TEMPERATURE EQUAL TO 4000 K

$\frac{A_{WCD}}{A_C} = 0.2$

$P_{TOT} = 395$ ATM

SEE TABLES II AND III FOR ADDITIONAL DATA

$R_{EOF} = 38.1$ CM

$(T^*_{BB})_{OUT} = 4000$ K

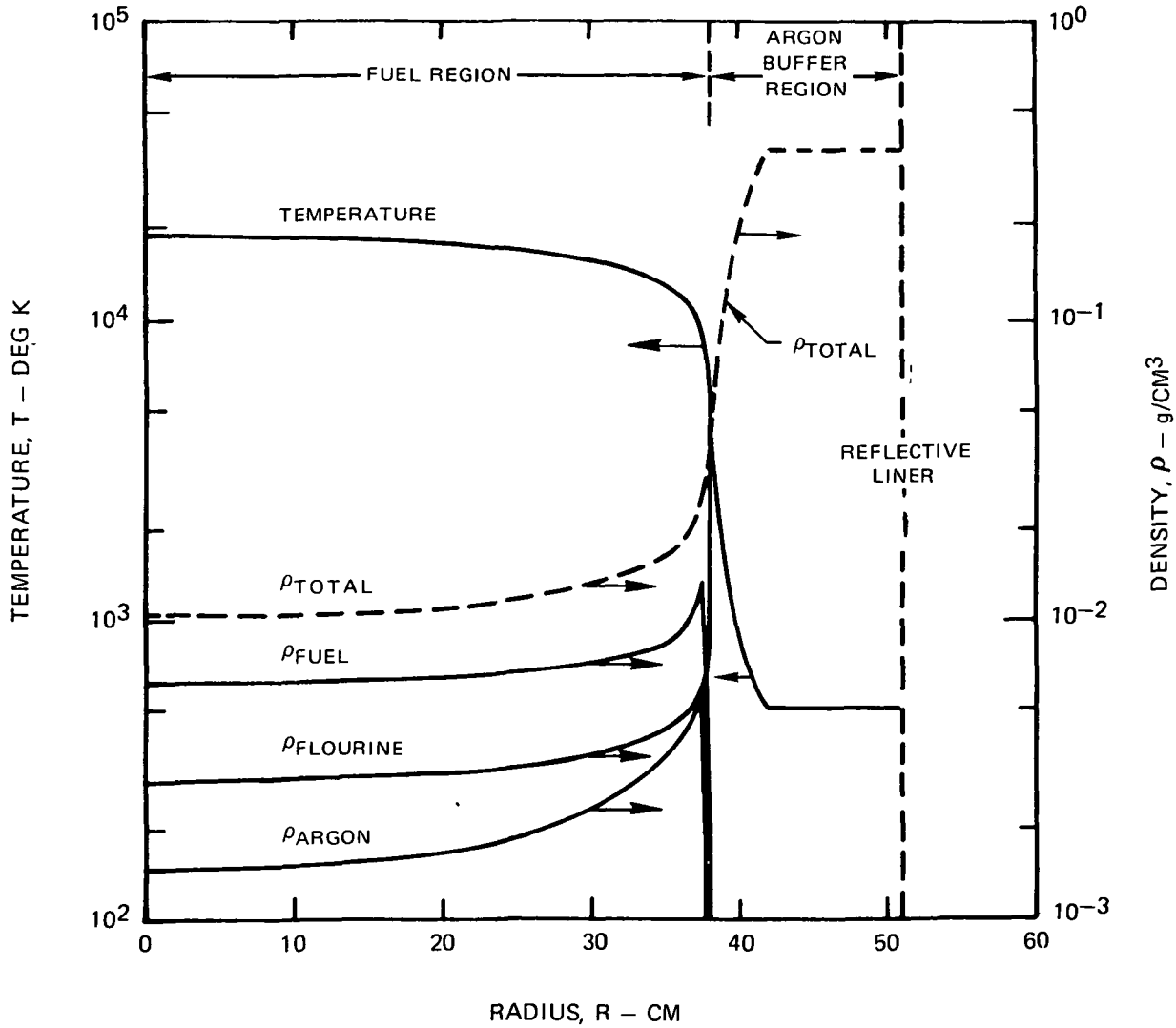

76–04–176–4

VARIATION OF FRACTION OF ENERGY ABSORBED BY REFLECTING SURFACE WITH REFLECTING SURFACE AREA RATIO FOR SEVERAL FUEL TO CAVITY RADIUS RATIOS

ALUMINUM REFLECTIVITY , $\mathcal{R}$ = 0 909

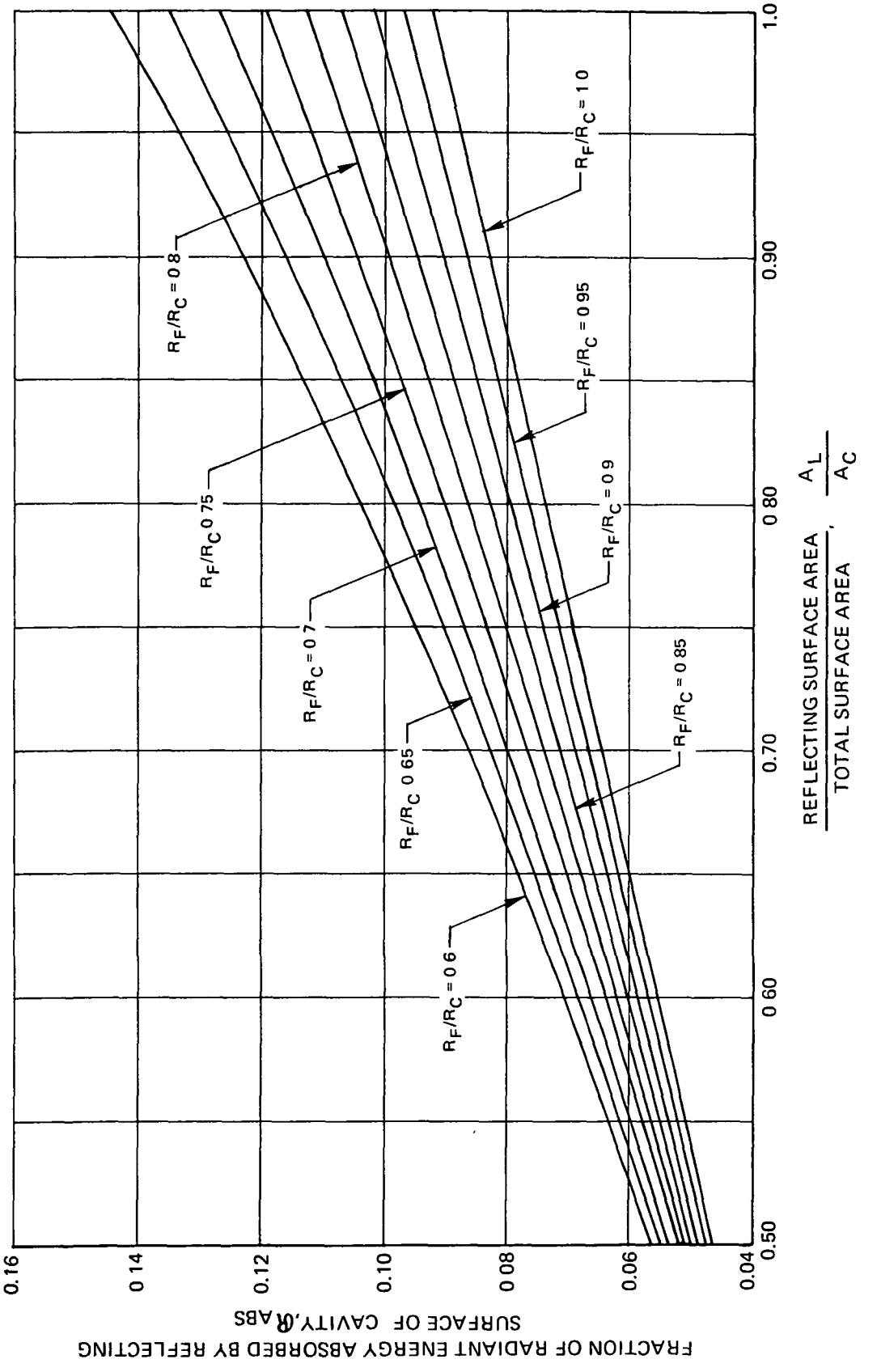

FIG.10

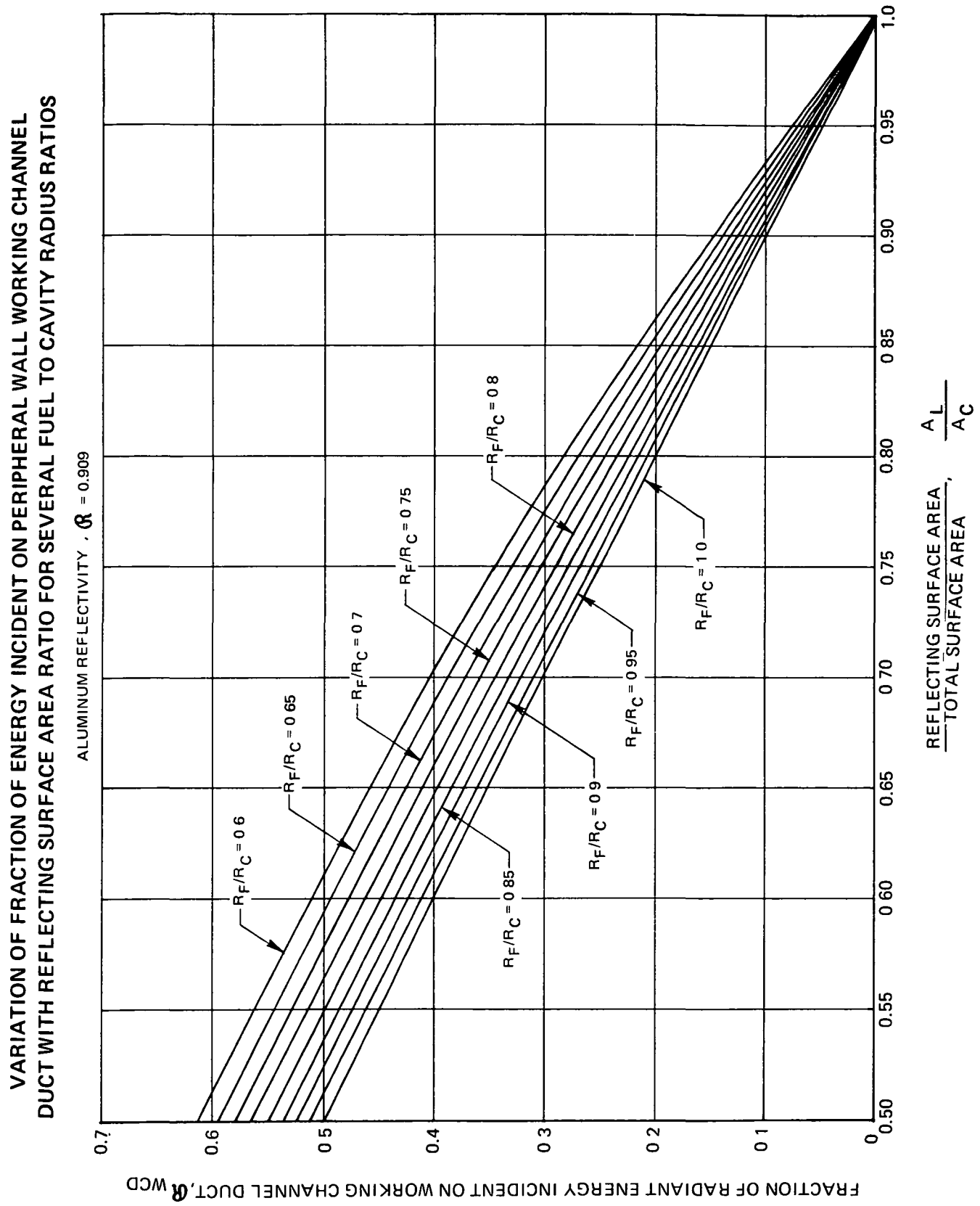
VARIATION OF FRACTION OF ENERGY INCIDENT ON PERIPHERAL WALL WORKING CHANNEL DUCT WITH REFLECTING SURFACE AREA RATIO FOR SEVERAL FUEL TO CAVITY RADIUS RATIOS
ALUMINUM REFLECTIVITY , ℜ = 0.909
FRACTION OF RADIANT ENERGY INCIDENT ON WORKING CHANNEL DUCT, α WCD
REFLECTING SURFACE AREA / TOTAL SURFACE AREA , A_L / A_C
R_F/R_C = 0 6
R_F/R_C = 0 65
R_F/R_C = 0 7
R_F/R_C = 0 75
R_F/R_C = 0 8
R_F/R_C = 0 85
R_F/R_C = 0 9
R_F/R_C = 0 95
R_F/R_C = 1 0
0.7
0.6
0 5
0.4
0 3
0 2
0 1
0
0.50
0.55
0 60
0.65
0 70
0.75
0.80
0 85
0.90
0.95
1.0

PLASMA CORE REACTOR WITH TRANSMISSION CELL CONFIGURATIONS FOR SPACE APPLICATIONS

(a.) MULTIPLE THRUST ROCKET AND/OR ELECTRIC POWER ENGINE

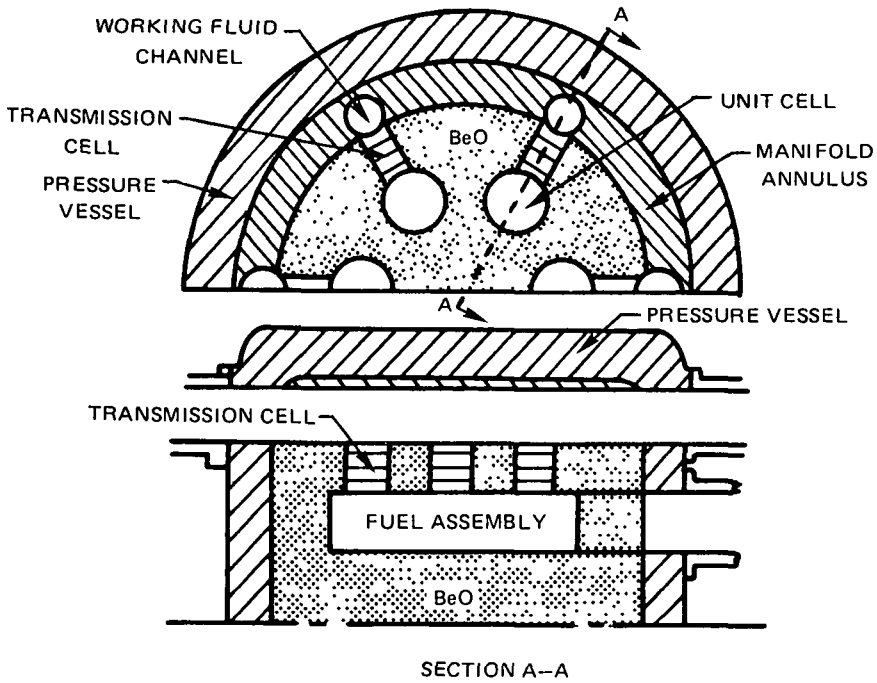

SECTION A–A

(b.) SINGLE THRUST ROCKET CONFIGURATION

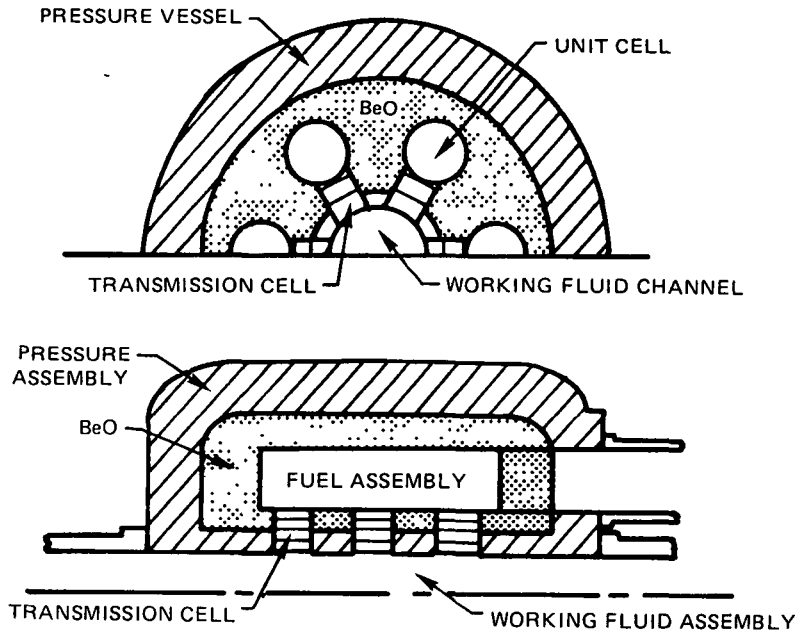

PLASMA CORE REACTOR TRANSMISSION CELL CONFIGURATION

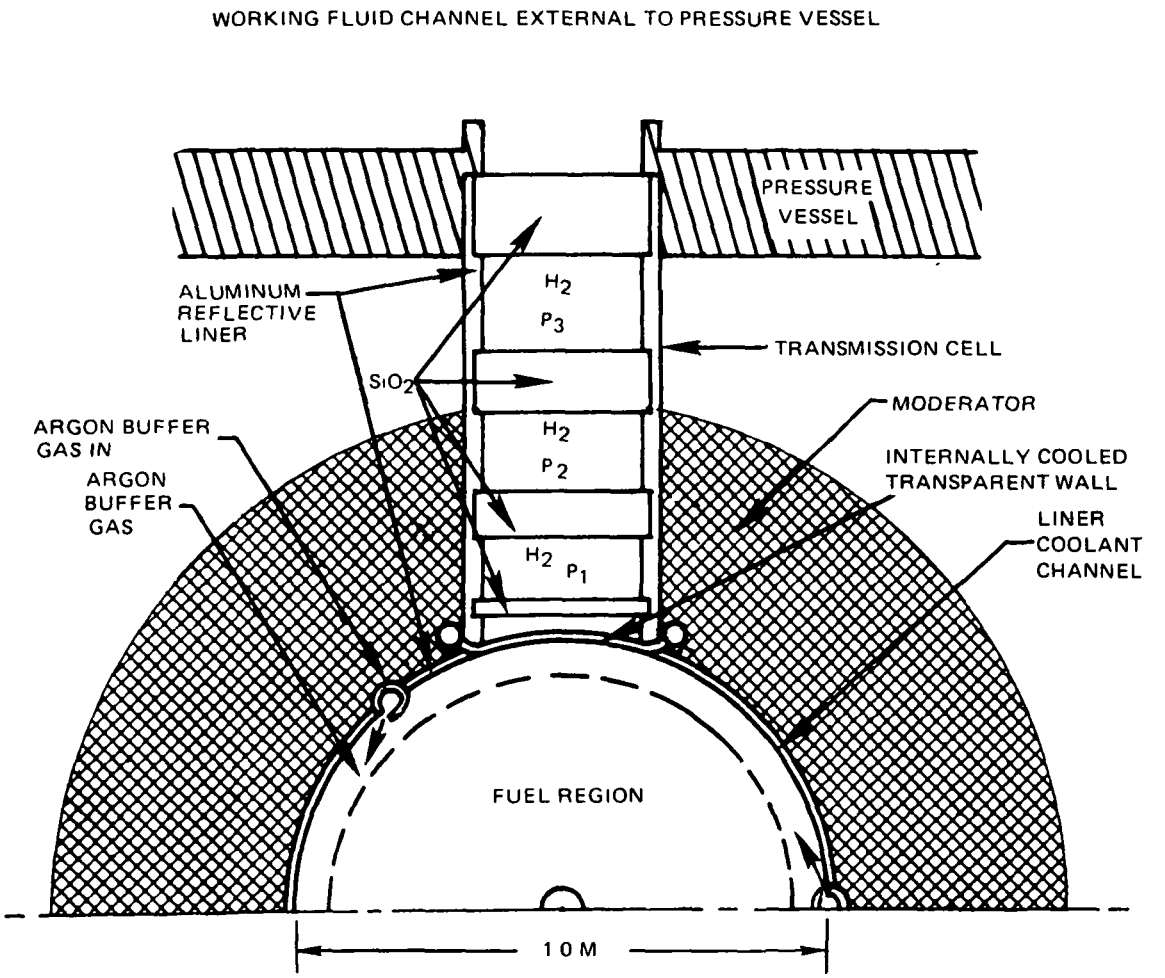

FIG. 13

SPECTRAL VARIATION OF ALUMINUM REFLECTIVITY, FUSED SILICA ABSORPTION COEFFICIENT, AND BLACK–BODY FRACTIONAL FLUX WITH WAVELENGTH

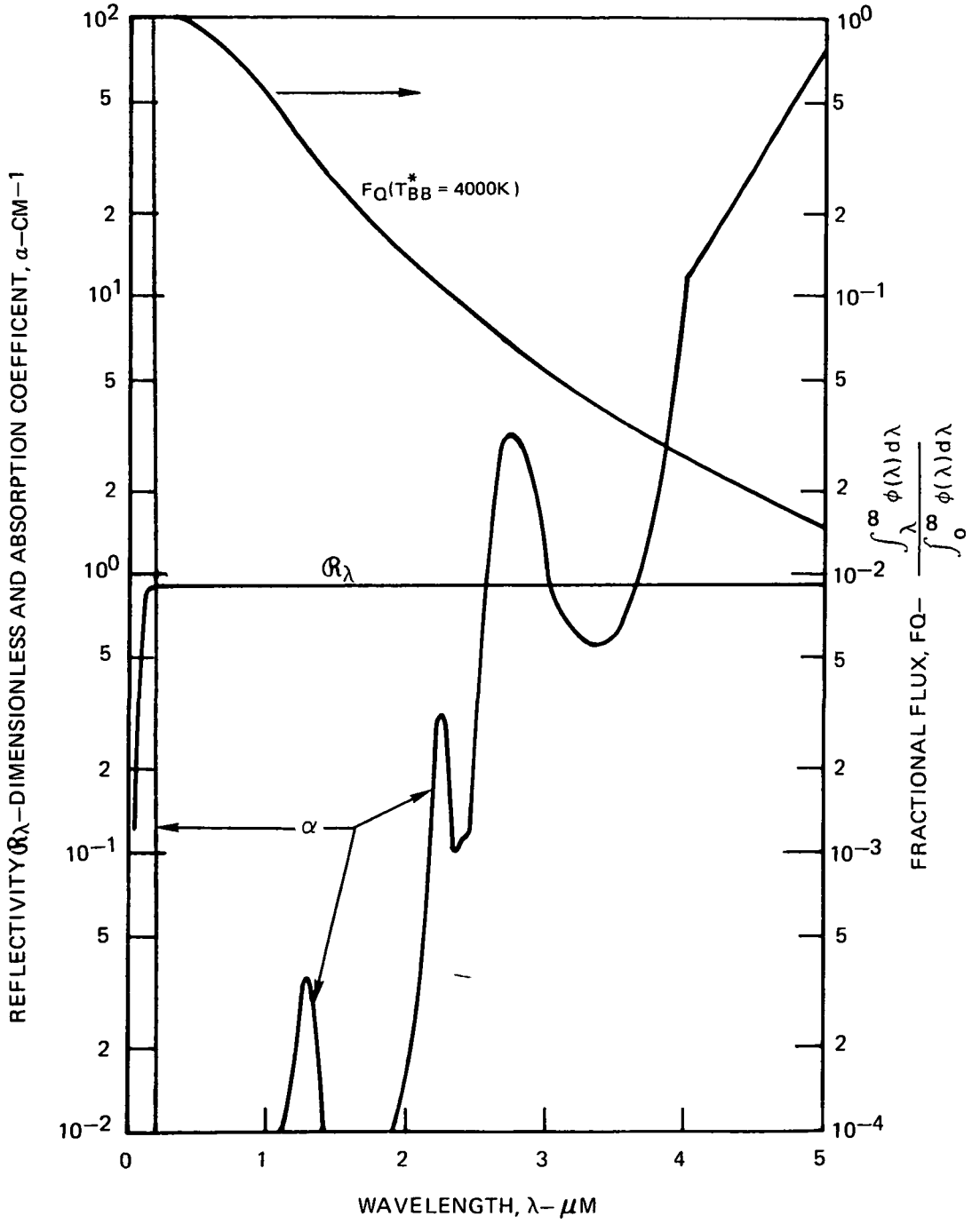

FIG. 14

VARIATION OF SURFACE HEAT FLUX WITH FUSED SILICA THICKNESS

T^*_{BB} = 4000K

$\frac{A_{WCD}}{A_C}$ = 0 2

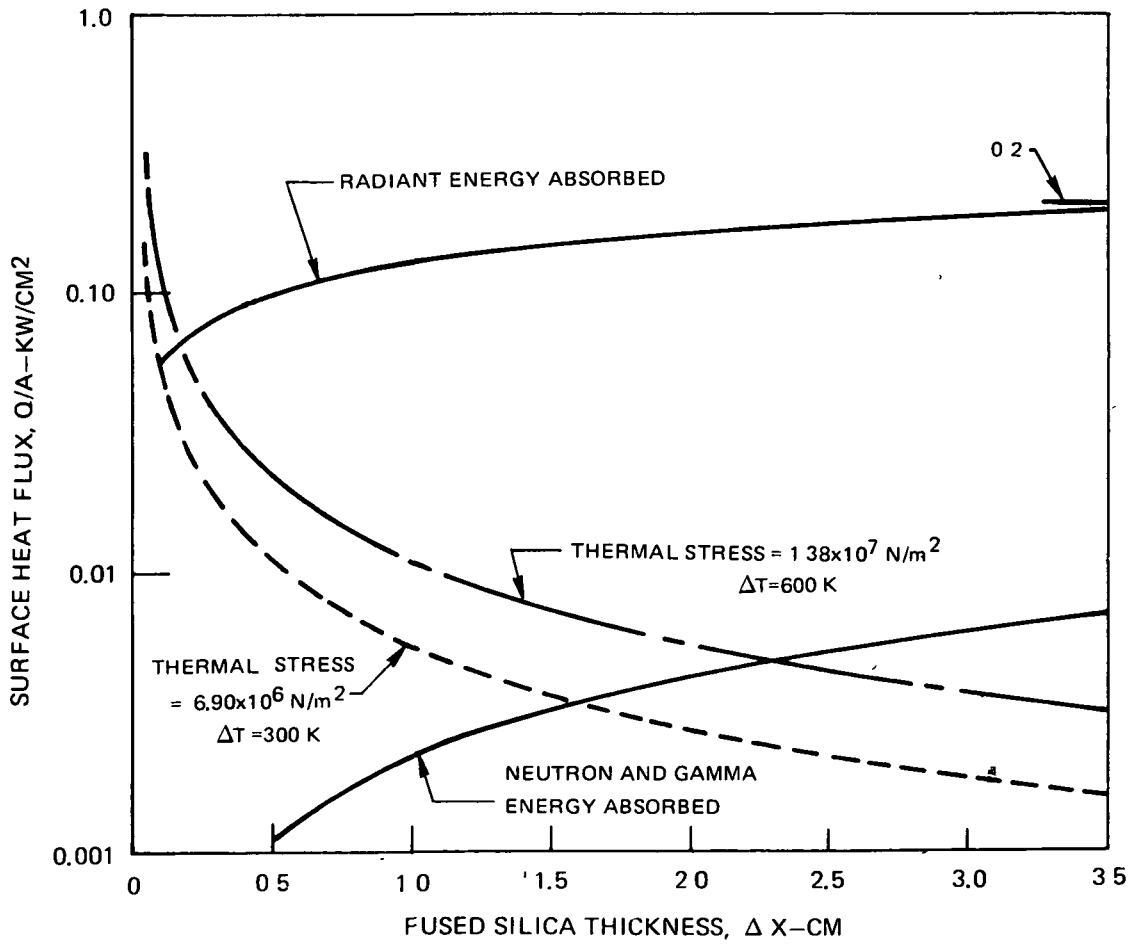

FIG. 15

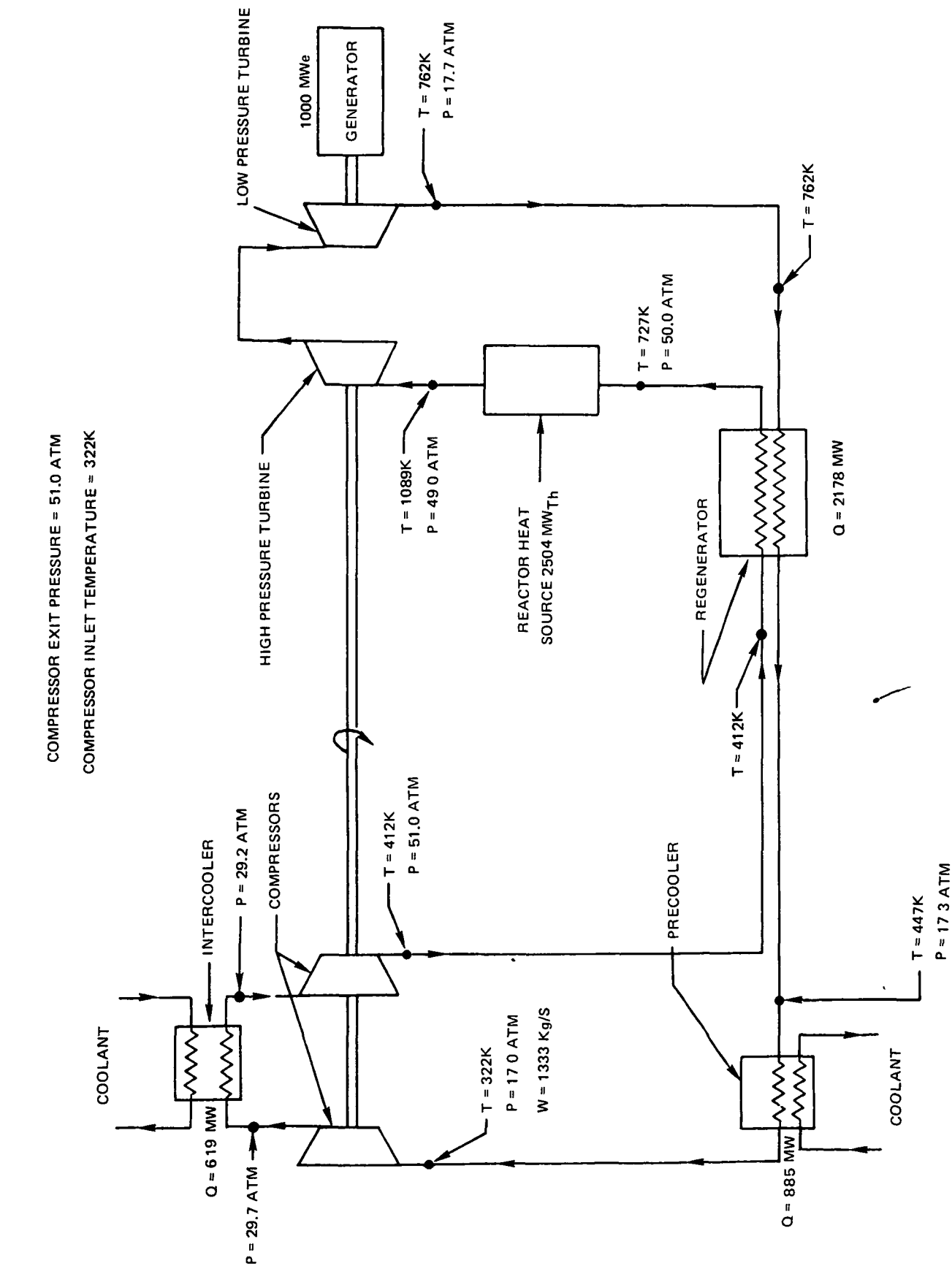
HELIUM CLOSED–CYCLE GAS TURBINE SYSTEM FOR TURBINE INLET TEMPERATURE OF 1089K
COMPRESSOR EXIT PRESSURE = 51.0 ATM
COMPRESSOR INLET TEMPERATURE = 322K
LOW PRESSURE TURBINE
1000 MWe
GENERATOR
T = 762K
P = 17.7 ATM
T = 762K
HIGH PRESSURE TURBINE
T = 1089K
P = 49 0 ATM
REACTOR HEAT
SOURCE 2504 MWTh
T = 727K
P = 50.0 ATM
REGENERATOR
Q = 2178 MW
T = 412K
INTERCOOLER
P = 29.2 ATM
COMPRESSORS
T = 412K
P = 51.0 ATM
PRECOOLER
T = 447K
P = 17 3 ATM
COOLANT
T = 322K
P = 17 0 ATM
W = 1333 Kg/S
Q = 619 MW
P = 29.7 ATM
Q = 885 MW
COOLANT

VARIATION OF CYCLE EFFICIENCY WITH COMPRESSOR PRESSURE RATIO

FLUID–HELIUM

$T_{COMPR\ INLET} = 322K$

$P_{COMPR\ OUT} = 51$ ATM

1 INTERCOOLER

REGENERATOR EFF = 0.90

ELECTR GEN. $\eta = 0.98$

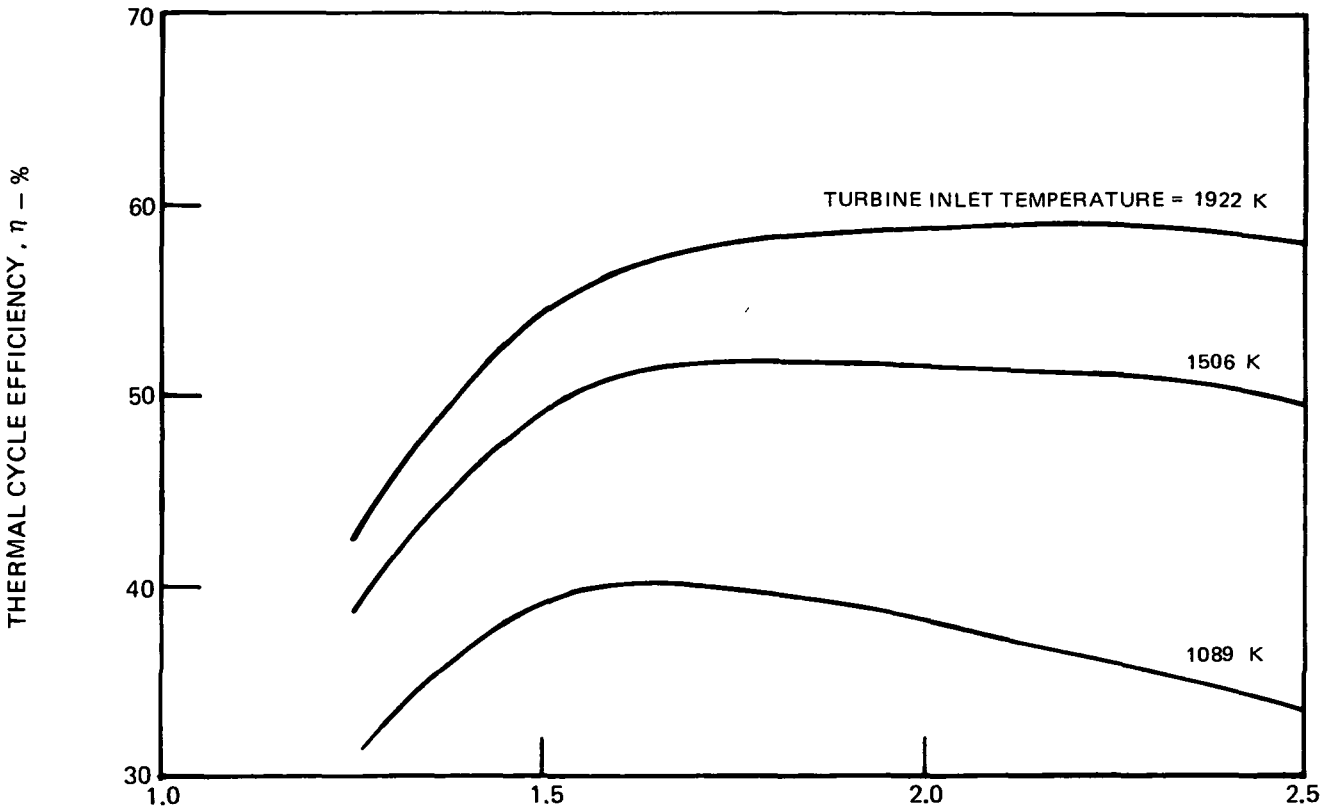

FIG.17

VARIATION OF CYCLE EFFICIENCY WITH TURBINE INLET TEMPERATURE

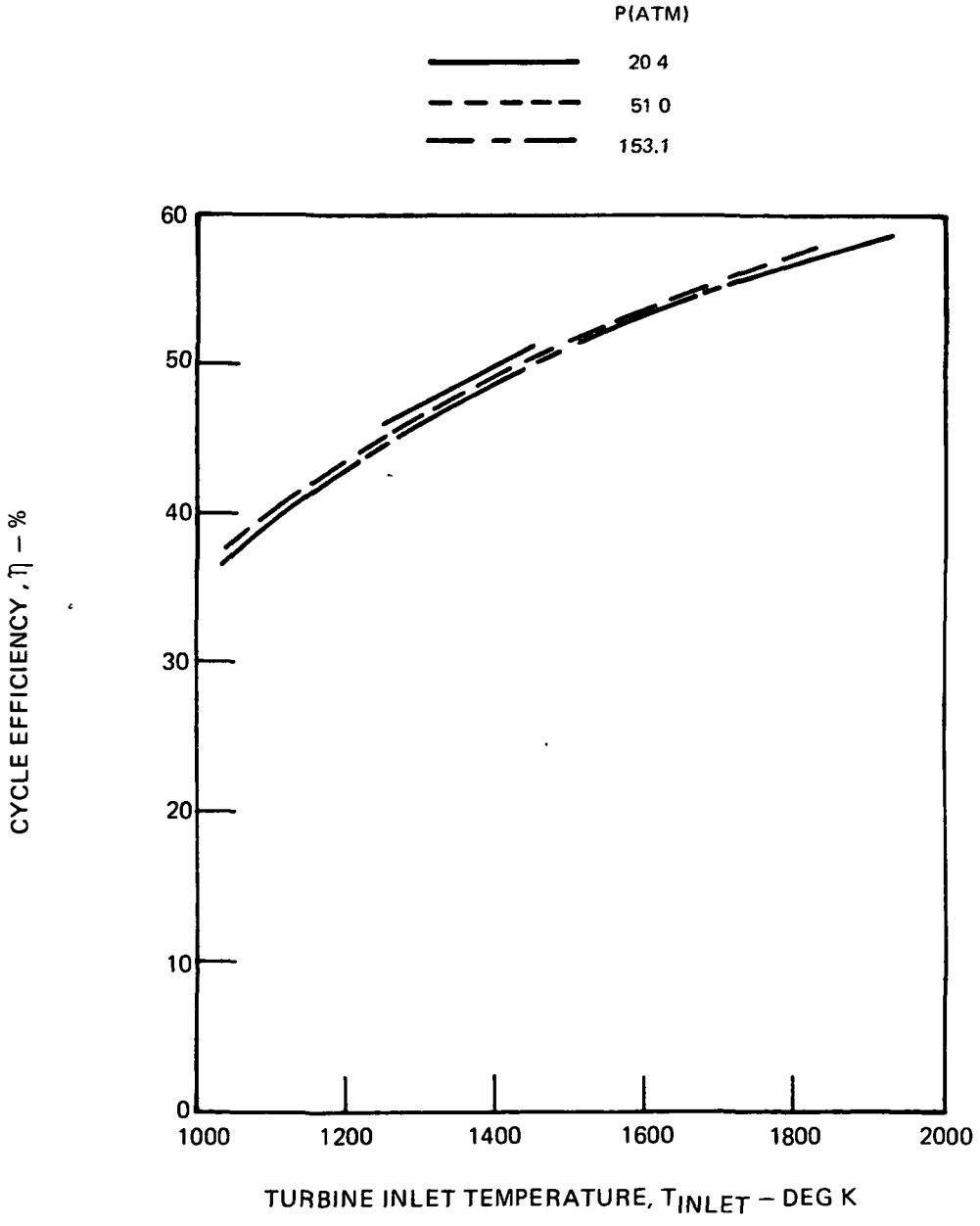

76–05–151–1

HELIUM CLOSED–CYCLE GAS TURBINE SYSTEM FOR TURBINE INLET TEMPERATURE OF 1506K

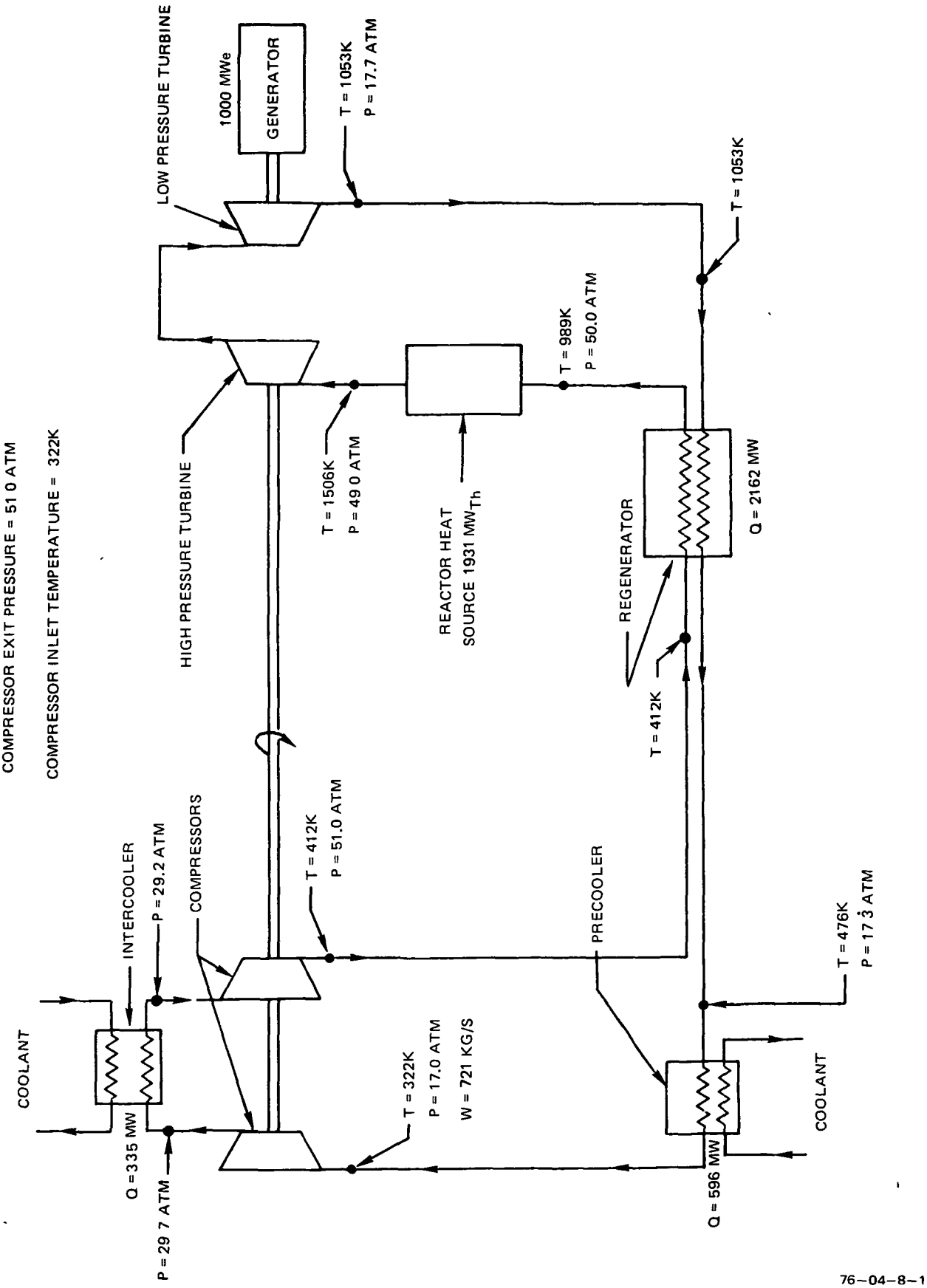

76–04–8–1

FIG. 19

HELIUM CLOSED–CYCLE GAS TURBINE SYSTEM FOR TURBINE INLET TEMPERATURE OF 1922K

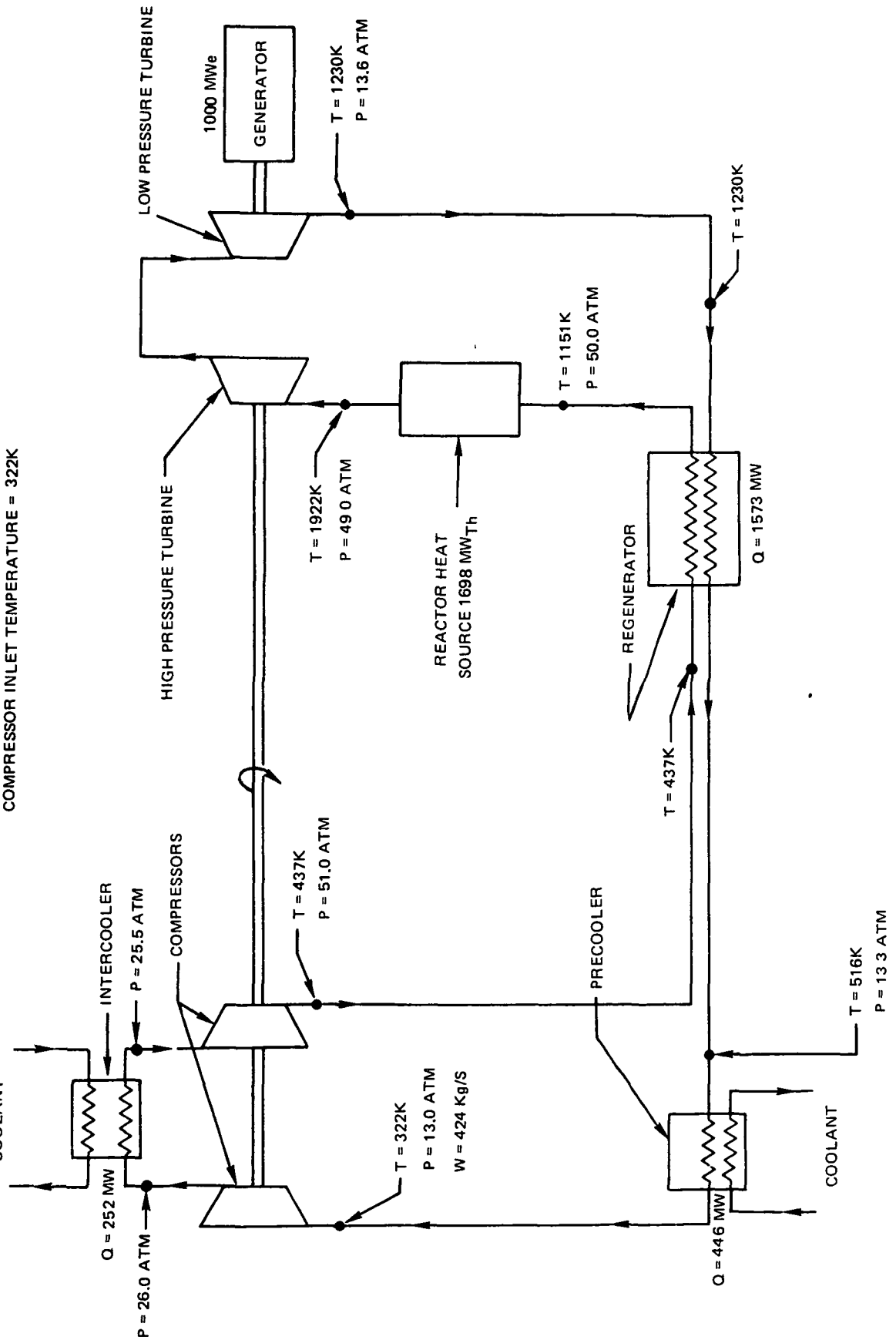

CALCULATED CYCLE EFFICIENCY FOR PLASMA CORE REACTORS WITH CLOSED–CYCLE GAS TURBINES

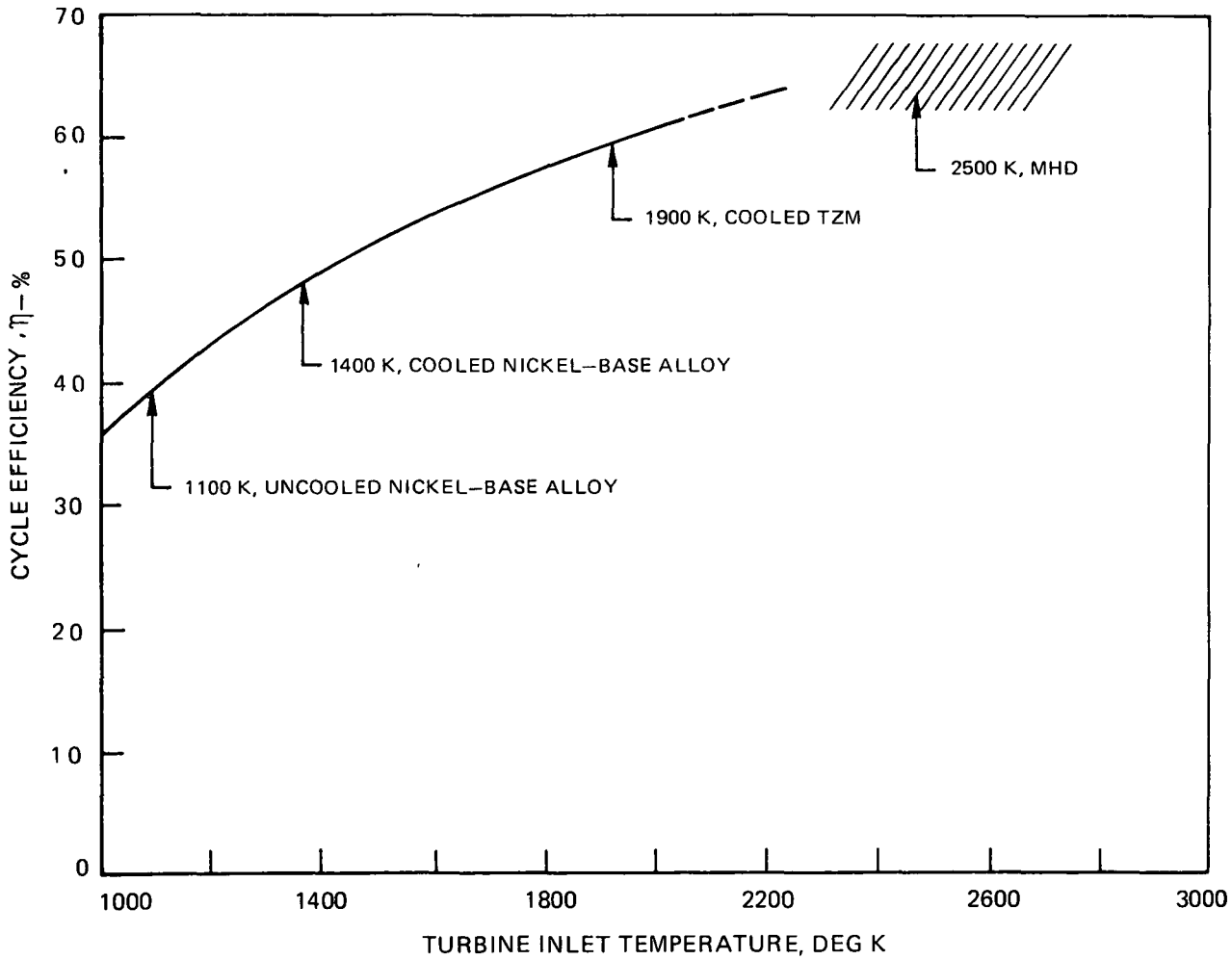

76–04–69–3

SCHEMATIC OF FUEL RECYCLE SYSTEM FOR UNIT CELL

Q_{TOT} = 479 MW T^* = 5000 K

Q_{CONV} = 18 MW M_{UF_6} = 21.45 Kg

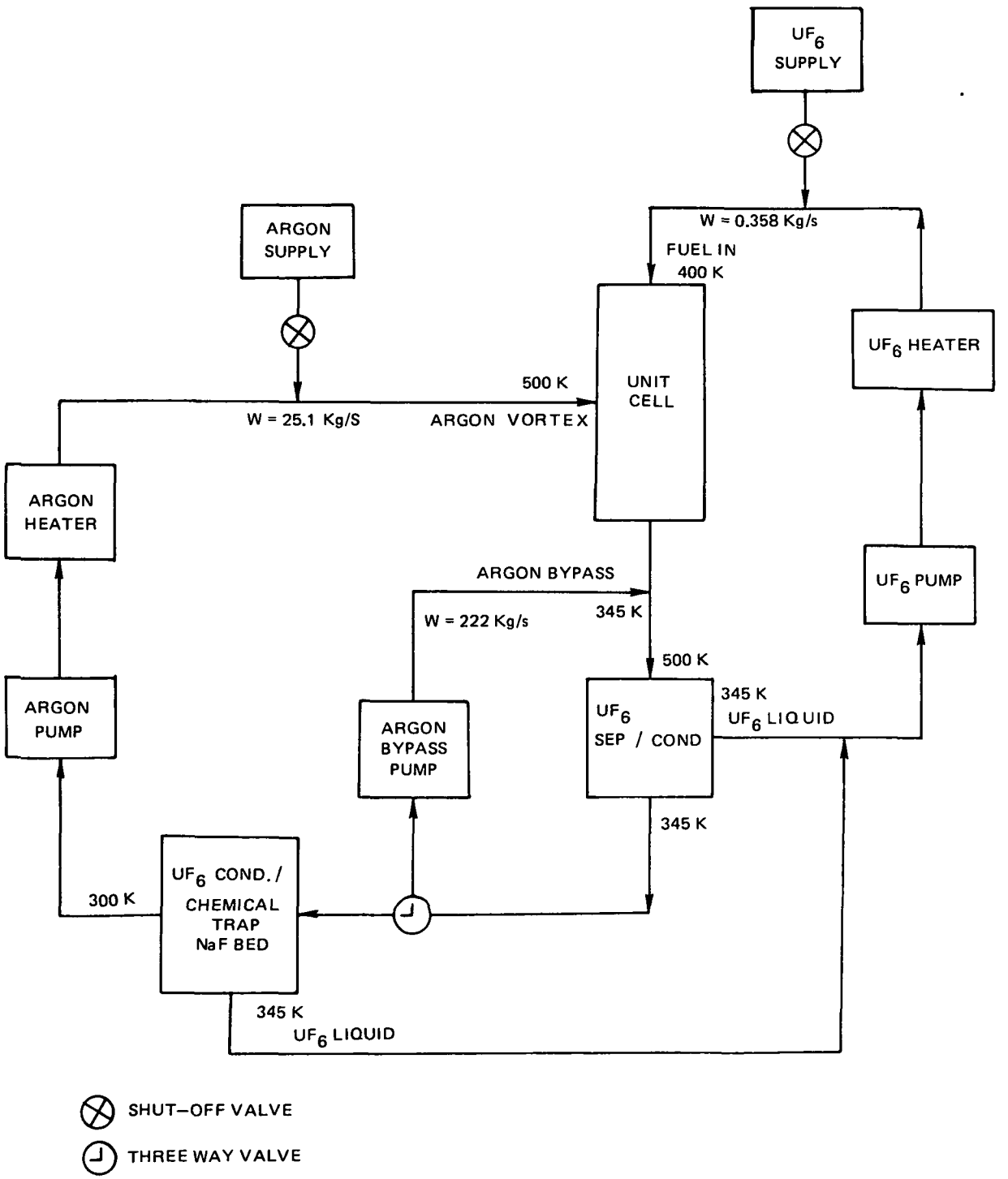

CONCEPT FOR HYDROGEN PRODUCTION FROM WATER BY PHOTO DISSOCIATION OF BROMINE AND IODINE GASES

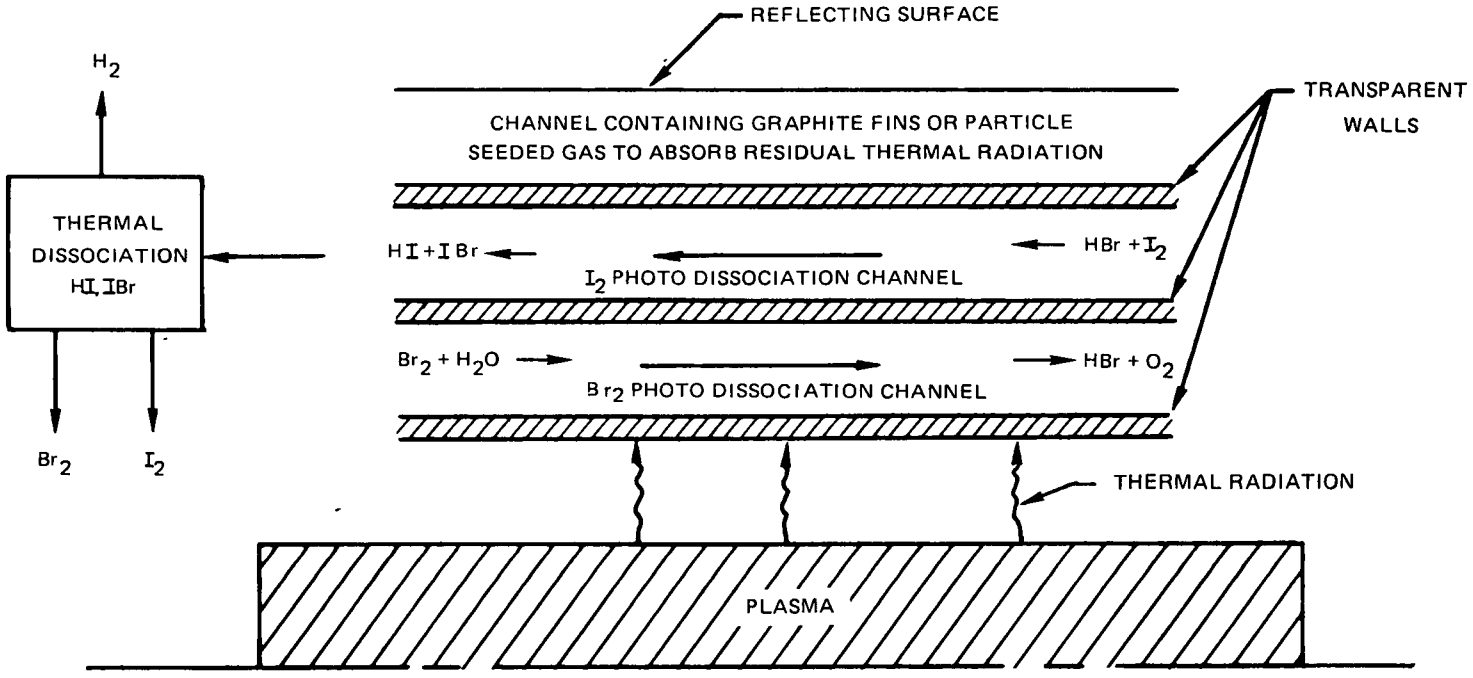

FIG. 22

COMPOSITION OF H_2O–Br MIXTURE AS A FUNCTION OF TEMPERATURE

P_{TOT} = 0.50 ATM

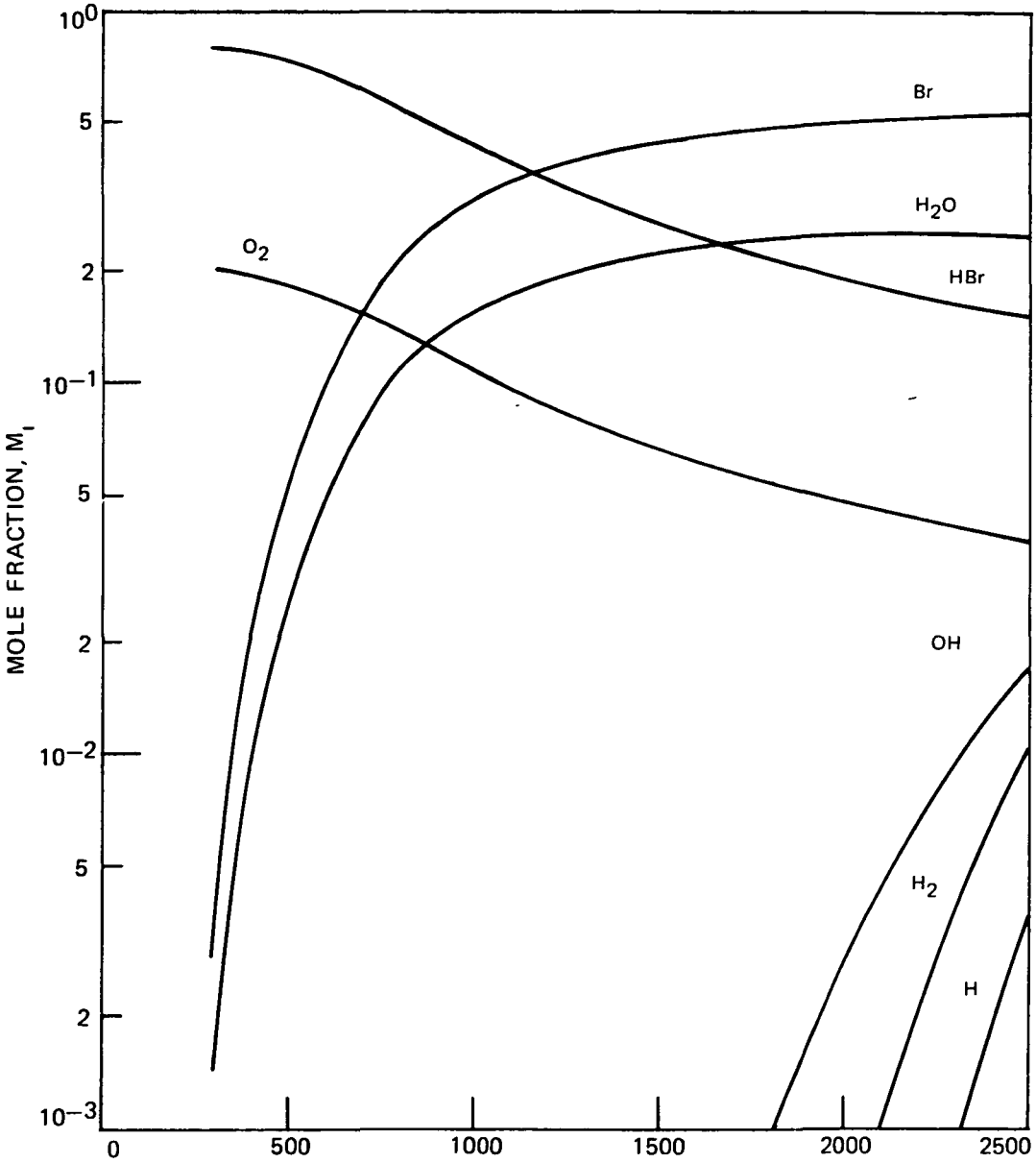

R06–227–2

FIG. 24

COMPOSITION OF CL_2, Br_2 AND I_2 AS A FUNCTION OF TEMPERATURE

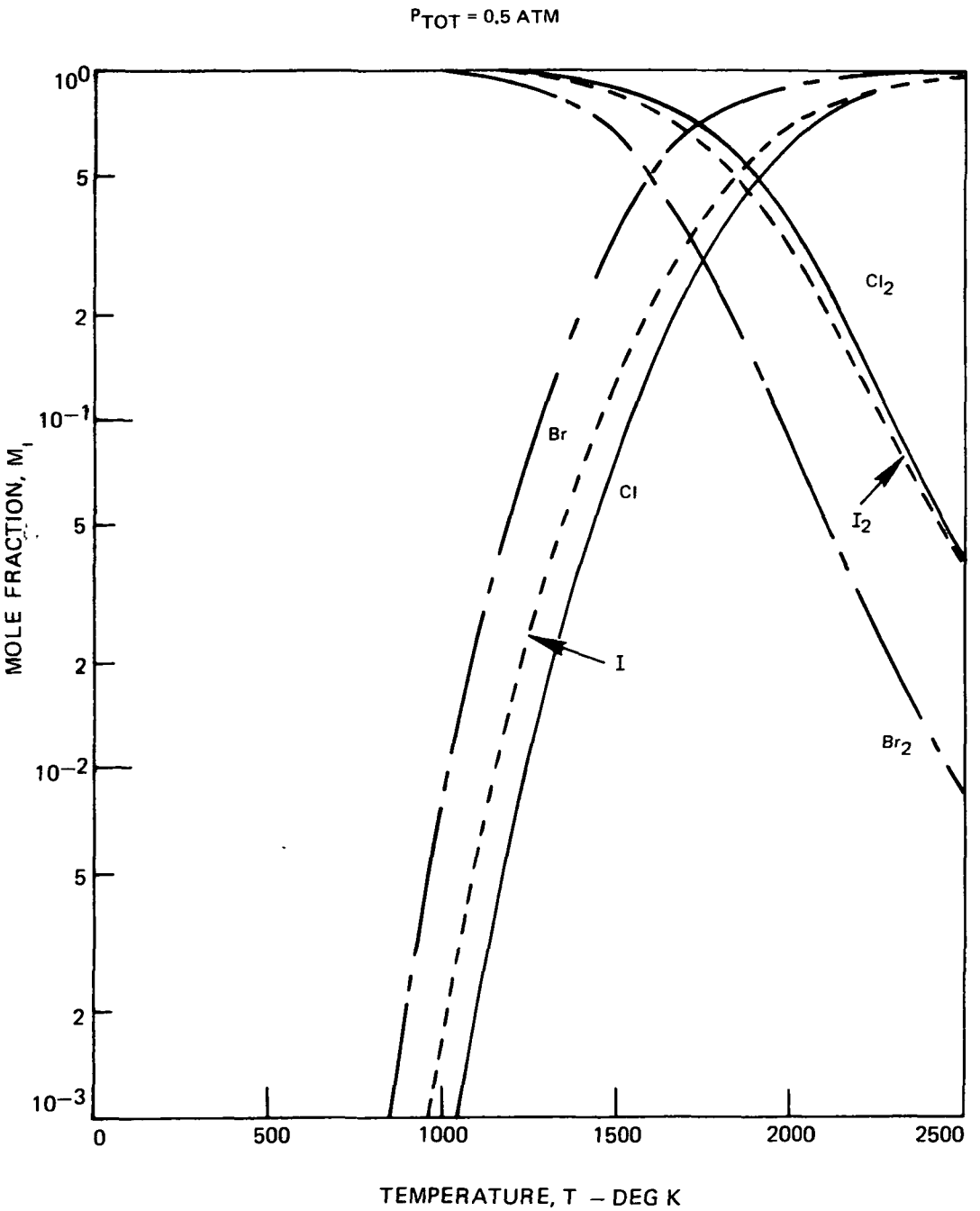

FIG. 25

BLACK–BODY FRACTIONAL FLUX DISTRIBUTION AT TEMPERATURE OF 4000 K AND PHOTO DISSOCIATION SPECTRAL ABSORPTION CROSS–SECTIONS FOR HALOGEN AND HALIDE GASES

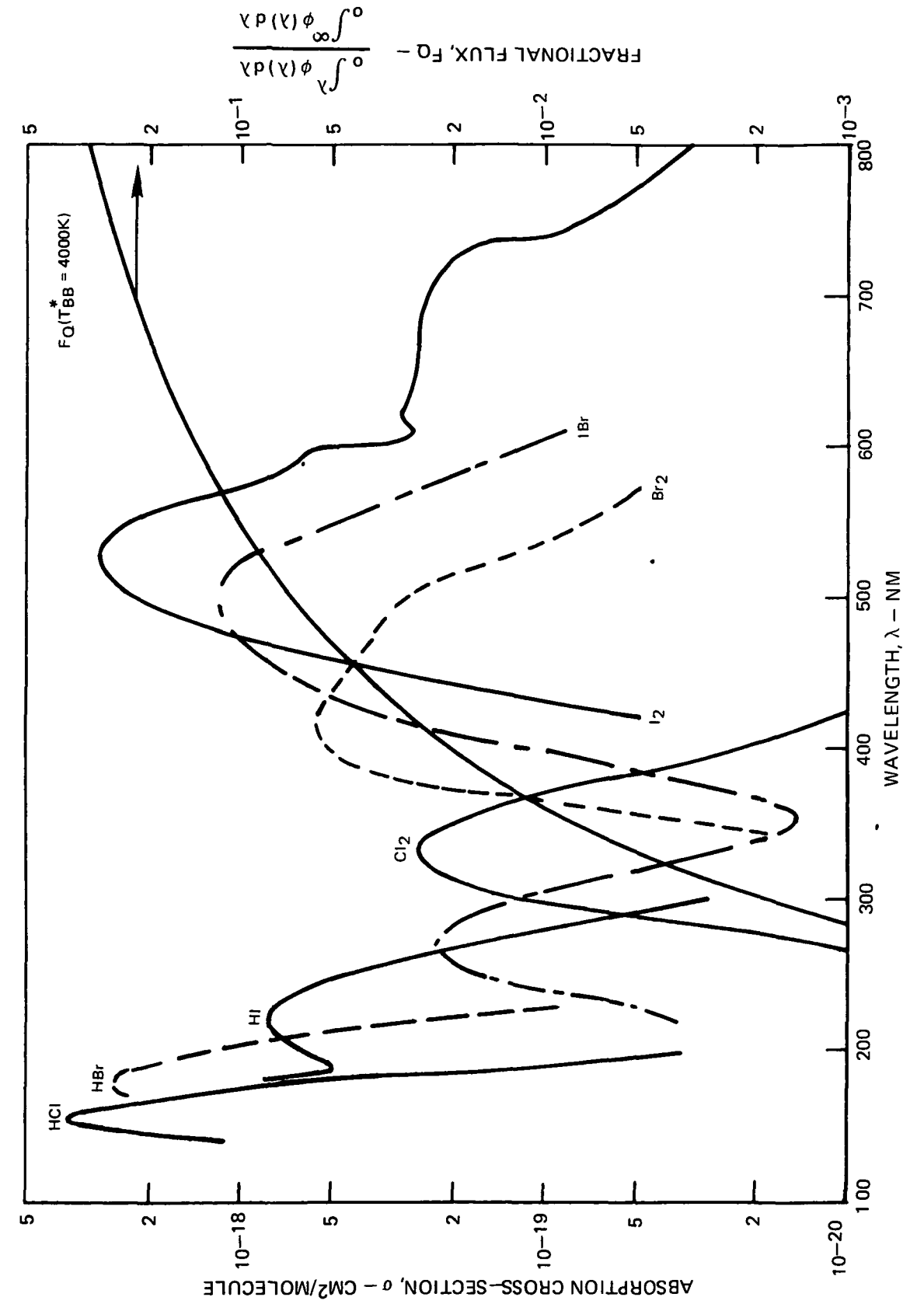

76–04–179–3

FIG. 26

DEGREE OF DISSOCIATION OF THE HALIDES HCL, HBr, HI AND IBr

P_{TOT} = 1.0 ATM

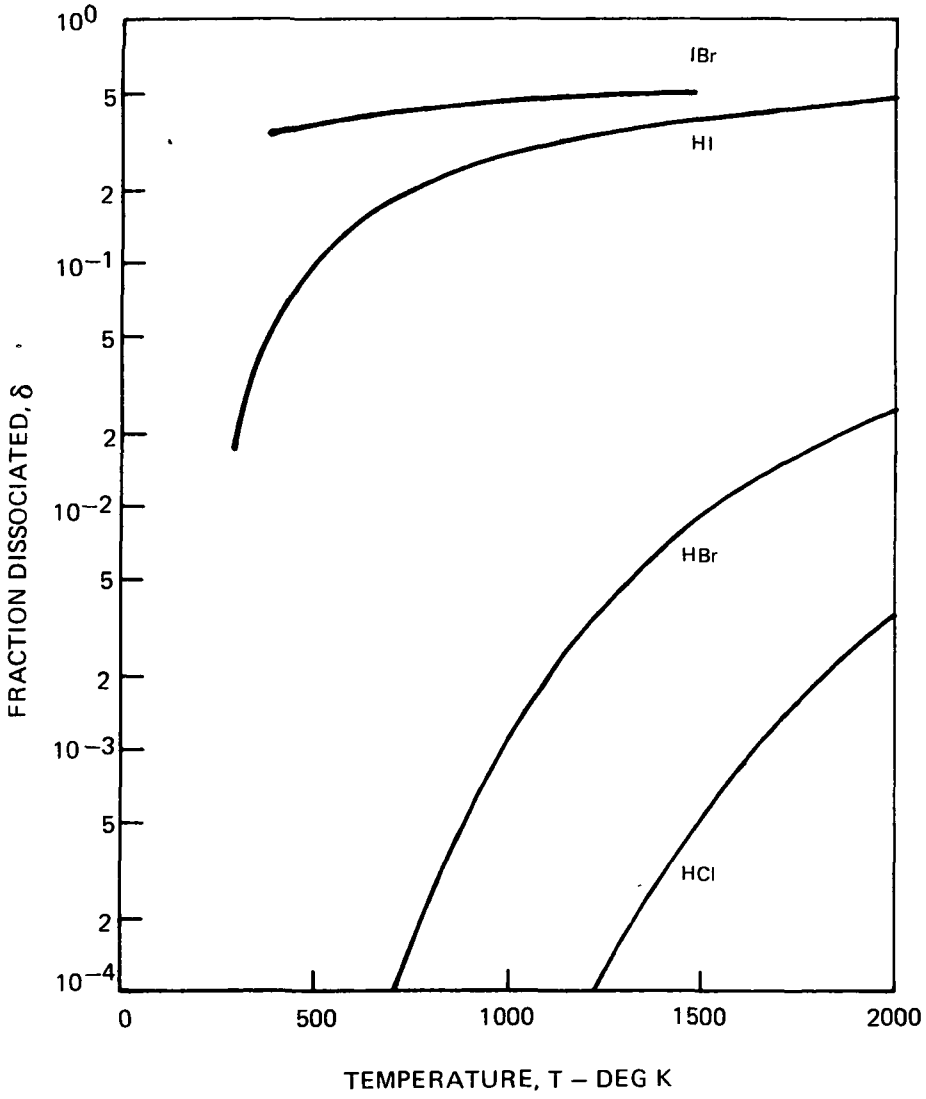

FIG. 27

PLASMA CORE BREEDER REACTOR FOR ELECTRIC POWER GENERATION

NOMINAL THERMAL POWER – 2500 MW

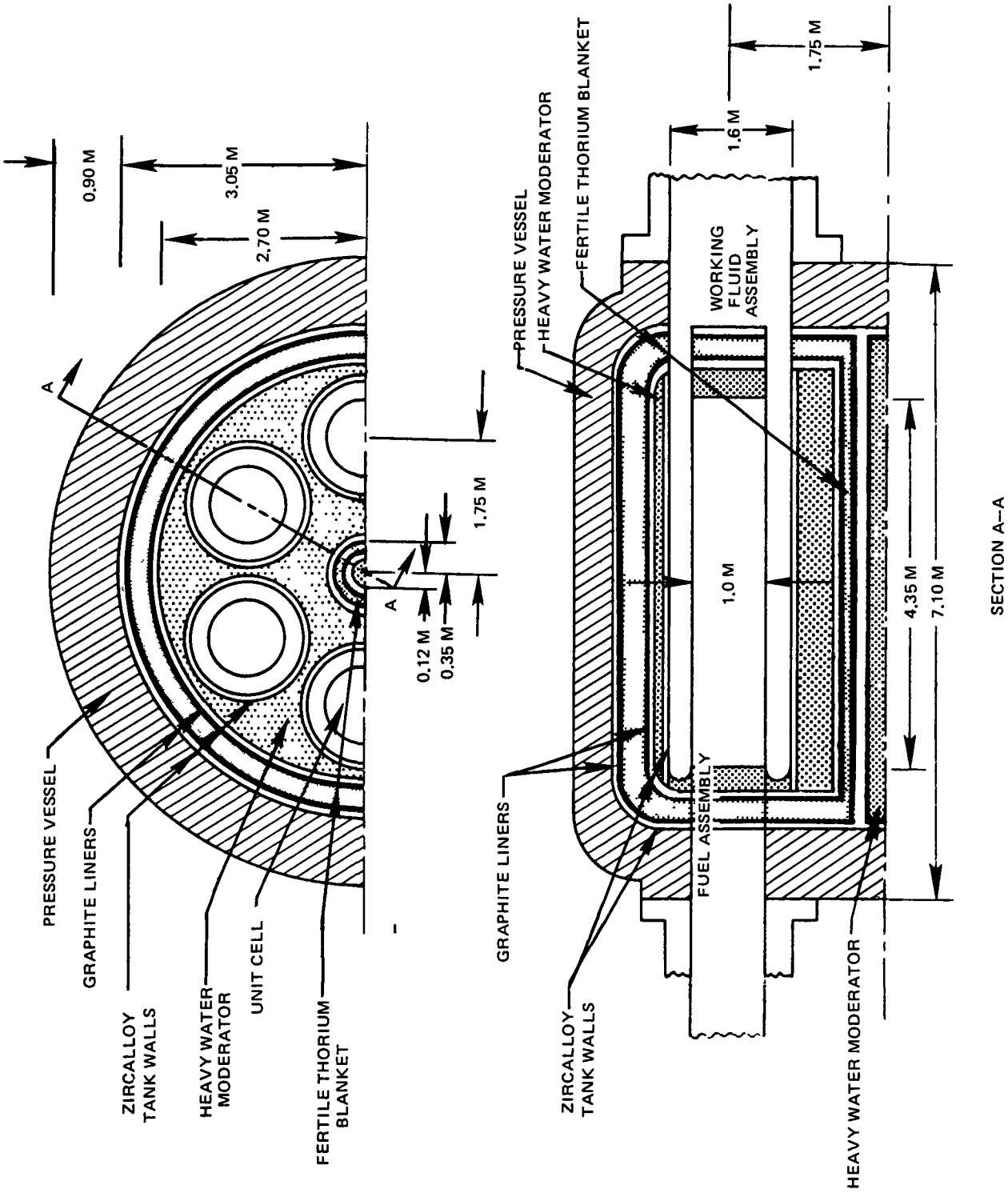

N11–148–1

CALCULATION MODELS FOR PLASMA CORE BREEDER REACTOR

(a) CYLINDRICAL FUEL CAVITY UNIT CELL

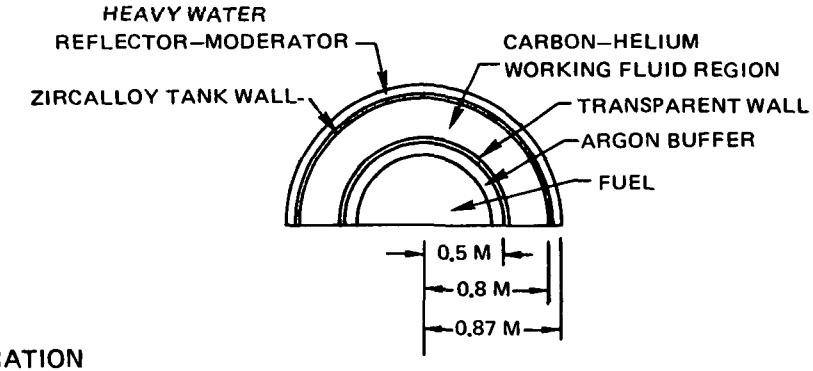

(b) SPHERICAL CONFIGURATION

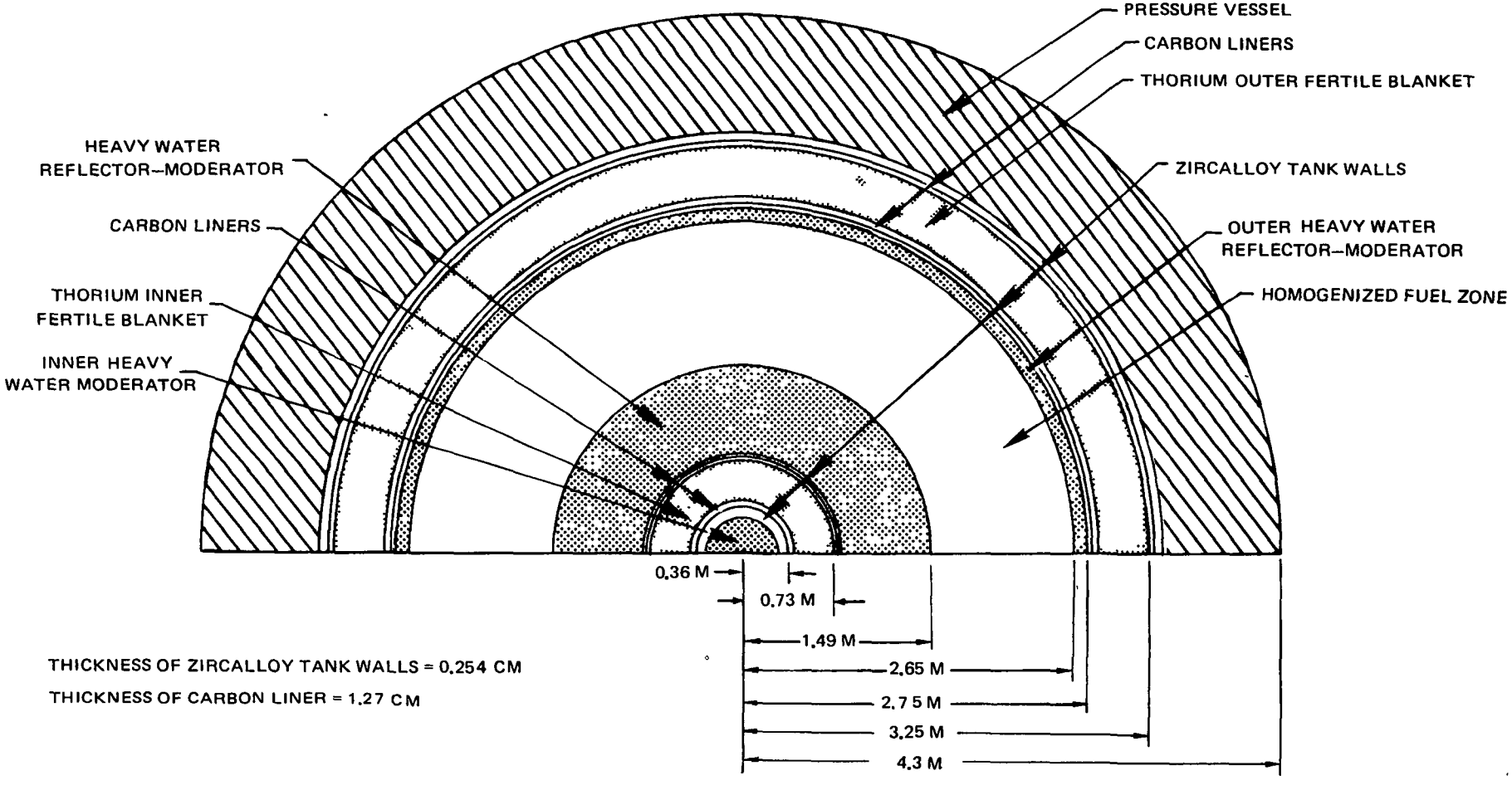

THICKNESS OF ZIRCALLOY TANK WALLS = 0.254 CM

THICKNESS OF CARBON LINER = 1.27 CM

R76–912204

FIG. 28

NUCLEAR REACTIONS IN TH^{232}–U^{233} MODIFIED BREEDING CYCLE CHAIN UNDER NEUTRON IRRADIATION

λ_{CP} = RECIPROCAL OF AVERAGE RESIDENCE TIME OF PROTACTINIUM ATOMS IN BREEDING BLANKET BEFORE CHEMICAL PROCESSING REMOVAL

λ_F = RECIPROCAL OF AVERAGE RESIDENCE TIME OF URANIUM ATOMS IN BREEDING BLANKET BEFORE FLUORIDATION REMOVAL

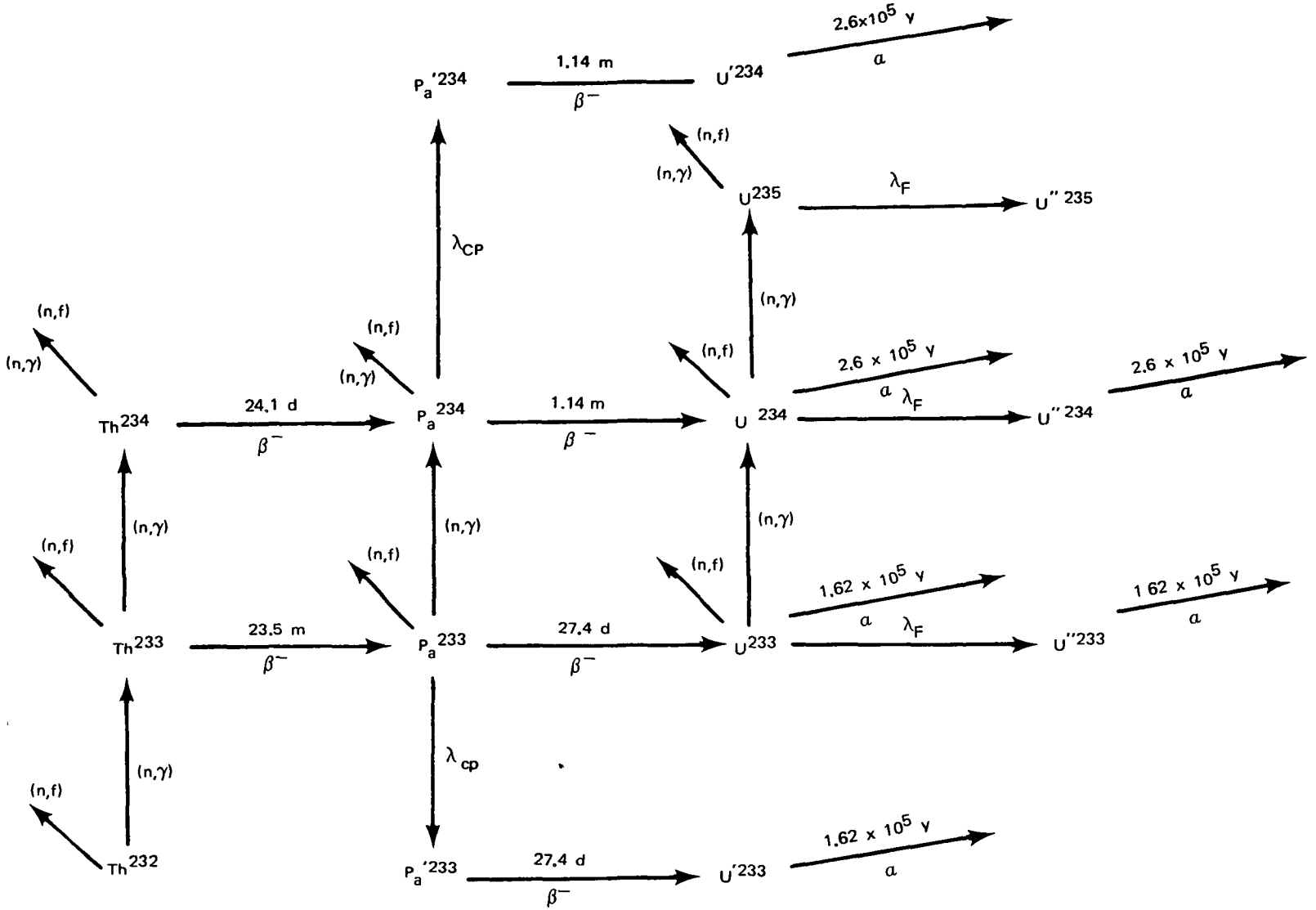

R76–912204

N12–40–1

FIG 29

FIG. 30

VARIATION OF BREEDING RATIO WITH TIME FOR Th -U–233 FUELED PLASMA CORE BREEDER REACTOR

TWO CHEMICAL PROCESSING AND FLUORIDATION REMOVAL RATES ARE CONSIDERED

POWER = 2500 MW THERMAL

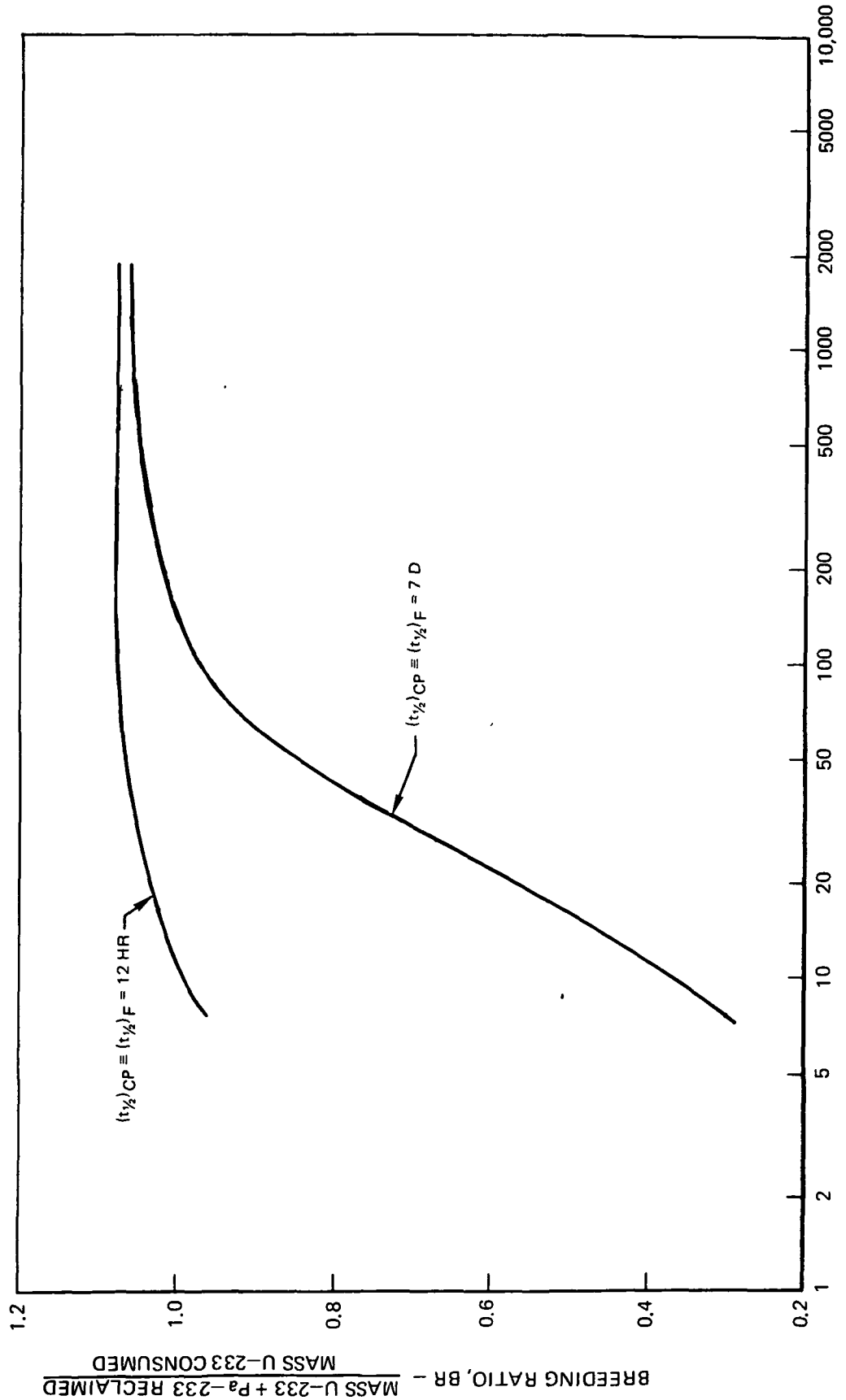

MASS OF URANIUM–233 AND PROTACTINIUM–233 RECLAIMED FROM THORIUM–232 BREEDING BLANKET FOR CHEMICAL PROCESSING AND FLOURIDATION HALF LIFE REMOVAL RATE OF TWELVE HOURS

POWER = 2500 MW THERMAL

M_{CRIT} = 84.4 Kg OF U–233

SEE FIG. 30 FOR BREEDING RATIO

SEE FIG 28 FOR GEOMETRY AND DIMENSIONS OF CONFIGURATION

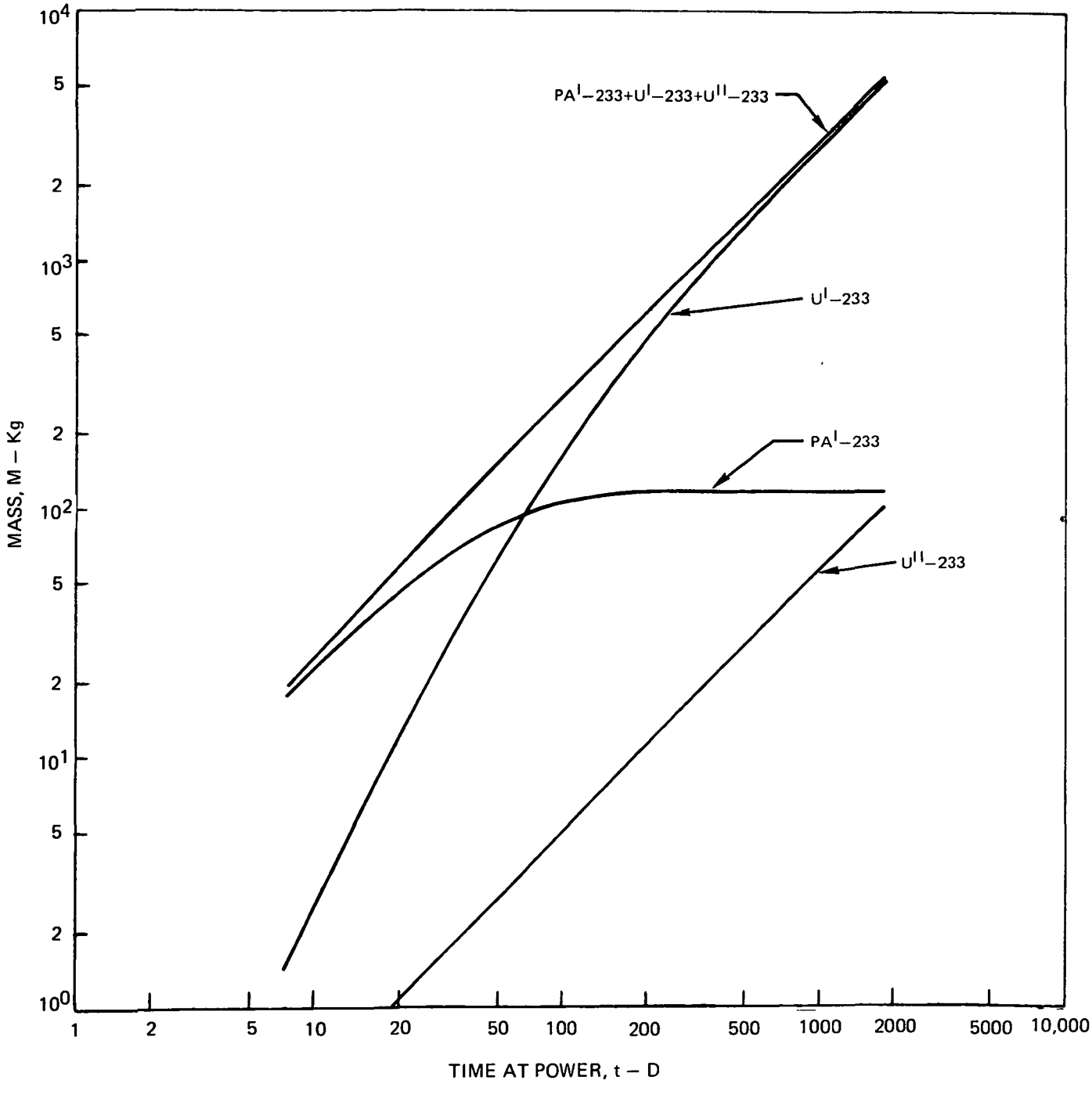

76–04–58–1

MASS OF URANIUM–233 AND PROTACTINUM–233 RECLAIMED FROM THORIUM–232 BREEDING BLANKET FOR CHEMICAL PROCESSING AND FLOURIDATION HALF LIFE REMOVAL RATE OF SEVEN DAYS

POWER = 2500 MW THERMAL

M_{CRIT} = 84.4 Kg OF U–233

SEE FIG 30 FOR BREEDING RATIO

SEE FIG 28 FOR GEOMETRY AND DIMENSIONS OF CONFIGURATION

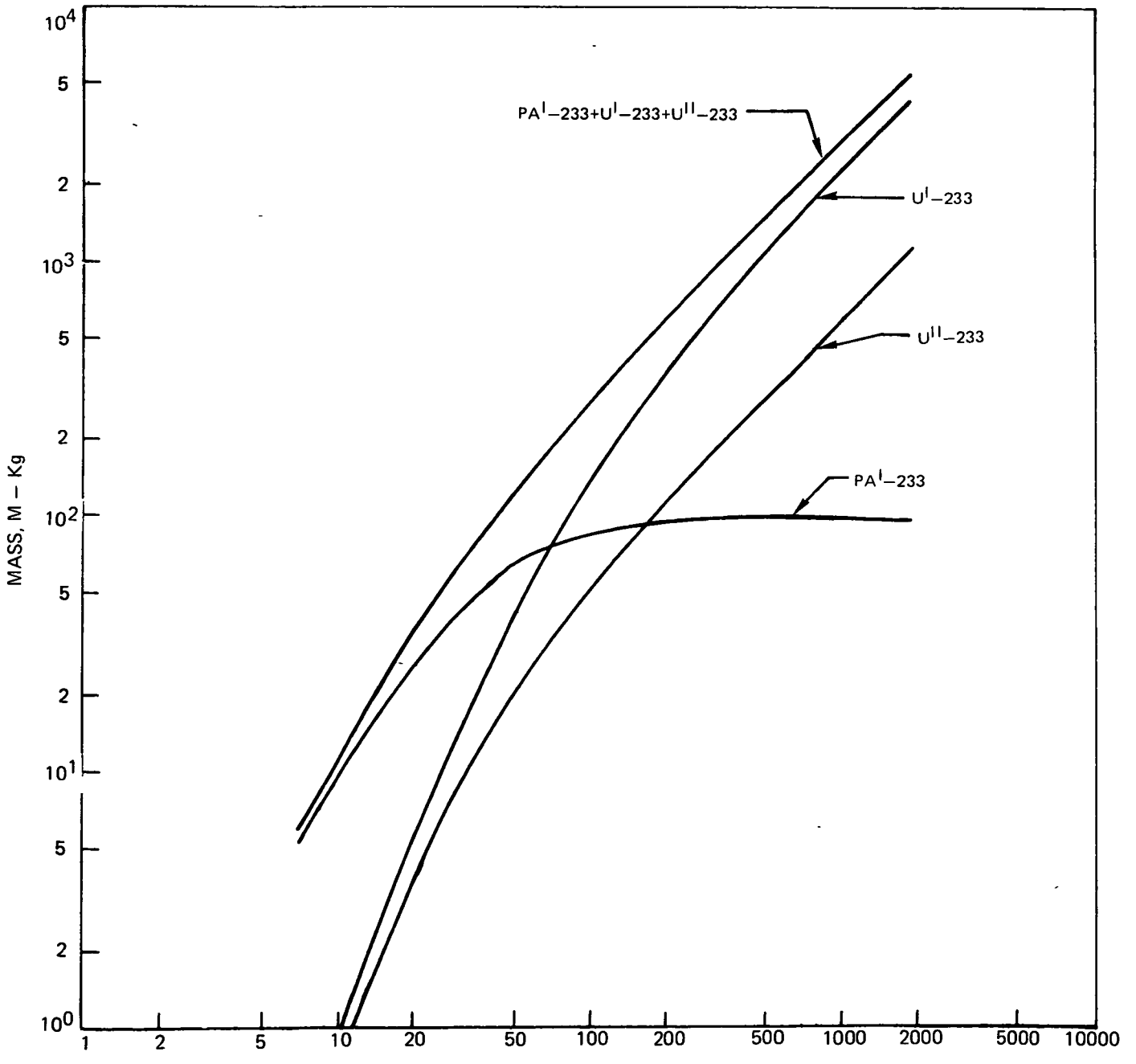

76–04–58–2